POLISH ACADEMY OF SCIENCES – WROCŁAW BRANCH
WROCŁAW UNIVERSITY OF TECHNOLOGY

# ARCHIVES OF CIVIL AND MECHANICAL ENGINEERING

Quarterly
Vol. IV, No. 3

WROCŁAW 2004

ARCHIVES OF CIVIL AND MECHANICAL ENGINEERING

Vol. IV 2004 No. 3

# Microstructure evaluation of hot-rolled sheet from ferritic stainless steel with 25% content of chromium

LIBOR CERNY
ISPAT NOVA HUT a. s., Technological Development and Environment,
Vratimovska 689, 707 02 Ostrava–Kuncice, Czech Republic, lcerny@novahut.cz

IVO SCHINDLER, STANISLAV RUSZ
VSB – Technical University Ostrava, Institute of Modelling and Control of Forming Processes,
17. listopadu 15, 708 33 Ostrava–Poruba, Czech Republic, ivo.schindler@vsb.cz

Structure-forming processes and hot deformation behaviour of stainless ferritic steel containing 25% of Cr were investigated both in a laboratory as well as in industrial conditions. To this end experimental equipment of the Institute of Modelling and Control of Forming Processes was utilized, including vacuum melting furnace, two-stand rolling mill Tandem and several electric-resistance furnaces. Experiments showed that the steel examined in as-cast and as-rolled states has a considerable susceptibility to grain coarsening. That phenomenon is difficult to eliminate because of appreciable inhibition of recrystallization processes due to high content of chromium. It takes place even during simulation of conventional and/or direct rolling. The influence of change of the processing parameters on the final structure has been determined.

Keywords: *microstructure evaluation, hot-rolled sheet, recrystallization*

## 1. Introduction

ISPAT NOVA HUT is the biggest steel producer and also sole hot-rolled strips producer in the Czech Republic. In the late 90ies, the management of the company decided to implement a wide-ranging modernization program. Within the frames of it also the production of hot-rolled strips was innovated.

For this purpose the reversible Steckel mill was selected, above all in order to optimize the investment and operational costs. The aim of ISPAT NOVA HUT is to produce more than one million tons of hot-rolled strips annually. The one-stand Steckel rolling mills are insufficient for such a level of production and therefore two-stand Steckel rolling mill was chosen to operate in ISPAT NOVA HUT (mill P1500). This type of rolling mill has not yet been constructed anywhere in the world, but because of the above-mentioned reason it seemed to be optimal.

Rolling mill P1500 is not equipped with rougher stand; however, it comprised the second finishing stand and vertical stand (see Figure 1). The slabs soaked in walking-beam furnace are rolled in reverse way by five or seven double-passes. Furnace coilers are located at entry and exit sides of stands and enable us to maintain temperature up

to 1050 °C. The roughing passes are performed without using furnace coilers, finishing passes with using them, which makes it possible to roll such a steel grade that is characterized by high flow stress [1].

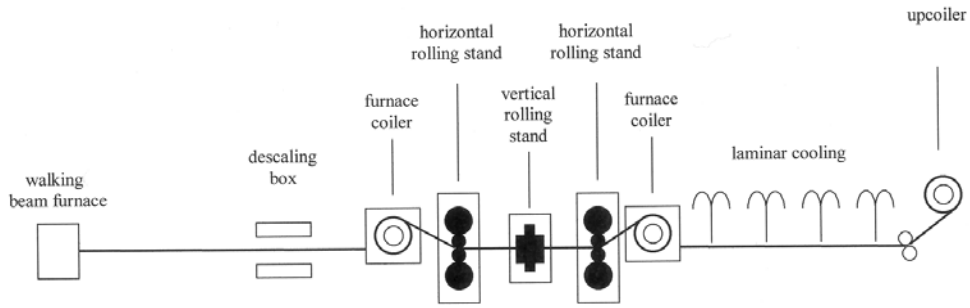


Fig. 1. Layout of two-stand reversible Steckel rolling mill in ISPAT NOVA HUT

Production schedule for the mill P1500 is composed of seven groups of steel grades according to their chemistry and subsequent using. One of them is stainless steel group. The mill P1500 came into operation in June 1999. After acquiring experience and knowledge about rolling and the properties of deep-drawing [2], structural [3], high-carbon [4] and high-strength low-alloyed steels [5] a technology for rolling of ferritic stainless steel has been developed.

The rolling process of the mill P1500 is very often and very effectively modelled with laboratory rolling mill Tandem at the Institute of Modelling and Control of Forming Processes at VSB – Technical University of Ostrava [6, 7]. This mill has been described in detail many times [8–10], so it is sufficient to emphasize that it has two stands and is equipped with two furnaces which perfectly simulate rolling process in the mill P1500.

## 2. Characteristics of the material tested

One of our aims was to study the deformation behaviour and possibilities of grain refinement of ferritic stainless steel 13Cr25 (i.e. 17153 according CSN) during various rolling processes. Initial status (slab) and also status after laboratory remelting in vacuum inductive furnace and casting into cast-iron mould have been investigated [1]. Shape and dimensions of a cast semi-product as well as its macrostructure in various sections are shown in Figure 2. The castings have been used for simulation of the as-cast structure rolling. The results of chemical analyses are presented in the Table. This Table shows an excellent correspondence of defined content of almost all elements. This means that the method of laboratory remelting of samples has been very well mastered.

Table. Chemistry of the samples analysed [wt. %]

| Species | Casting | Slab |
|---|---|---|
| C | 0.067 | 0.074 |
| Mn | 0.312 | 0.33 |
| P | 0.028 | 0.028 |
| S | 0.010 | 0.009 |
| Si | 0.74 | 0.78 |
| Cu | 0.10 | 0.10 |
| Ni | 0.43 | 0.43 |
| Cr | 25.4 | 25.5 |
| Mo | 0.15 | 0.15 |
| W | 0.05 | 0.05 |
| V | 0.08 | 0.08 |
| Al | 0.04 | 0.07 |

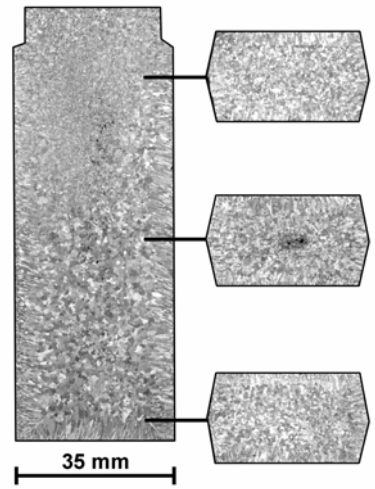


Fig 2. Macrostructure of laboratory cast

The initial microstructure of rolled slab has been investigated mostly in surface parts in longitudinal and transverse sections with respect to rolling direction by means of optical spectroscopy (Figure 3). It has been found that the structure was quite coarse-grained, but equiaxial – no marked differences in grain shape in longitudinal and transverse directions have been found. The grain in central parts is slightly rougher than the grain in surface parts. Grain boundaries are occasionally bordered with carbides.

a) b)

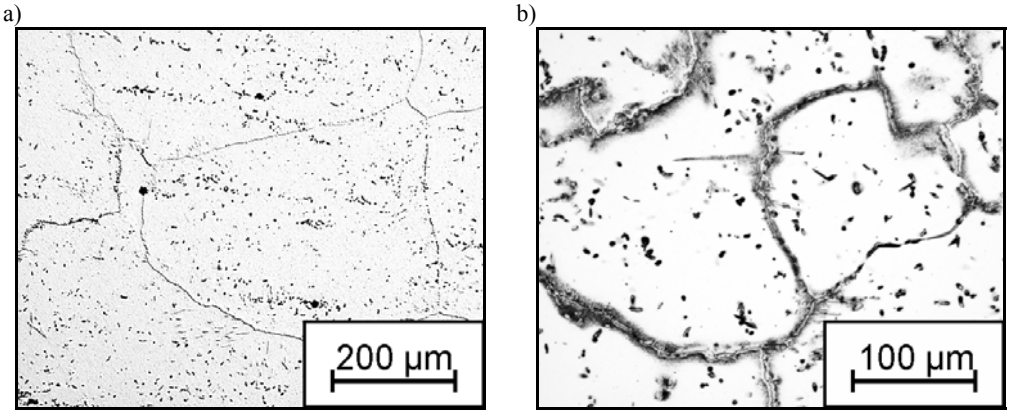


Fig. 3. Initial microstructure of slab: a) central part, longitudinal section, b) edge, longitudinal section – detail

Microstructure in the corner parts is quite different. The grains in these parts are elongated and are more unequal with respect to grain size. The steel tested contains a considerable amount of precipitates. The amount of globular inclusions, mainly of complex character, does not exceed grade 2 according to standard CSN 42 0240.

The structure of laboratory cast has been investigated in transverse section in a half of height of its body (the so-called representative locality [12]). It is obvious (Figure 4) that grain size in all places is comparable with grain size of manufactured rolled slab (with the exception of the corner parts of a slab). Cast microstructure is surprisingly homogeneous, grains are mostly perfectly equiaxial. Some pictures show (especially at corner places) wavy, as though shaky grain boundaries. Primarily poured polyhedral grains are bigger than hundreds micrometers and acicular precipitates occur in these grains. Grain boundaries in some places are sharp and straight which is typical of as-cast structures.

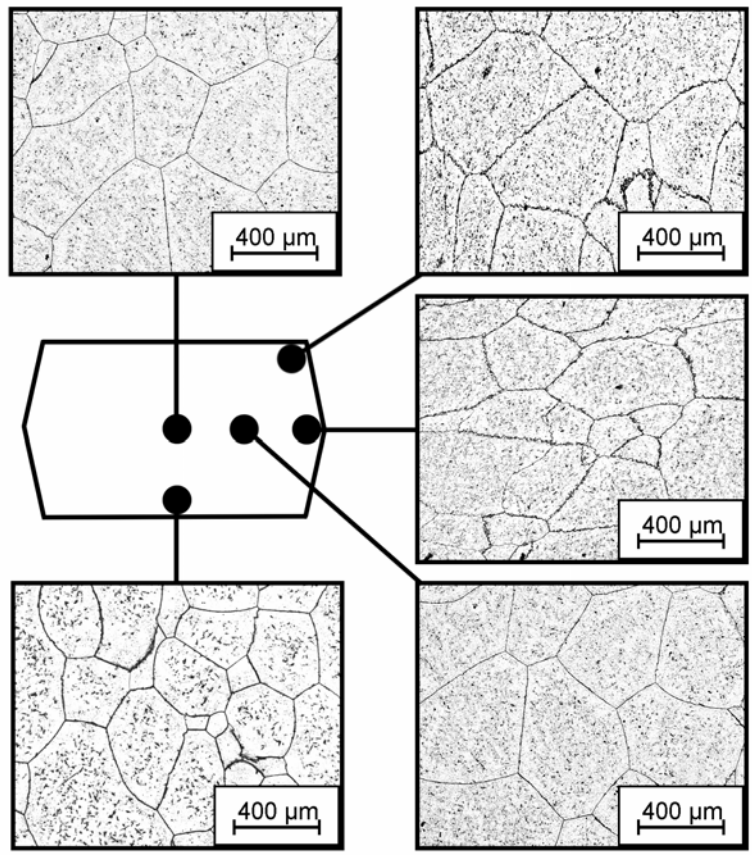


Fig. 4. Transverse section microstructure of laboratory casting

Other grain boundaries of cast (but also of rolled slab) are wavy, especially at corner parts. This is probably due to internal tension in the casting. The casting solidifies firstly at surface and therefore the highest tension in these parts can be expected. This makes the formation of dislocations and their slip to grain boundaries possible. The fact that the largest amount of cumulated energy is here has been stated also after rolling when the recrystallization occurs preferentially at grain boundaries.

## 3. Experimental procedures

Ferritic steel 13Cr25 (see the Table for chemical composition) has been chosen for operational rolling with the mill P1500. The specimens of the same chemistry have been prepared from a slab for laboratory rolling with the mill Tandem.

Slab with the cross-section dimensions of 750×120 mm has been rolled into the strip of 765×4 mm with the mill P1500. This slab has been heated for approximately 300 minutes at the temperature of 1180 °C. After heating and descaling a rolling process with ten passes follows. Relative strain $\varepsilon_h$ varied from 0.18 to 0.36 in particular passes. Temperature of deformation $t_{\mathrm{def}}$ dropped from 1070 °C to 870 °C. Coiling temperature was about 540 °C. The specimens for metallographical analyses have been taken from the finished strip.

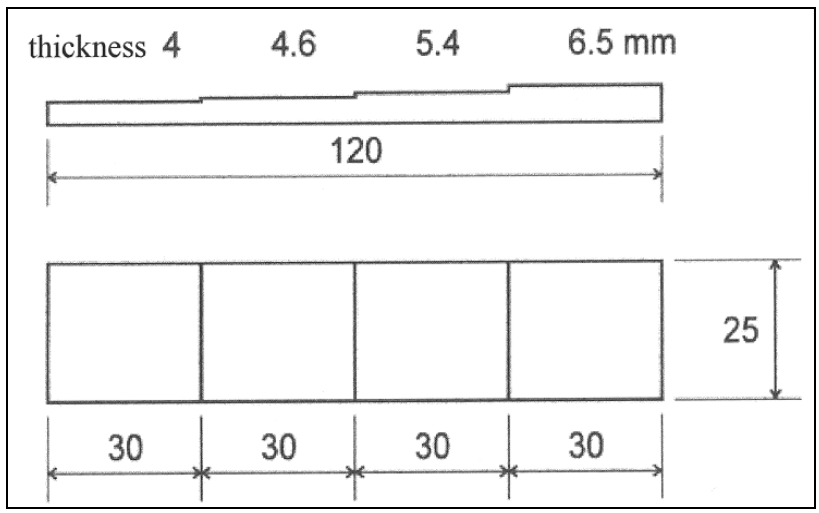


Fig. 5. Flat samples with graded thickness

The flat samples with graded thickness (see Figure 5) have been laboratory-rolled under various conditions. After heating at a uniform temperature of 1150 °C the samples have been rolled out by one pass to obtain a final thickness. The equivalent strain *e* varied within one specimen from 0.10 to 0.51. Deformation temperature ranges be-

tween 800 °C and 1100 °C. 0.5 s or 2 s after rolling the finished strips have been quenched in oil. Four specimens for metallographical analyses have been taken from each laboratory strip.

## 4. Discussion of results

Ferrite and carbides have formed the microstructure of industrial hot-rolled strips. The structure is markedly inhomogeneous which is evidenced by different size and shape of ferritic grains. Slightly deformed ferritic grains dominate in the surface. Thin layer (0.3–0.4 mm) with very fine-grained structure occurs just under the surface (see Figure 6). Strongly deformed and rough grains dominate in central parts of strip (see Figure 7). Small particles of carbide have been found on the boundaries of rough ferritic grains. All structural characteristics are more strongly marked in longitudinal than in transverse sections (see Figures 8 and 9).

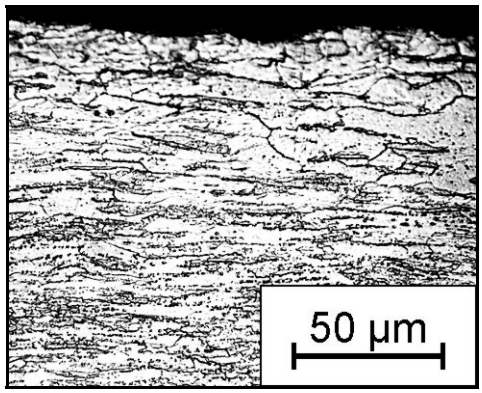


Fig. 6. Structure of hot-rolled strip in surface (longitudinal section)

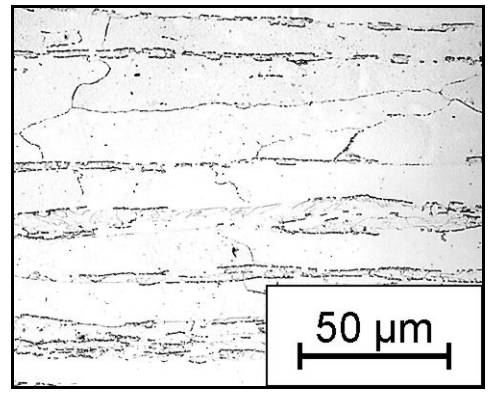


Fig. 7. Structure of hot-rolled strip in central parts (longitudinal section)

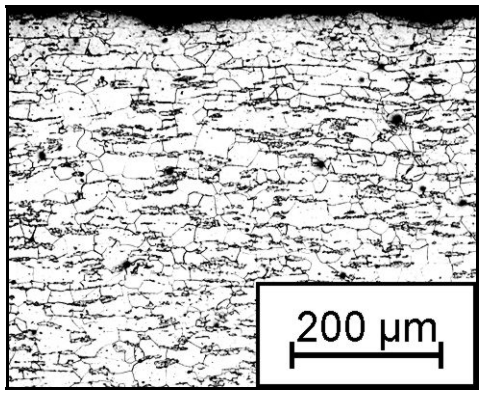


Fig. 8. Structure of hot-rolled strip in surface (transverse section)

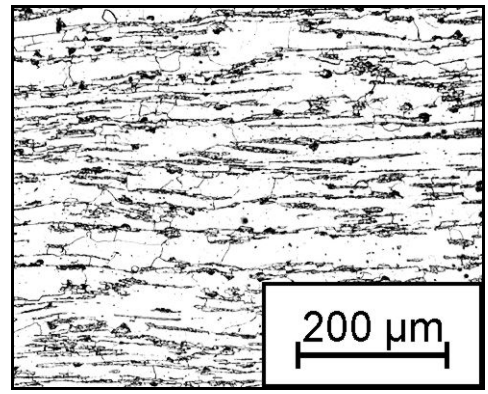


Fig. 9. Structure of hot-rolled strip in central parts (transverse section)

The grain size of final microstructure of hot-rolled sheets is very strongly influenced by total strain intensity. If the strip thickness approaches 2 mm, the final microstructure is very fine-grained (see Figure 10). If the strip thickness is about 5 mm and more, the final microstructure is coarse-grained (see Figure 11) and grain size is much greater than in thin strips.

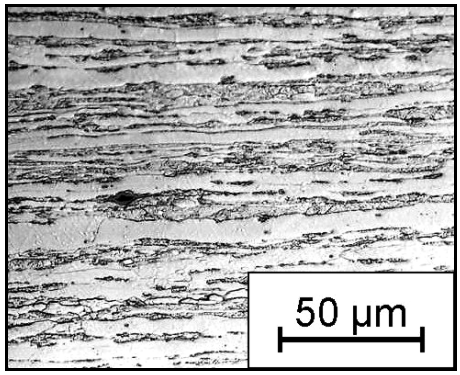


Fig. 10. Structure of central parts of hot-rolled strip with 2.2 mm thickness

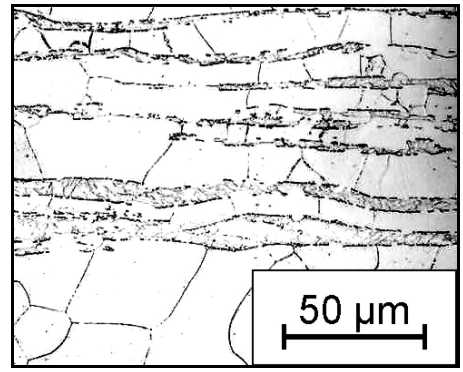


Fig. 11. Structure of central parts of hot-rolled strip with 5.7 mm thickness

Ferrite and carbides along the ferritic grain boundaries have formed the microstructure of the laboratory-rolled specimens. The dependence of grain size on the deformation temperature has not been surprisingly apparent and a final structure has been very coarse-grained (see Figures 12 and 13).

On the other hand, the dependence of grain shape on the strain has been evident (see Figures 14–17). It is very probable that status of final microstructure has been markedly influenced by structural heterogeneity of initial slab. Longer delaying after deformation before quenching has not had any influence on final structure of laboratory-rolled samples (see Figures 18 and 19).

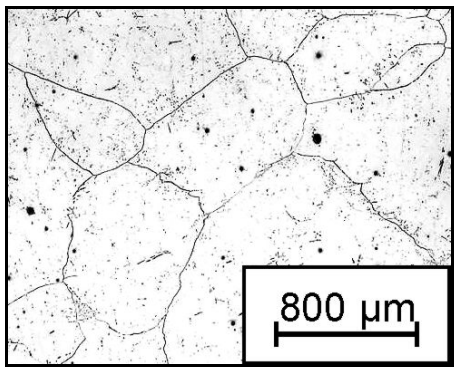


Fig. 12. Structure of laboratory-rolled sample ($e$ = 0.11, $t_{def}$ = 1100 °C)

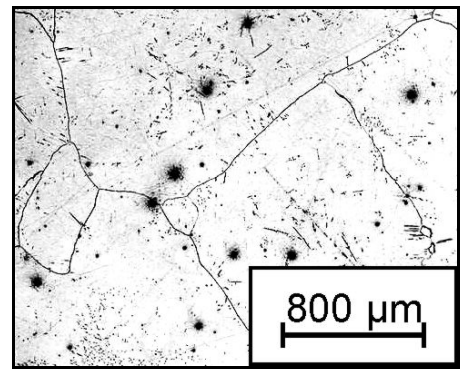


Fig. 13. Structure of laboratory-rolled sample ($e$ = 0.10, $t_{def}$ = 800 °C)

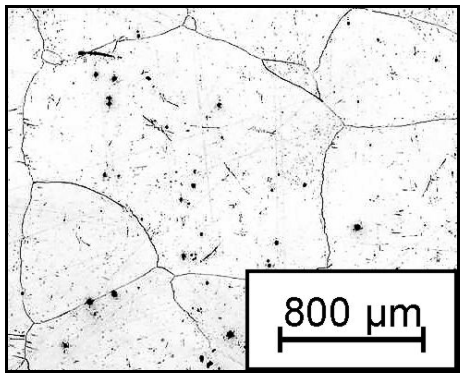


Fig. 14. Structure of laboratory-rolled sample ($e$ = 0.11, $t_{def}$ = 1000 °C)

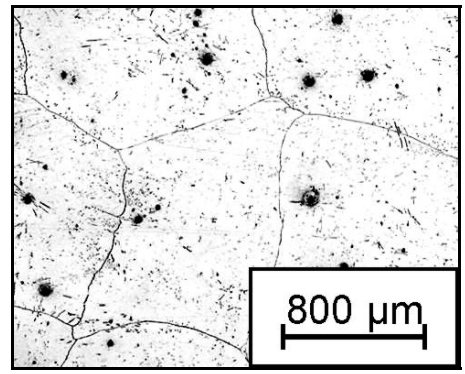


Fig. 15. Structure of laboratory-rolled sample ($e$ = 0.20, $t_{def}$ = 1000 °C)

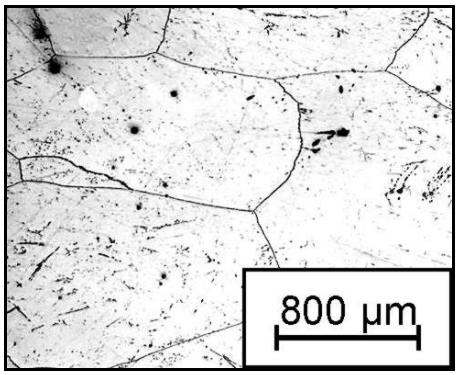


Fig. 16. Structure of laboratory-rolled sample ($e$ = 0.34, $t_{def}$ = 1000 °C)

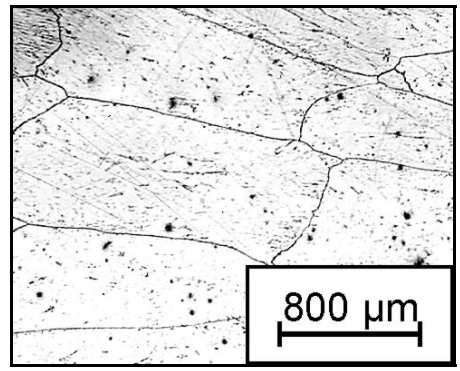


Fig. 17. Structure of laboratory-rolled sample ($e$ = 0.47, $t_{def}$ = 1000 °C)

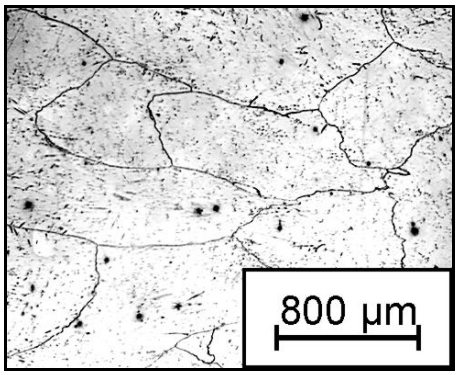


Fig. 18. Structure of laboratory-rolled sample ($e$ = 0.47, $t_{def}$ = 1100 °C, quenched in oil for 0.5 s

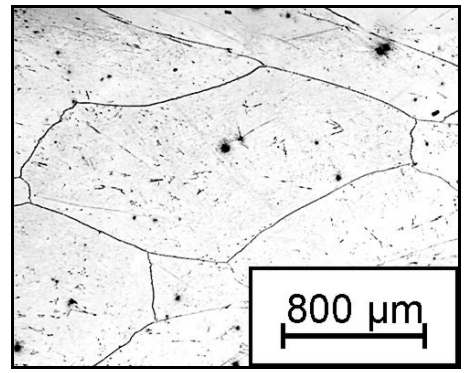


Fig. 19. Structure of laboratory-rolled sample ($e$ = 0.48, $t_{def}$ = 1100 °C, quenched in oil for 2 s

after deformation) after deformation)

Quantitative microstructure has been evaluated based on measuring the grain size in all directions. Twenty grains have been measured within one sample. The grain size measured has ranged from 0.3 mm up to 4.2 mm. Average value of $N_v$ (number of grains in 1 mm$^3$) has been 0.25 up to 0.67. The average grain size $G$ according to standard CSN 42 0462 thus has reached the value of –4. In agreement with calculated minimum and maximum values of $N_v$ the grain size $G$ has varied between 0 and –7. Nevertheless the value $N_{v\,\max}$ in all samples has reached similar size, but higher value of $N_{v\,\min}$ has been found in the samples rolled at higher temperature. This means that these samples consisted of higher number of fine grains originated by dynamic or metadynamic restoration. Dispersion of the results has been so considerable that the dependence of $N_{v\,\mathrm{avg}}$ on strain could not be definitely determined at any sample.

Mean elongation of grains, i.e. rate of their width to thickness and length to thickness, has been negatively influenced by heterogeneity of initial structure. Grain elongation in width direction (in cross-section) increases fairly uniformly with strain – from the value of about 1.1 at $e = 0.1$ up to the value of about 2.5 at $e > 0.6$. By contrast, grains have been elongated very unequally in the length direction (in longitudinal section). Dependence of grain elongation on strain has been quite indefinable. Elongation of grain has been calculated at $e > 0.6$ in the range from 2.3 up to 4.2 [13].

The expected dependence of grain elongation on the strain $e$ has been found at the deformation temperature of 800 °C only (see Figure 20). The increase in the grain elongation with the strain $e$ has been observed in all other samples, but this parameter has decreased relatively at the largest strain (see Figure 21). This fact indicates that some stretched grains have been broken into fine and more equiaxial formation.

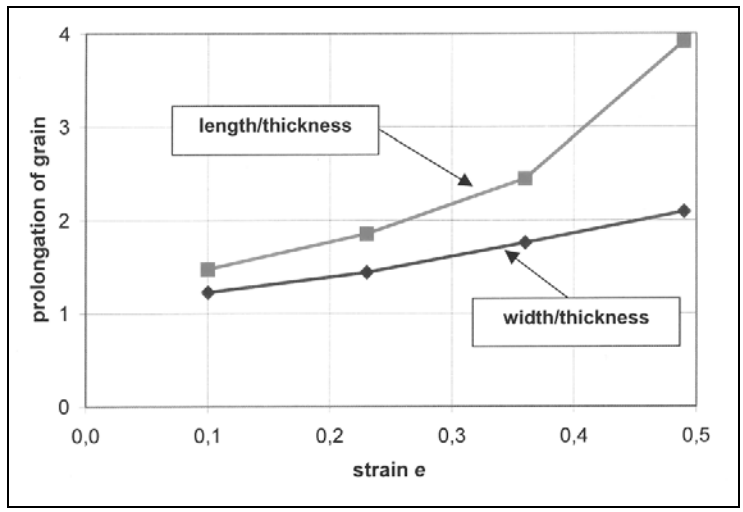


Fig. 20. Grain elongation versus strain

(deformation temperature $t_{def}$ = 800 °C)

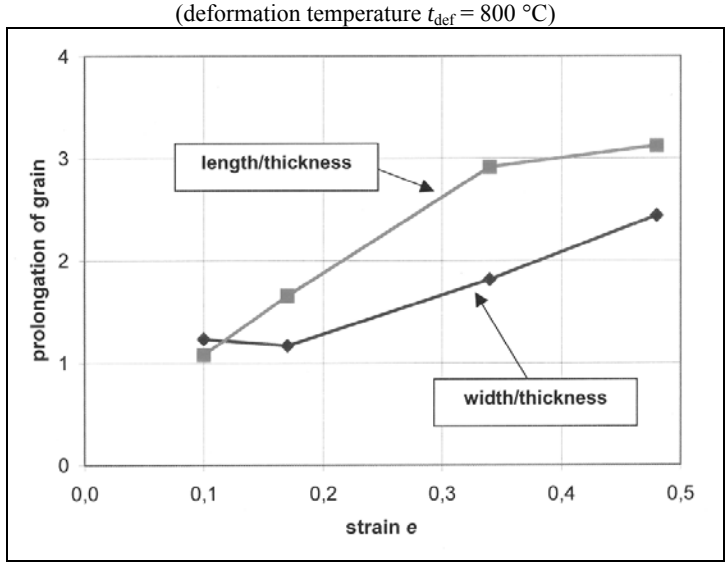


Fig. 21. Grain elongation versus strain
(deformation temperature $t_{def}$ = 1100 °C)

## 5. Summary

- Microstructure of industrial and also laboratory-rolled strips is found to be very heterogeneous. The grains larger than several millimeters are observed practically in all samples. Final microstructure is very markedly influenced by initial structure of rolled material.
- Because of a high chromium content it is very difficult to initiate complete recrystallization of deformed structure in a ferritic stainless steel under operational and laboratory conditions that simulate rolling process with the mill P1500. Static recrystallization is considerably inhibited and competes with polygonization that is considered to be a less effective structure-forming process.
- It is possible to decide whether dynamic recrystallization occurs under the conditions tested. On the other hand, it has to be stressed that it is extremely difficult to differentiate between recrystallization and recovery in the steel.
- Laboratory rolling mill Tandem appears to be a very suitable for modelling of rolling process with the mill P1500 and for a detailed research of recrystallization processes.

**Acknowledgements**

The research was financially supported by the Ministry of Trade and Business of the Czech Republic (grant project FD-K/032) and by the Grant Agency of the Czech Republic (grant project 106/01/0371).

**References**

[1] Chowaniec F. et al.: *Latest result from the production of peritectic steel grades in a medium–slab caster and a tandem Steckel mill at Nova Hut, Czech Republic*, VAI 8th Continuous Casting Conference, Linz, Austria, 2000.
[2] Cerny L.: *Hodnoceni vlastnosti tepleho pasu hlubokotaznych jakosti valcovanych na trati P1500* (final report of research project), Nova hut, Ostrava, 2001.
[3] Cerny L.: *Hodnoceni vlastnosti tepleho pasu jakostnich rad 34, 37 a 52 valcovanych na trati P1500* (final report of research project), Nova hut, Ostrava, 2001.
[4] Cerny L., Vavros P.: *Technologie valcovani tepleho pasu jakosti CSN 12071 na trati Steckel*, Ocelove pasy 2001, Spolecnost Ocelove pasy, Roznov pod Radhostem, 2001, pp. 137–142.
[5] Sykora P.: *Valcovani mikrolegovanych oceli na trati P1500* (final report of research project), Nova hut, Ostrava, 2002.
[6] Cerny L., Schindler I.: *Vliv teploty ohrevu a parametru ochlazovani na vyslednou mikrostrukturu za tepla valcovaneho pasu z hlubokotazne oceli*, FORM 2002, VUT Brno, Brno, 2002, pp. 109–114.
[7] Cerny L., Schindler I.: *Studium deformacniho chovani nizkouhlikove oceli pri finalnim dvoupruchodu na pasove trati Steckel za tepla*, 12th International Metallurgical Conference METAL 2003, TANGER Ostrava, Hradec nad Moravicí, 2003, paper No. 57.
[8] Schindler I. et al.: *Optimization of the hot flat rolling by its modelling at the laboratory mill Tandem*, 6th ICTP, Springer-Verlag, Berlin, Nürnberg, 1999, pp. 449–454.
[9] Schindler I. et al.: *Modelovani tvarecich procesu na laboratornich valcovacich tratach*, Hutnicke listy, 1999, Vol. 54, No. 7–8, pp. 79–85.
[10] www.fmmi.vsb.cz/model
[11] Schindler I. et al.: The 5th International *ESAFORM* Conference on Material Forming, Krakow, Akapit Krakow, 2002, pp. 387–390.
[12] Schindler I. et al.: The 10th International Metallurgical and Materials Conference *METAL 2001*, Ostrava, Tanger, 2001.
[13] Schindler I. et al.: *Studium deformacniho chovani a vyvoje struktury feritickych korozivzdornych oceli* (final report of contract for work), VSB – TU Ostrava, 2002.

**Określenie mikrostruktury walcowanej na gorąco cienkiej blachy z 25% zawartością chromu**

W warunkach laboratoryjnych oraz przemysłowych badano zmiany struktury podczas odkształcania na gorąco nierdzewnej stali ferrytycznej o zawartości 25% Cr. Do realizacji prób laboratoryjnych wykorzystano znajdujące się na wyposażeniu Instytutu Modelowania i Stero-

wania Procesami Przeróbki Plastycznej urządzenia: piec próżniowy do wytapiania, dwuklatkową walcarkę Tandem i elektryczne piece oporowe. Eksperymenty pokazały, że badana stal w stanie odlewanym oraz przerobionym plastycznie wykazuje znaczącą skłonność do rozrostu ziarna. Ta tendencja jest trudna do usunięcia, ponieważ duża zawartość chromu powoduje istotne hamowanie procesu rekrystalizacji w trakcie odkształcania na gorąco. Zostało to również potwierdzone podczas symulacji walcowania konwencjonalnego, w którym określono wpływ parametrów przeróbki plastycznej na końcową strukturę stali.

ARCHIVES OF CIVIL AND MECHANICAL ENGINEERING

Vol. IV 2004 No. 3

# The influence of plastic strain on twinning stress in Cu-8at.%Al single crystals

T. BAJOR, M.S. SZCZERBA
University of Mining and Metallurgy, Department of Structure and Mechanics of Solids, 30-059 Cracow, al. Mickiewicza 30/A2

Face-centred cubic (FCC) metals and alloys usually are deformed plastically by slip and twinning. Deformation twinning becomes especially important when FCC materials are subjected to large plastic deformations (e.g. rolling, drawing). The main aim of this paper is to emphasize the necessity of incorporating of this mode of plastic deformation into the model of mechanical properties of FCC metals and alloys subjected to large deformations. The paper gives an experimental evidence of the influence of plastic strain on the critical resolved shear stress for twinning and also some other experimental observations of plastic anisotropy of the deformed Cu-8at.%Al single crystals.

Keywords: *face-centred cubic crystals, mechanical twinning, twinning stress, large plastic deformations*

## 1. Introduction

Metals and alloys with FCC crystal lattice usually are deformed by slip, but at large strains and especially low temperature the mechanical twinning is also significantly involved. FCC mechanical twinning may occur when stresses in a crystal lattice are high enough, therefore this phenomenon can take place only if an appreciable amount of work hardening due to slip has to be already imposed on a material. According to one of the three necessary conditions of the criterion proposed by Szczerba et al. [1], the onset of twinning may take place in a particular twin system only when the resolved shear stress is higher than a minimum stress ($\tau_{RSS} > \tau_{MIN}$), and according to the dislocation theory [8], the minimum stress must be higher than $\gamma/b$ ($\gamma$ is the value of stacking fault energy, and $b$ is the Burgers vector of twinning dislocation). There were many attempts reported in the literature [2–7] to determine important structural factors influencing the twinning stress value. A series of semi-empirical equations trying to determine twinning stress was obtained, e.g. the following equation proposed by Haasen and King [4]:

$$\tau = \frac{1}{n'}\frac{\gamma}{b'} + Gb'\sqrt{N}\,, \tag{1}$$

where $\gamma$ is the value of stacking fault energy, $n'$ is the stress concentration factor connected with, for example, pile-ups of dislocation on the Lomer–Cottrell barriers, $G$ is an elastic shear modulus, $N$ is an average dislocation density, $b'$ is an length of twinning dislocation vector.

According to the Equation (1) the twinning stress is strongly dependent on the stacking fault energy $\gamma$ of a material as well as on its density of dislocations. If the dislocation density of a material is low, the first part of Equation (1) connected with $\gamma$ should control the shear stress value. On the other hand, it is well known that each cold working process, for instance rolling or drawing at room temperature, is usually associated with large plastic strains and hence with a significant increase in the material dislocation density $N$. Therefore, at large plastic deformations the second part of Equation (1) will become more important and will have a basic influence on the twinning stress value or other strengthening properties (e.g. microhardness) of a deformed material. Moreover, as a result of the mechanical twinning, the existing material dislocation substructure is transformed into a stronger configuration [9], which additionally increases the material strengthening. There is no doubt that mechanical twinning must be taken into account in modelling the processing technologies of metals and alloys which lead to the production of high-strength plastic materials. In order to model successfully the technological processes, it is important to know fundamental physics of the mechanical twinning that can be relatively easy observed in single crystals. Taking advantage of the investigations of Cu-8 at.%Al single crystals we aim at delivering the experimental evidence and the physical explanation of the effect of a plastic deformation on the critical twinning stress in FCC materials.

## 2. Experimental procedure

The samples of Cu-8 at.%Al single crystal were used in the investigation. The single crystals were grown from a seed in purified graphite moulds in a vertical temperature gradient furnace and in a vacuum better than $10^{-5}$ hPa. The shape of the samples was a rectangular prism with the dimensions: 3 mm × 30 mm × 150 mm. According to the (0 0 1) stereographic projection, the samples had primary crystallographic orientation such that tensile axis was parallel to the [–1 4 5] crystallographic direction, and the side surfaces (KN) and (KP) were parallel to the cross-slip plane (1 –1 1) and to the (–3 –2 1) plane, respectively (Figure 1).

The samples were deformed by tension at room temperature and the strain rate of $10^{-3}$ $s^{-1}$ using Instron 5566 tensile testing machine. The primary crystals, called further the ‘parent’ crystals, were deformed until the critical point appeared on the stress–strain curve (Figure 2), which was associated with a sudden tensile load drop, the appearance of the first twin lamella in the crystal sample and the audible acoustic emission.

The critical state of the ‘parent’ crystals is described by the tensile stress value and crystallographic orientation of the tensile axis (the crystallography of the deformed samples was taken after {111} pole figures’ X-ray measurements), which allowed us to calculate the resolved shear stresses acting in all possible slip or twin systems in a crystal lattice.

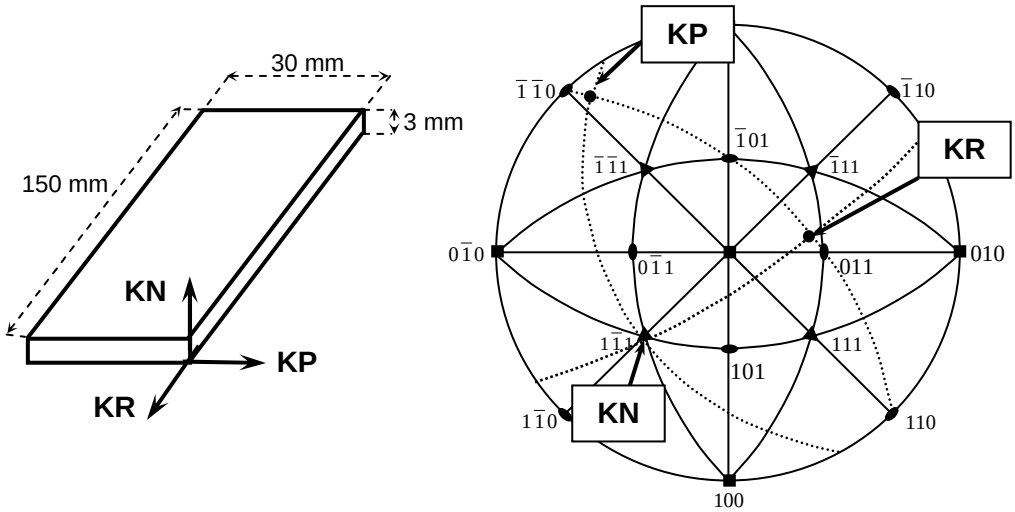


Fig. 1. Geometry of the primary single crystal samples (a) and their crystallography presented on the (0 0 1) stereographic projection (b)

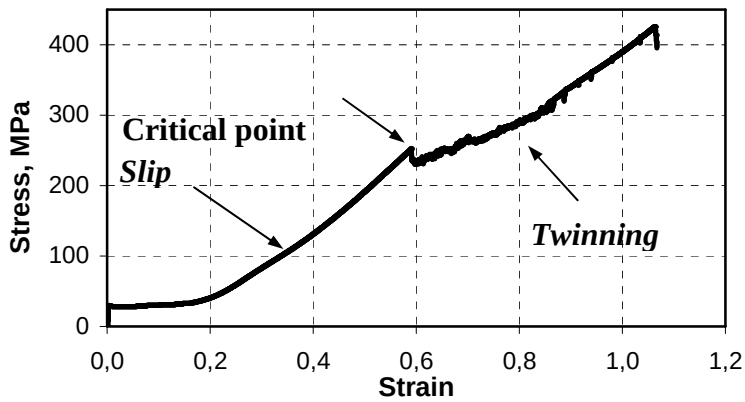


Fig. 2. The stress–strain curve of the Cu-8at.% Al single crystals with the [–1 4 5 ] tensile direction. The deformation stages of slip and twinning and the onset of mechanical twinning are shown by arrows

Then, the secondary samples ($T_1$, $T_2$) were cut out from the 'parent' crystals in various directions with respect to the to main axis $KR_D$ (Figure 3a). The secondary samples were cut out by means of the Dwell precise diamond wire saw, and then in order to remove any damage caused by cutting, they were mechanically and electro-chemically polished. The samples prepared in such a way were deformed again by tension along the new crystallographic directions ($T_1$, $T_2$), at room temperature and the strain rate of $10^{-3}$ $s^{-1}$. The secondary tensile directions specially chosen allow us to control the most stressed deformation system that is initiated during the secondary

test. So, the tensile direction $T_1$ favoured the C3 twin system, whereas the tensile direction $T_2$ – the BIV slip system (Figure 3b). The deformed secondary samples were subjected to structural and crystallographic observations in order to check which deformation system was really initiated during the secondary tension. Now, it was possible to find the critical resolved shear stresses of the C3 and BIV deformation systems. Since the samples $T_2$ do suffer during the secondary tension, it was possible to investigate the influence of the plastic strain on the critical twinning stress of the C3 twin system.

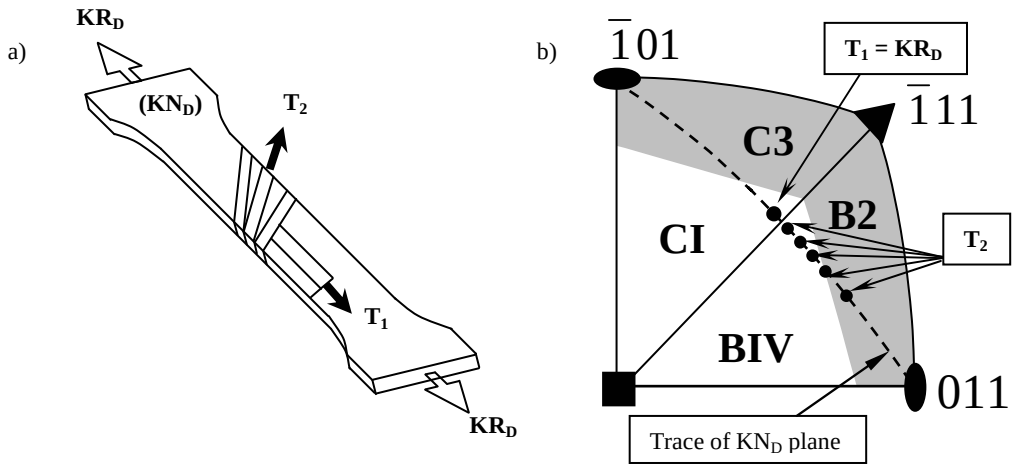


Fig. 3. Schematically drawn geometry (a) and the crystallography shown on the stereographic projection (b) of the 'parent' crystals' wide surface ($KN_D$) and the secondary tensile samples ($T_1$, $T_2$).

## 3. Experimental results and discussion

Two kinds of plastic response were observed during the deformation of secondary samples: (i) the samples with the tensile axis $T_1$ are deformed by mechanical twinning which originates in the C3 twin system (Figure 4a); (ii) the samples with the tensile axis $T_2$ start to deform in the BIV dominant system, and then after an appreciable amount of the deformation by slip they do continue the deformation by mechanical twinning, which originates again in the C3 twin system (Figure 4b). It is important to emphasize that in both cases of the onset of the C3 twin system the tensile axis takes the identical crystallographic orientation and that it was checked after the (111) pole figures X-ray measurements (see the inserts of the Figures 4a and 4b).

The second case of plastic response (Figure 4b) was systematically observed in order to check the influence of the angular distance of the axis $T_2$ from the $KR_D$ direction on the critical value of resolved shear stress of the C3 twin system, $\tau_{C3}$, and the results are collected in the Table. These results prove unambiguously that the structural changes, the increase in density of dislocations which is taking place during the incu-

bation period of crystal deformation by slip, can significantly affect the value of critical stress for twinning in FCC materials.

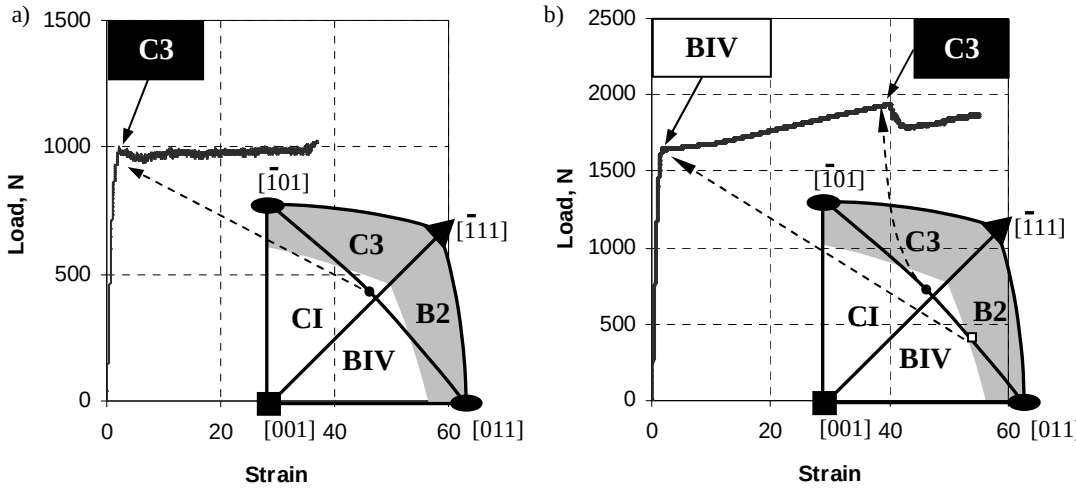


Fig. 4. Tensile stress–strain characteristics of the chosen secondary samples of the initial tensile orientation $T_1$ (a), and $T_2$ (b)

Table. Critical stresses of the C3 twin system as a function of the angular distance α of the orientation of the $T_2$ tensile axis of the secondary sample taken from the $KR_D$ direction

| $\alpha$ | $\tau_{C3}$ |
|---|---|
| 0º | 98.4 MPa |
| 3º | 103.3 MPa |
| 7º | 104.7 MPa |
| 10º | 119.4 MPa |
| 12º | 122.8 MPa |
| 15º | 129.0 MPa |
| 17º | 130.4 MPa |

Taking advantage of the results obtained, another experiment, involving the 'parent' –'child' – 'grandchild' sequence of the samples tested, has been performed (Figure 5) and the results of cumulative deformation characteristics are shown in Figure 6. The results show that in the 'grandchild' sample, cut from the secondary ('child') sample in the same way as the 'child' sample was cut out from the 'parent' crystal, the tensile stress of almost 0.5 GPa or, alternatively, the resolved shear stress of about 200 MPa is necessary to activate the C3 twin system. So, one can see that for a given material an initial crystal orientation and the deformation temperature, the twinning stress of the same twin system may differ by more than a factor of two. Moreover, it is not unreasonable to conclude that because the work hardening capacity

of the ‘grandchild’ sample was still not exhausted, the critical twinning stress is expected to be even higher than 200 MPa at room temperature.

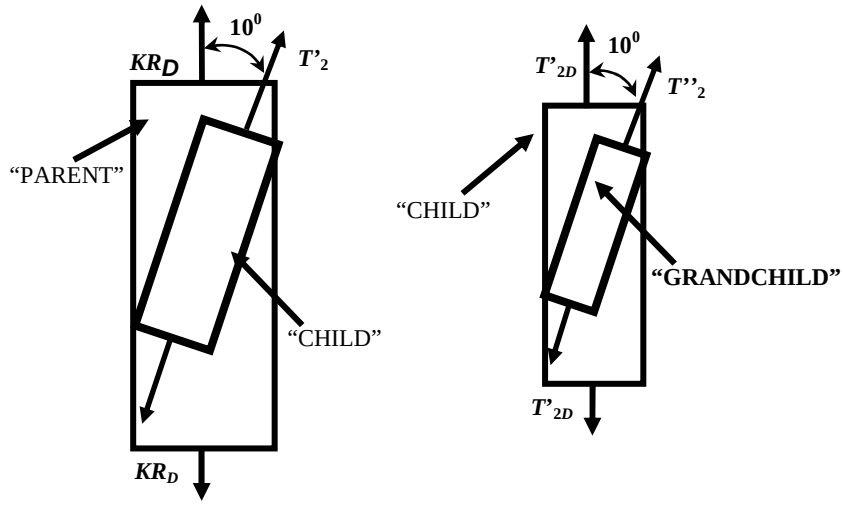


Fig. 5. Schematic illustration of the experimental procedure, which allowed us to obtain the cumulative stress–strain characteristics shown in Figure 6

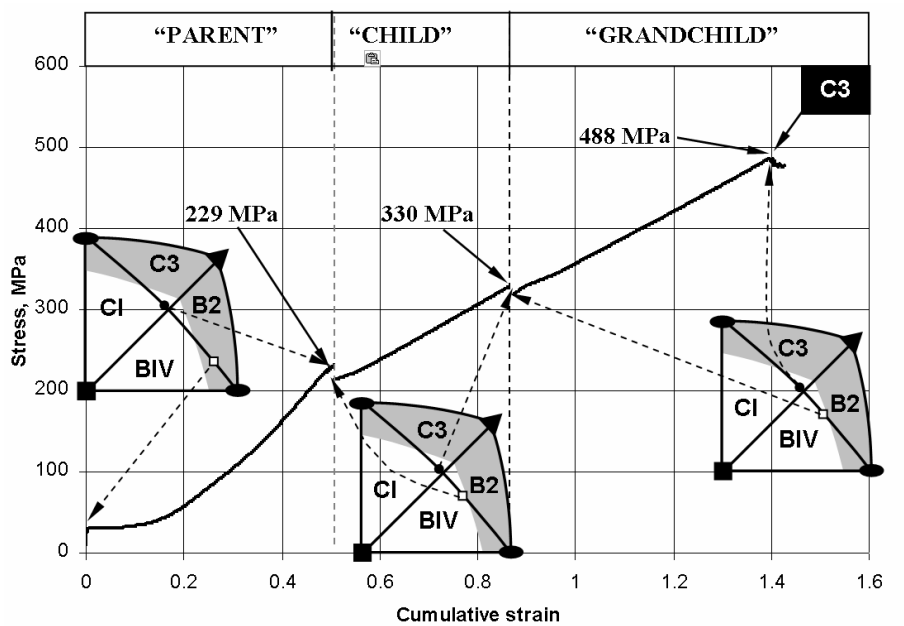


Fig. 6. Cumulative mechanical characteristics of the ‘parent’, ‘child’ and ‘grandchild’ samples, see comment in the text

## 4. Conclusions

As it was checked in the case of Cu-8at.%Al single crystals, twinning stress in FCC materials at room temperature may strongly depend on the amount of strain by slip during the incubation period (prior to the onset of mechanical twinning), or alternatively, on an average density of crystal dislocations. This effect should be especially important when a material is subjected to large plastic strains, and hence it is strictly necessary to take it into account in deformation codes that are incorporated into a modelling of technological processes of plastic forming of metals and alloys.

### References

[1] Szczerba M.S., Bajor T., Tokarski T.: *Is there a critical resolved shear stress for twinning in face centred cubic crystals?* Philosophical Magazine, in print.
[2] Cottrell A.H., Bilby B.A.: *A Mechanism for the Growth of Deformation Twins in Crystals*, Philosophical Magazine, Vol. 42 (1951), 573.
[3] Suzuki H., Barrett C.S.: *Deformation Twinning in Silver-Gold Alloys*, Acta Metallurgica, Vol. 6 (1958), 156.
[4] Haasen P., King A.: *Verfestigung und Stapelfeherenergie von Kupfer-Legierungskristallen*, Z. Metallkunde, Vol. 51 (1960), 722.
[5] Venables J.A.: *Deformation Twinning in Face-Centered Cubic Metals*, Philosophical Magazine, Vol. 6 (1961), 379.
[6] Venables J.A.: *The Nucleation and Propagation of Deformation Twins*, Journal of Physics and Chemistry of Solids, Vol. 25 (1964), 693.
[7] Thornton P.R., Mitchell T.E.: *Deformation Twinning in Alloys at Low Temperatures*, Philosophical Magazine, Vol. 6 (1961), 361.
[8] Hirth J.P., Lothe J.: *The Theory of Dislocations*, II edition, published by John Wiley, New York, 1982.
[9] Basinski Z.S., Szczerba M.S., Niewczas M., Embury J.D., Basinski S.J.: *The transformation of slip dislocations during twinning of copper-aluminium alloy crystals*, Revue de Métallurgie – Science et Génie des Matériaux, 1997, 1037.

**Acknowledgements**
This work was supported by the State Committee for Scientific Research of Poland under grant number 0782/T08/2002/22 and 11.11.180.255.

### Wpływ odkształcenia plastycznego na naprężenie bliźniakowania w monokryształach Cu-8at.%Al

W technologii przetwórstwa metali bardzo często dąży się do poprawienia własności wytrzymałościowych materiałów, w czym pomocny może stać się proces bliźniakowania. Wystąpienie zjawiska bliźniakowania jest bowiem związane z dużymi naprężeniami w sieci krystalicznej i dlatego zaczyna się ono dopiero po pewnym okresie odkształcenia plastycznego, wtedy

gdy substruktura dyslokacyjna wewnątrz materiału zostanie odpowiednio naprężona. Deformacja przez bliźniakowanie staje się szczególnie istotnym sposobem deformacji w obszarach dużych odkształceń plastycznych (np. walcowania, ciągnienia). Zatem aby poprawnie zamodelować proces technologiczny, należy wziąć pod uwagę działające mechanizmy deformacji w skali podstawowej, czyli uwzględnić zmiany zachodzące w pojedynczym ziarnie. Niniejsza praca, oparta na badaniach monokrystalicznego stopu Cu-8at.%Al, ma na celu wyjaśnienie przyczyn poprawienia własności wytrzymałościowych badanego materiału, który odkształca się plastycznie zarówno przez poślizg, jak i przez bliźniakowanie. Przeprowadzono, więc eksperyment z tak zwaną nieciągłą zmianą orientacji. Polegał on na tym, że wyjściowe monokryształy o określonej geometrii zostały odkształcone na etapie deformacji pierwotnej do punktu pojawienia się pierwszego pasma bliźniaczego. Następnie z tak przygotowanej próbki wycięto pod różnymi kątami względem głównej osi odkształconego kryształu wyjściowego próbki wtórne, uaktywniając za każdym razem inny główny system deformacji. Podczas deformacji próbek wtórnych zaobserwowano dwa sposoby ich odkształcania się: (i) bliźniakowanie oraz (ii) bliźniakowanie poprzedzone okresem inkubacyjnym deformacji przez poślizg. Przypadek drugi poddano systematycznym badaniom doświadczalnym, w wyniku których określono wpływ odchylenia kątowego osi próbek wtórnych od kierunku rozciągania odkształconego kryształu wyjściowego na wielkość naprężenia bliźniakowania w systemie bliźniakowania C3. Uzyskane wyniki pokazują jednoznacznie, że podczas oddalania się z osią rozciągania próbki wtórnej „dziecka” od osi próbki „matki” okres inkubacyjny deformacji kryształu przez poślizg wydłuża się, a wartość naprężenia krytycznego dla transformaty bliźniaczej C3 staje się w wyniku umocnienia odkształceniowego coraz wyższa. Takie zachowanie się próbek wtórnych skłoniło autorów do przeprowadzenia eksperymentu rozszerzonego o kolejny krok, czyli przygotowania z próbki wtórnej kolejnej próbki – „wnuka”. Otrzymane wyniki doświadczalne w pełni potwierdziły istotny wpływ odkształcenia plastycznego przez poślizg lub, alternatywnie, gęstości dyslokacji na wielkość krytycznego naprężenia bliźniakowania w materiałach RSC badanych w temperaturze otoczenia. Stwierdzono, że w badanych monokryształach Cu-8%at.Al naprężenie bliźniakowania może zmieniać się co najmniej dwukrotnie i osiągać wartość około 200 MPa, co koresponduje z wartością 0.5 GPa naprężenia rozciągania i wynika z istotnego wzrostu gęstości dyslokacji na etapie inkubacyjnego okresu odkształcenia przez poślizg. W pracy wskazano ponadto na konieczność uwzględnienia zjawiska bliźniakowania mechanicznego podczas modelowania procesów odkształcenia plastycznego materiałów RSC, szczególnie w obszarach dużych deformacji, a zatem w tych obszarach, które mają duże znaczenie w technologii przetwórstwa metali i stopów.

ARCHIVES OF CIVIL AND MECHANICAL ENGINEERING

Vol. IV 2004 No. 3

# Computer system of selecting blanks used for forming car body elements

A. PIELA, F. GROSMAN
Silesian University of Technology, Krasińskiego 8, 40-019 Katowice

In order to facilitate the selection of blanks for producing the specified type of drawpiece, a suitable computer database has been set up. In a proper selection of blanks, the analysis of drawing process based on the finite elements method is employed. Database contains a lot of information on advanced steel grades used for the production of drawing blanks such as: basic mechanical properties (including the drawability determined on the basis of technological tests and limit curve of forming), the description of structure, the characteristics of surface zone, essential data for simulation of forming process employing FEM, the process guidelines developed and the examples of practical application. Data-ordering structure has been created in order to gain an easy access to the stored information and thus the structure created has also enabled us to establish the computer base. The paper presents basic assumptions of the program design as well as the database related to it.

Keywords: *computer base, selection of blanks for drawing, car body elements*

## 1. Introduction

Currently manufactured car bodies are produced mainly from steel blanks. Deeply drawable blanks of higher strength are used for car body elements [1]. High standard requirements of car industry regarding drawability properties and strength resulted in developing several steel grades which can be used for producing drawing blanks and this, in turn, gives wide variety of material offer for car industry [2]. At present blank producers' offer exceed the accepted standards which define only a basic level of requirements. Furthermore, many types of blanks are produced according to individual car manufacturers' demands. A computer database program has been designed to facilitate the selection of the most suitable blanks for producing a specified type of drawpiece. The analysis of drawing process that is based on finite-elements method (FEM) has also been involved [3].

## 2. Database

Computer database has been developed to enable an appropriate selection of blanks for producing the required type of drawpiece. The database contains information about modern types of blanks used for production of drawing blanks. The following features have been taken into account: mechanical properties, including drawability defined on the basis of technological tests and limit forming curve, description of the structure,

characteristics of the surface area, essential data for simulating forming process using FEM, production guidelines and the examples of application [3, 4]. Easy access to the required information has been made possible by creating the structure of data subordinating which allowed us to make a computer database being well co-ordinated with the program of an immediate selection and presentation of data.

*Database* contains the following information about blanks, steel strips for cold working:

- thickness from 0.3 mm to 3.0 mm,
- width of 550 mm or more,
- non-coated, electrolytically coated, metallic hot-dip coated,
- low-carbon (including very low-carbon contents, i.e. < 0.002%) and of higher strength with
- additives of such elements as: silicon, manganese, phosphorus, sulphur, aluminium, niobium, boron, titanium, copper,
- those which feature:
  - low strength of yield point up to 200 MPa,
  - high strength of yield point from 200 up to 550 MPa,
  - extremely high strength of yield point above 550 MPa,
- hot rolled or cold rolled from the following types of steel:
  - soft low-carbon,
  - microalloyed,
  - interstitial free (IF),
  - rephosphorized,
  - ferric-martensitic (dual phase DP),
  - back hardenable (BH),
  - isotopic (IS),
  - transformation induced plasticity type (TRIP),
  - martensitic,
  - complex phase (CP),
- special materials, e.g. tailored blanks.

***Tailored blanks*** – database includes flat-rolled products such as blanks and wide strips, slit strips or belts obtained in the process of strip slitting.

***Application of the program*** – assisting the process of selecting appropriate tailored blanks used for forming a desired type of drawpiece or choosing corresponding tailor blanks as well as introducing a new type of tailored blanks so as to improve the quality of the final product. Information included in the database enables us to carry out both physical and virtual analyses of forming process.

***Characteristics of the blanks*** incorporates a set of information about such items as: mechanical properties with the emphasis put on drawability (with examples of limit forming curve), chemical constitution, pattern of structure, examples of application, data concerning friction specification in the process of forming blanks with particular

kind of coating, strain resistance of blanks being exposed to impact or flexibility for being tailored in the process of welding, laser welding [5] or soldering.

## 3. Description of the program

The database is the most essential part of the program. Group of steel and steel grade are the elements which identify the database. Any information which is an important item of the database is assigned to a given steel grade. Interactive display and direct visualisation of the results of actual searching are another qualities of the program. They enable us to make a direct initial estimation of searching results which in turn makes it possible to interfere if necessary and to choose data for further variant calculations by simulation of the forming process by means of the finite elements method. Features of models employed in the process, necessity of using the dynamic database, the use of graphic and chart functions as well as the need of easy access to searching required the application of object programing elements with background procedures.

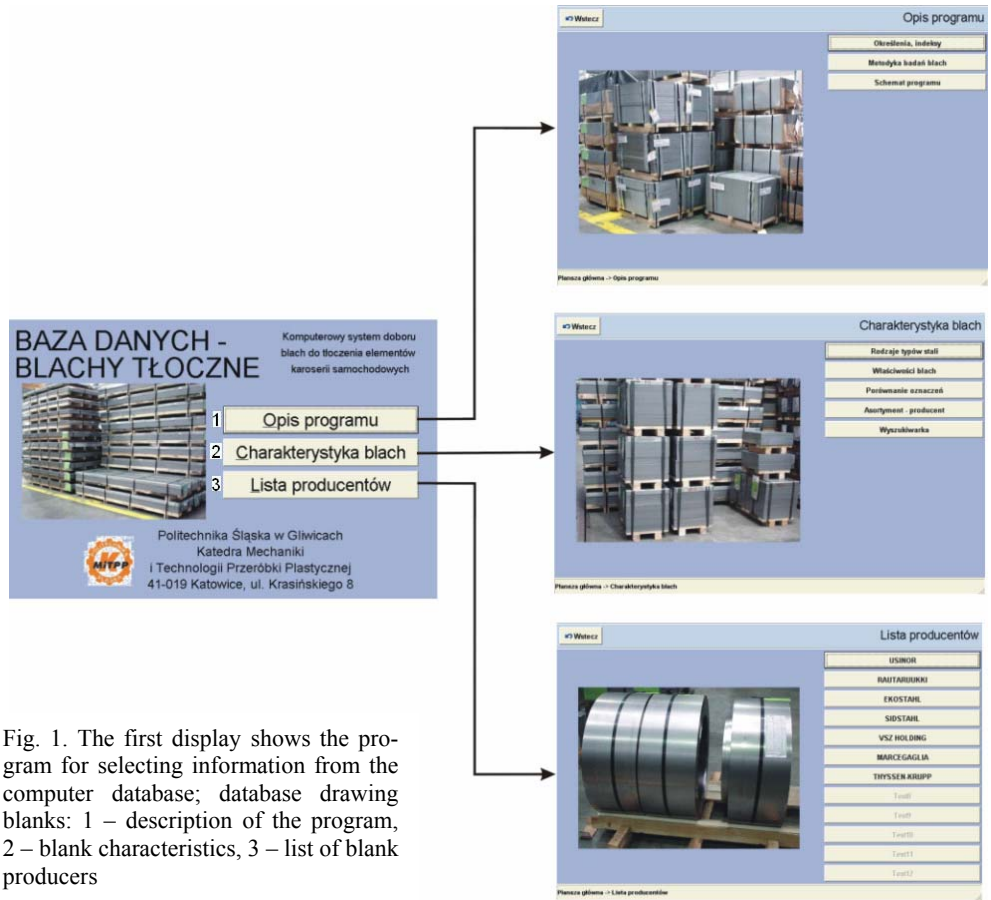


Fig. 1. The first display shows the program for selecting information from the computer database; database drawing blanks: 1 – description of the program, 2 – blank characteristics, 3 – list of blank producers

Figure 1 presents initial parts of display demonstrating the program which services the database. The first display allows the user, simply by pressing an appropriate key, to select the following information:

- explanation of how the program works,
- characteristics of the blanks,
- information about the producer or supplier of the blanks.

The program presented has been based on materials provided by representatives of the following companies: ACERALIA, EKO-ZINC, EKO-STHAL, INTER STHAL, MARCEGAGLIA, RAUTARUUKKI, SALZGITTER AG, SIDSTHAL, SCHMOLZ + BICKEN-BACH, THYSEN KRUPP STHAL AG, USINOR, VOEST-ALPINE, and VSZ HOLDING. They represent individual blank producers or galvanising shops as well as groups of producers. The database contains information on a wide variety of steel grades and mechanical properties of blanks of particular forming qualities together with information about blanks of high strength after the process of cold plastic strain. It also gives an overview of the quality of top coating. Blanks with coating which facilitates shaping in the process of forming have also been listed. They should be abrasion-resistant and strip-resistant with a specified macro- and microstructure.

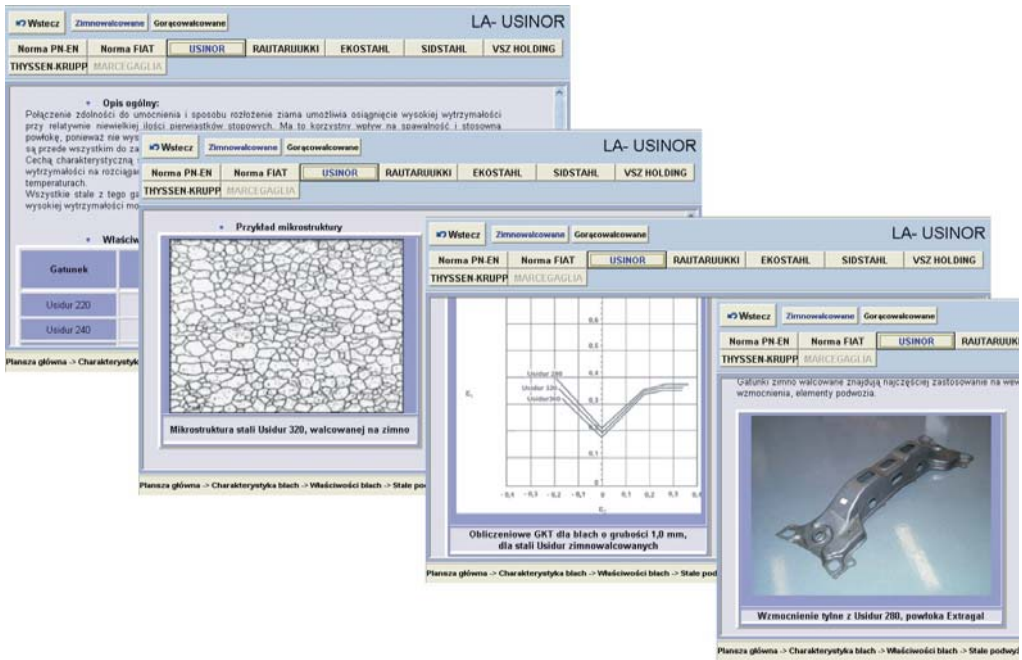


Fig. 2. Displayed examples of characteristics of blanks made of microalloyed steel of higher yield point

Some displays have been shown in Figure 2 as examples of microalloyed steel of a higher yield point with appropriate data regarding mechanical properties, structure and limit forming curve as well as some applications of such steel.

## 4. Summary

The offer of blanks used for car body elements is very wide. It contains blanks of different properties and various coatings. That is why choosing a suitable blank or making instant comparison of blank properties manufactured by different producers is difficult and time-consuming. Introducing the catalogues with characteristics of blanks produced by different manufacturers, information on suppliers and standards would not save much time, therefore the computer database prepared allows an easy access to the required information. There is also an explorer which makes it possible to get an easy access to any necessary information on the desired mechanical properties of the blanks. At the same time the structure of database enables adding or changing particular characteristics according to the current market offer of blank producers.

**Acknowledgement**

This work was supported by the State Committee for Scientific Research in Warsaw under the grant No. 10 T08 054 2000 C/5339. This support is gratefully acknowledged.

**References**

[1] Grosman F., Woźniak D.: *Postęp w technologii i produkcji blach dla motoryzacji*, Hutnik – Wiadomości Hutnicze, 2002, No. 5, 196.
[2] Grosman F.: *Nowoczesne stale na blachy tłoczne dla motoryzacji*, XV Conference – Design and Technology of Drawpieces and Die Stampings, 17–19 June, 2002, Poznań, 7.
[3] Piela A., Grosman F.: *Struktura komputerowej bazy, wspomagającej dobór blach do tłoczenia elementów karoserii samochodowych*, X Conference KomPlasTech 2003, Eds.: F. Grosman, A. Piela, J. Kusiak, M. Pietrzyk, „Akapit", Kraków, 185.
[4] Piela A., Grosman F.: *Współczesne metody wyznaczania kompleksowych charakterystyk technologicznej plastyczności blach do tłoczenia*, Hutnik – Wiadomości Hutnicze, 2002, Vol. 69, No. 5, 201.
[5] Piela A.: *Tłoczność wykrojów spawanych laserem*, Rudy i Metale Nieżelazne, 2001, Vol. 46, No. 11, 527.

**Komputerowy system doboru blach do tłoczenia elementów karoserii samochodowych**

Aby ułatwić dobór odpowiedniej blachy do wytwarzania określonego typu wytłoczki, w tym również przy użyciu analiz procesu tłoczenia metodą elementów skończonych, podjęto prace nad budową komputerowej bazy danych. W bazie tej zebrano szereg informacji dotyczących nowoczesnych gatunków stali stosowanych do produkcji blach tłocznych. Informacje te obejmują: podstawowe właściwości mechaniczne, w tym tłoczność określoną na podstawie prób technologicznych oraz granicznej krzywej tłoczenia, opis struktury, charakterystykę war-

stwy wierzchniej, dane niezbędne do symulacji procesu kształtowania MES, wytyczne przetwórstwa oraz przykłady zastosowania. W celu łatwego i szybkiego wyszukiwania informacji opracowano strukturę porządkowania danych, która umożliwiła opracowanie bazy komputerowej. Przedstawiono też podstawowe założenia budowy programu oraz współpracującej z nim bazy danych.

ARCHIVES OF CIVIL AND MECHANICAL ENGINEERING

Vol. IV 2004 No. 3

# Method of evaluating drawability of laser-welded tailored blanks

J. LISOK, A. PIELA
Silesian University of Technology, Krasińskiego 8, 40-019 Katowice

Methods of examining drawability which allow us to evaluate the flexibility of steel sheets for body-making processing have been presented. Basic mechanical examinations and technological simulation tests reveal that the weld influences the changes in the deformation scheme which together with different thickness of component blanks and their properties result in the changes of the stability loss which leads to drawpiece cracking. Our experience enables us to foresee the behaviour of tailored blanks in the process of forming the elements for car bodies which is associated with typical deformation schemes. Thus in order to verify the stamping process of tailored blanks, a computer simulation was used.

Keywords: *sheet-metal working, plastic processing, material model, laser-welded blanks, drawability*

## 1. Introduction

There are many advantages of using the laser-welded tailored blanks for forming car-body elements. The most significant of them can be itemized as follows: reduction of a car weight, reduction of the number of both drawpieces and tailored blanks which improve a car quality. The laser-welded tailored blanks can be used in the drawing process, provided that right solutions to numerous technological problems are found. In order to draw non-homogeneous tailored blanks, we have to develop the methods of evaluating their drawability which is essential for setting up the properties of laser-welded tailored blanks during the process of forming.

Laser-welded blanks flow in different mode due to the relationship between various thickness and strength of welded strips and the properties of the weld [1–5]. Thus, the same kind of tests as those carried out for homogeneous steel sheets ought to be conducted to assess the drawability of laser-welded tailored blanks, but a diversified flow of the actual tailored blank needs to be evaluated on the basis of these characteristics and numerical simulation of the drawing process [6–10].

In general, the research deals with such issues as: the way of evaluating plastic characteristics of any laser-welded pass and determining the parameters which allow us to analyze (applying numerical methods) the mode of flow of that kind of tailored blanks. In this way, process engineers at a stamping press can design the drawing process of tailored blanks more effectively, since high heterogeneity of mechanical properties and diversification of geometry are the biggest drawbacks of the process.

## 2. Methods of examination

Research on the development of welding and forming technologies [9–12] have revealed that the influence of a weld upon the process of plastic flow of the pass in the zone of joining can be examined using the same kind of tests as those used for evaluating the drawability of homogeneous sheets. However, the tools for drawability tests applied in technological trials appeared not to be suitable enough for trials on tailored blanks which are of different thickness. Therefore a series of experiments allowing evaluation of drawability of laser-welded tailored blanks has been performed. In such experiments, the thickness of steel sheets is not of particular importance. A detailed analysis carried out proved that such characteristics as those obtained in tensile tests of welded strips and the weld itself can only be appropriate for preparing preliminary classification of laser-welded tailored blanks. Thus it is of great importance to examine all the welds, taking into account different ways of joining steel sheets in a given tailored blank so that full assessment of drawability of laser-welded tailored blanks can be made. The examinations should include:

- technological tests, e.g. cup drawing test, cupping (Swift's method); KWI, hydraulic bulging and bending tests,
- evaluation of microstructure of the welded zone,
- measurements of microhardness distribution alongside the weld.

In the case of tailored blank shown in Figure 1, it was necessary to evaluate drawability of three welds which joined blanks A–B, B–C, C–D, C–D (Figure 2). Appropriate washers made of steel sheet, which would level the differences in thickness of tailored blanks, had to be used in technological trials.

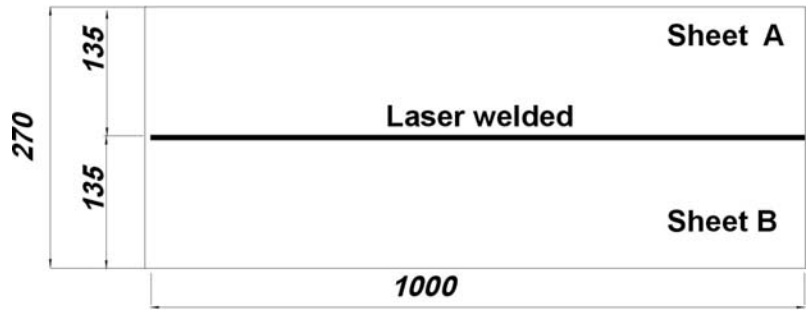


Fig. 1. Examples of joining sheet strips: A–B

Figure 3 presents the chart of the distribution of samples in a strip of laser-welded tailored blank. It was difficult to fix the samples (the samples were from laser-welded tailored blanks of different thickness, with the weld positioned in accordance with the direction of stretching) inside flat jaws of a tensile testing machine, therefore a special kind of fixture with a hole for blocking out the sample was used.

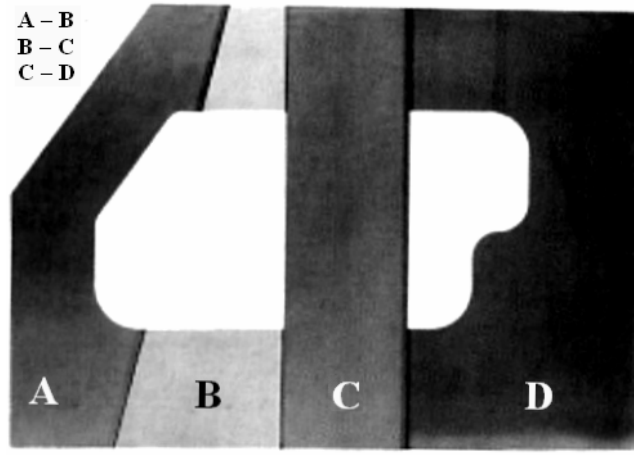


Fig. 2. Laser-welded tailored blank composed of sheet strips of A–B–C–D type

a)

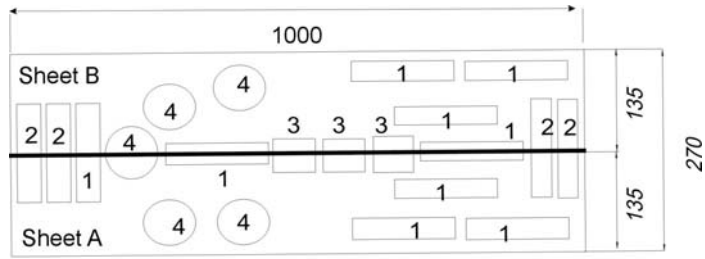


b)

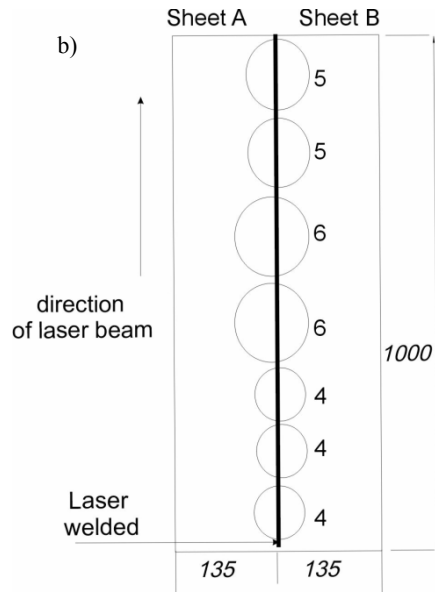


Fig. 3. Pattern of taking samples from the exemplary strip. Tests notation: 1 – tensile test, 2 – bending test, 3 – cup drawing test, 4 – cupping (Swift's method), 5 – KWI test – bugle forming of the hole, 6 – hydraulic bulging

Photographs of a fixture with a model sample have been shown in Figure 4. All the suggested mechanical properties of the sample as well as the parameters of its work-hardening curve (flow curve) which are essential for designing a material model of welded zone used for the simulation of laser-welded tailored blanks forming process, applying the finite elements method (FEM), have been determined as well [6–8].

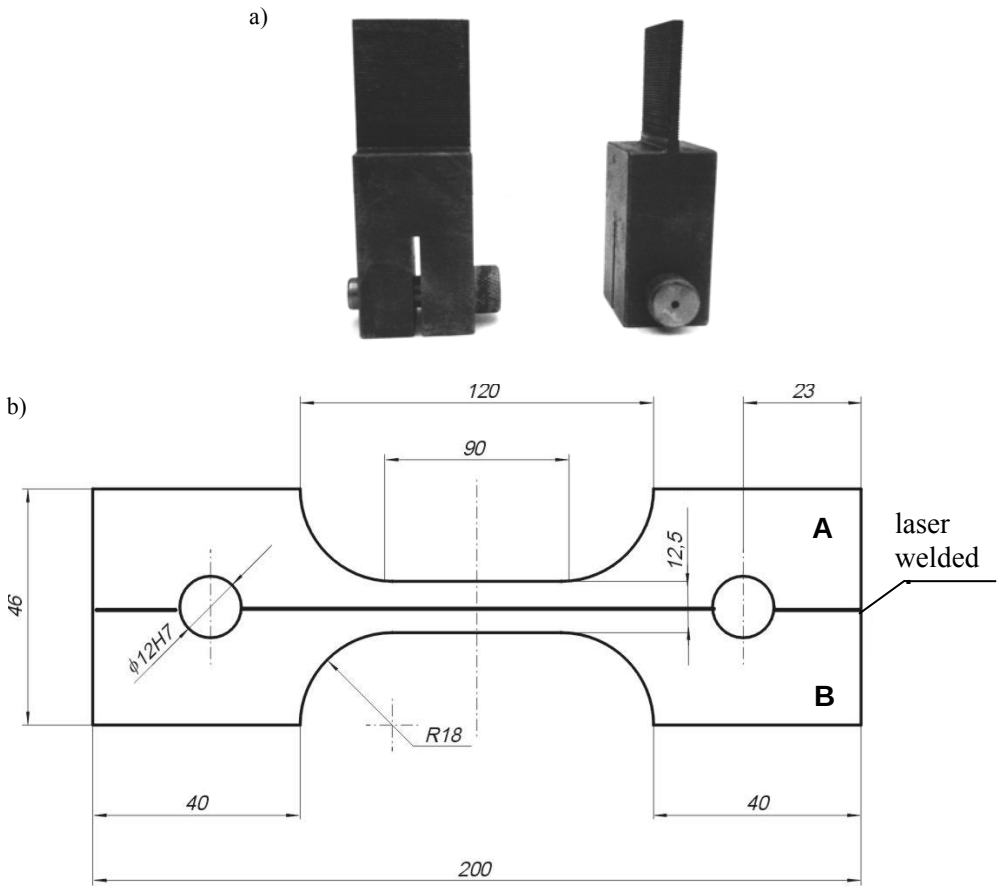


Fig. 4. Photograph of the fixture (a) and diameters of the sample with the hole, (b) the sample was cut out from a laser-welded tailored blank used in tensile test

Method of evaluating the drawability of laser-welded tailored blanks used for analyzing an actual process of forming has been presented. It seems to be quite satisfactory and evidences that introducing laser-welded tailored blanks instead of conventional steel sheets which have been previously used is far more advantageous. The presented example of a center pillar in Audi A3 (Figure 5) illustrates it best because the location of the weld and the type of tailored blanks have been selected on the basis of examination results.

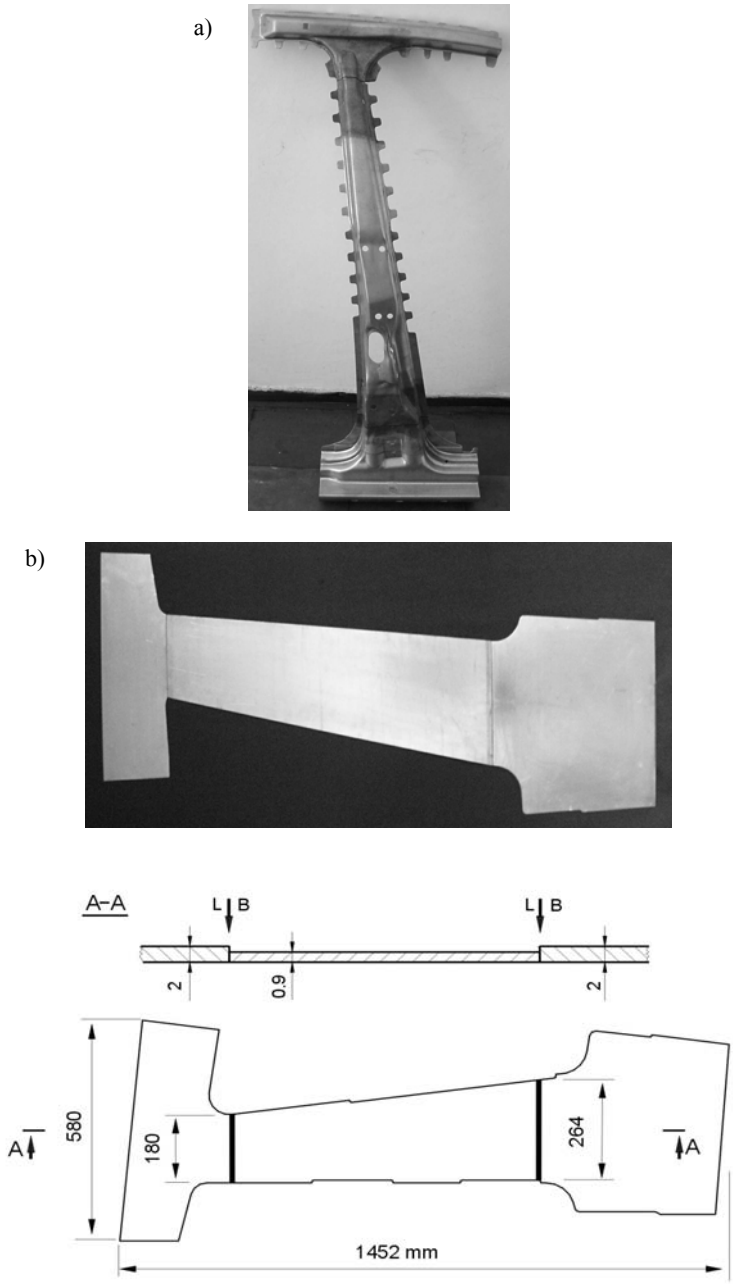


Fig. 5. Welded pass of laser-welded tailored blank: (a) the picture of the final form of a drawpiece-center pillar in Audi A3, (b) after the process of forming

## 3. Summary

This, in turn, allowed us to produce the drawpieces of a high quality which improved the strength of car's door step and drip moulding areas. It was also possible to determine the parameters of material model of a welded zone. Such a model is indispensable in forming industrial drawpiece applying finite elements method. The results of examining this subject have been presented in papers [8–13].

### Experimental study and numerical simulation of tailor-welded blanks

### Uniaxial tension tests

In order to assess forming behaviour of tailor-welded blanks under tension and influence of weld orientation, the uniaxial tension tests have been conducted for welded specimens with the weld line oriented at different angles with respect to the direction of load. The specimens were cut from a tailor-welded blank made from the same material. Thus the influence of weld hardening could be observed better.

Typically fractured specimens with different orientation of weld line are shown in Figure 6 together with a homogenous specimen (without weld). Generally, a weld is characterised by higher strength and lower plasticity in comparison to base material. Hence, the weld influences the strain distribution in tailor-welded specimens. This phenomenon depends strongly on the direction of the weld against the direction of tensile load. The lowest strains occur in the specimen with a longitudinal weld.

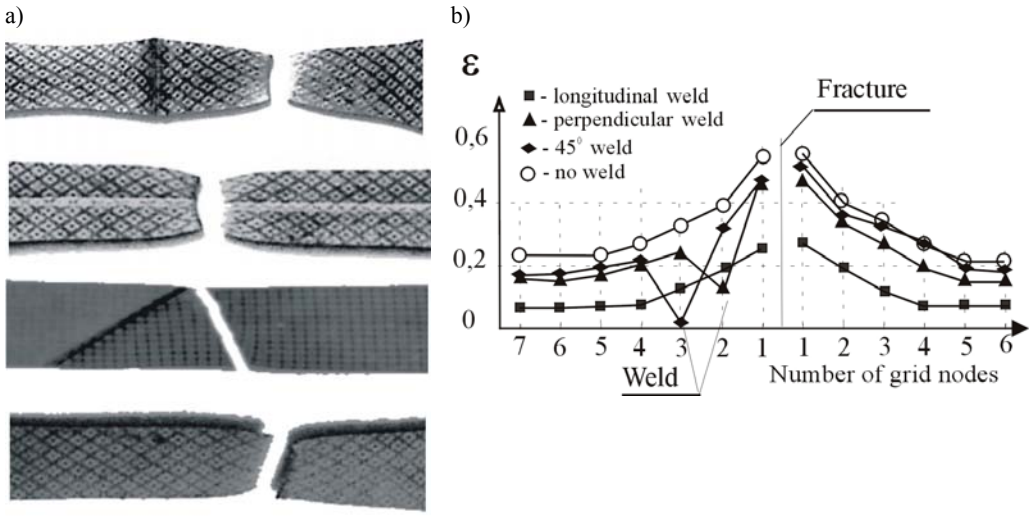


Fig. 6. Tension test – fractured specimens with different orientation of weld line (a), the results of tension tests – distribution of local strains along load direction (b)

## The Erichsen test

The Erichsen test has been carried out for a tailor-welded blank made from base sheet components of steel ST12.03 of different thickness (0.7 mm and 1.2 mm). Fracture of the material occurred in a thinner base material along the line parallel to the weld line which is shown in Figure 7. This result confirms that in the case of the base sheet components of different strength, the strain can be close to the weld line in a weaker base material. Figure 7 also presents characteristic movement of the weld line towards a stronger material.

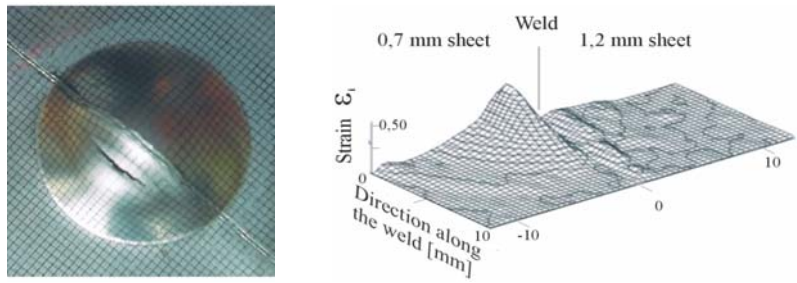


Fig. 7. The Erichsen test – fractured tailor-welded blank and local strain distribution

## Deep drawing of a cylindrical cup

Deep drawing of a cylindrical cup from homogeneous and tailored blanks was done in order to observe the influence of the hardening of the weld on the material flow and to study the flow of the material of the tailor-welded blanks made from similar and different base sheet components. Punch diameter was 50 mm and initial blank diameters were 100 mm.

Figure 8a shows a cup drawn from the tailor-welded blanks made from the same base material. It clearly demonstrates a reduced elongation of the material along the weld. Figure 8b shows view of the cup drawn from the tailor-welded blank made from material of different thickness, i.e. 0.8 and 1.2 mm. Significant movement of the weld line towards a thicker side can be seen.

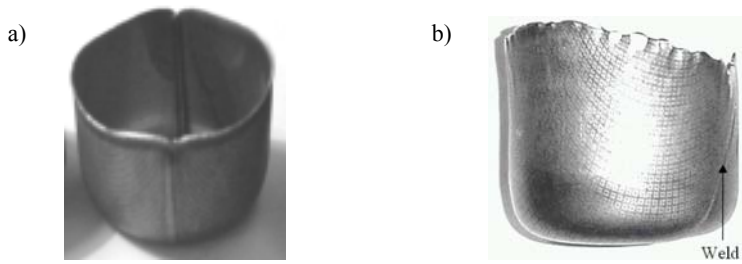


Fig. 8. Cylindrical cups drawn from tailor-welded blanks: a) 1.2 mm + 1.2 mm, b) 0.8 mm + 1.2 mm

## Numerical model of tailor-welded blanks

Experimental results show that the forming properties of tailor-welded blanks differ considerably from those of homogeneous blanks. Material of the weld joint and heat-affected zone hardens during welding (Figure 9). Numerical model should be capable of reproducing a restraining action of the weld. Experiments on tailored blanks led to the presentation a physical model of the joint, in which three material zones are represented: weld area, heat-affected zone and base material [11, 12]. It can be assumed that material behaviour of the weld and heat-affected zone can be described by elastoplastic constitutive model with isotropic hardening given by the power law:

$$\sigma = K(a + \varepsilon_p)^n, \tag{1}$$

where $K$, $a$ and $n$ are the material constants, and $p$ is the effective plastic deformation.

Since tension tests for the material of welded zone are practically impossible, it is assumed that the parameters of hardening law for the weld zone can be determined indirectly by means of microhardness measurements of the weld zone and base materials, cf. [13]. Assuming a direct proportionality of the material yield stress $\sigma_Y$ to its microhardness $\mu HV$ (cf. [12]), the yield stress of the weld area is given by

$$\sigma_Y^{\text{weld}} = \sigma_Y^{\text{sheet}} \frac{\mu HV^{\text{ weld}}}{\mu HV^{\text{ sheet}}}. \tag{2}$$

Geometry of the zones representing the weld area can also be determined by microhardness measurements (Figure 9). It can be assumed approximately that the width of a zone representing the weld bead and two heat-affected zones is equal to an average thickness of the joined sheets.

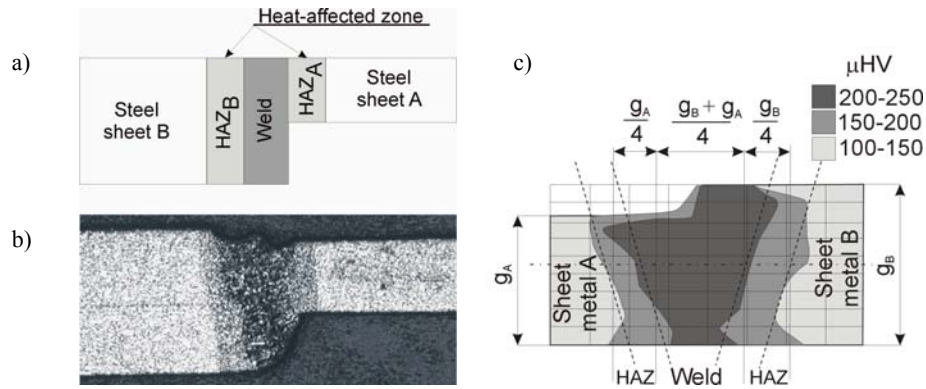


Fig. 9. Five-zone model of tailored blank (heat-affected zone – HAZ) (a); microphotograph of a weld zone (b); microhardness distribution in the weld zone (c)

## Model of the parent material

Numerical models of tailor-welded blanks have been implemented in the explicit dynamic finite element code, cf. [5, 11–13]. Parent material discretized with best elements is treated as an elastoplastic material with normal anisotropy in plasticity governed by the Hill 48 yield criterion [9]

$$\sigma_{11}^2 + \sigma_{22}^2 - \frac{2r}{1+r}\sigma_{11}\sigma_{22} + \frac{2(1+r)}{1+r}\sigma_{12}^2 = \sigma^2 , \tag{3}$$

where: $\sigma_{11}$, $\sigma_{12}$, $\sigma_{22}$ are the Cauchy stress tensor components, $\sigma$ is the equivalent yield stress, $r$ – average Lankford coefficient. Stress–strain relationship has been assumed according to the power law represented by Equation (1).

## Uniaxial tension tests – numerical simulation

Simulation of uniaxial tension tests being described in section 2.1 has been carried out for specimens with the weld orientation of 45º and 90º to the loading direction. The specimens were cut from a tailor-welded blank made from the same material, steel ST12.03, 1.0 mm thick. Two different models of bead (shell and beam) were used. Both models allowed us to obtain similar results. The results of simulation for the beam model of the weld are presented in Figure 10, where the blocking effect of the weld on the material deformation can be seen. Numerical results can be compared with the experimental results presented in Figure 1.

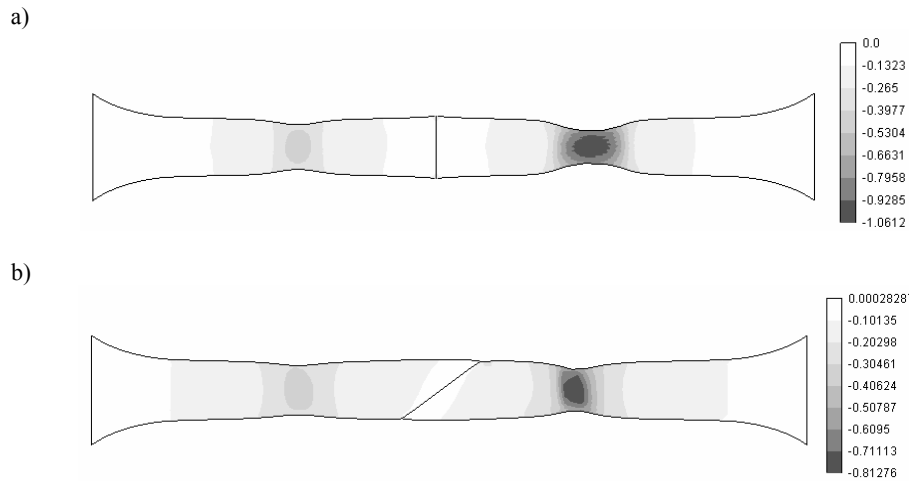


Fig. 10. Simulation of a tension test – weld line orientation of:
a) 90° to the loading direction, b) 45° to the loading direction

**Numerical simulation of deep drawing of tailor-welded blanks**

Calculations were done for the test of deep drawing of a cylindrical cup tested (section 2.3). The cases of the tailored blanks of initial diameter of 100 mm made from the same base materials (steel DC04, 1.2 mm thick) and from different base materials (steel DC04, 1 mm and steel DX54D+Z, 1.5 mm thick) were analysed. The weld and heat-affected zone were modelled by beam elements.

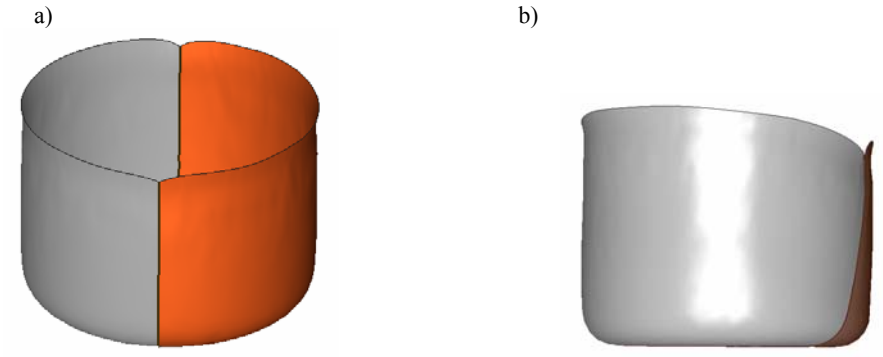


Fig. 11. Numerical shapes of cylindrical cups drawn from the tailored-welded blank: a) made from the same base materials, b) made from different base materials

Figure 11a presents simulation results for the tailor-welded blank made from the same base materials. The final shape obtained in the numerical analysis corresponds closely to the shape of a real drawpiece (Figure 11a). A reduced deformation along the weld line can be observed. A numerical shape of a cup drawn from the tailor-welded blank made from different base materials is shown in Figure 6b. Here the restrained action of the weld along its length is reproduced in the simulation together with its movement towards the thicker component sheet. Simulation reproduces correctly the experimental results (Figure 11b).

## 4. Concluding remarks

Flow of tailor-welded blanks in a process of deep drawing is considerably different from the flow of homogeneous blanks. In the case of tailor-welded blanks, reduced elongation along the weld line is observed. Another effect present in drawing of tailor-welded blanks made from the base materials of different strength or thickness is a movement of the weld line towards the material of greater strength or thickness. In order to obtain correct results, it is important to take into account different mechanical properties of the weld zone in numerical modelling of tailor-welded blanks. Therefore a physical model of the weld zone has been proposed here with mechanical properties of the weld- and heat-affected zones identified using microhardness measurements.

A numerical model of tailor-welded blanks was implemented in the FEM program. Various finite-element discretization methods for the two models were considered. Beam/shell model taking into account the deformation of the weld along the weld line is computationally effective and adequate for practical engineering use. The results of numerical simulation are in a good agreement with experimental results of deep drawing of tailor-welded blanks.

**Acknowledgement**

This work was supported by the State Committee for Scientific Research in Warsaw under the grant No. 4 T08C 011 23. This support is gratefully acknowledged.

**References**

[1] Piela A.: *Tłoczność wykrojów spawanych laserem*, Rudy i Metale Nieżelazne, Vol. 46, 11 (2001), 527–532.
[2] Piela A., Grosman F.: *Współczesne metody oceny technologicznej plastyczności wsadów stosowanych do tłoczenia elementów karoserii samochodowych*, Obróbka Plastyczna Metali, Vol. 13, 4, (2002), 17–26.
[3] Lisok J.: *Tailored Blanks*, Conf. Proc. Junior-Euromat 2000, Switzerland, Lousanne, 28.08.2000–01.09.2000, 334.
[4] Piela A., Hyrcza M., Lisok J.: *Wsady do tłoczenia spawane laserem*, Przegląd Mechaniczny, 4 (2001), 19.
[5] Piela A., Kocańda A., Zimniak Z.: *FEM simulation of drawing of tailored blanks*, Numiform 2001, The 7th International Conference on Numerical Methods in Industrial Forming Processes, 18–21.06.2001, Toyohashi, Japan, 795–800.
[6] Piela A.: *Analiza płynięcia blachy w procesie tłoczenia niejednorodnych wykrojów wsadowych typu Tailored Blanks*, XIII Konferencja Sprawozdawcza Komitetu Metalurgii PAN, Metalurgia 2002, Krynica, 17–20.04.2002.
[7] Piela A.: *Nowe materiały do tłoczenia – Tailored blanks*, XIV Konferencja Naukowo-Techniczna Obróbki Plastycznej nt. Konstrukcja i Technologia Wytłoczek i Wyprasek, Poznań – Czerniejewo, 14–16.06.2000, 87–94.
[8] Pilarczyk J., Piela A., Banasik M.: *Wykroje blach „tailored blanks" spawane laserem*, Przegląd Spawalnictwa, 6 (2003), 1–4.
[9] Lisok J., Piela A.: *Model złącza spawanego we wsadach do tłoczenia blach „tailored blanks"*, Przegląd Spawalnictwa 6 (2003), 5–9.
[10] Piela A., Lisok J.: *Modelowanie procesu tłoczenia blach łączonych laserem*, Informatyka w Technologii Materiałów, Wydawnictwa AKAPIT, Vol 1, 3–4 (2001), 166–180.
[11] Rojek J., Piela A., Lisok J.: *Numerical simulation of tailor welded blanks*, The 15th International Conference on Computer Methods in Mechanics CMM-2003, Gliwice-Wisła, 3–6.06.2003, 305.
[12] Piela A., Lisok J., Rojek J.: *Experimental study and numerical simulation of tailor welded blanks*, International Conference on Advanced Materials & Processing Technologies AMPT 2003, 8-11.07.2003, Dublin City University, Ireland.

[13] Piela A., Rojek J.: *Weryfikacja wyników numerycznej symulacji procesu tłoczenia. Część II. Tłoczenie niejednorodnych blach głębokotłocznych typu tailored blanks*, Materiały IX Konferencji „Informatyka w Technologii Metali", Szczawnica, 13–16.01.2002, 239.

**Metoda oceny tłoczności wsadów spawanych laserem**

Opisano metodę oceny tłoczności nowoczesnych wsadów z blach łączonych laserowo, które stosuje się do tłoczenia elementów karoserii samochodowych. Stwierdzono, że tradycyjne podejście do oceny blach tego typu na podstawie wyników prób podstawowych i technologicznych jest niewystarczające, ponieważ ocena tłoczności dokonywana na podstawie badań blach składowych nie pozwala prognozować przebiegu procesu tłoczenia blachy łączonej. Dlatego też do analizy procesu tłoczenia tego rodzaju wsadów niezbędne jest zastosowanie symulacji metodą elementów skończonych (MES).

ARCHIVES OF CIVIL AND MECHANICAL ENGINEERING

Vol. IV 2004 No. 3

# Analysis of power-energy effects for processes with forced deformation path

J. PAWLICKI, F. GROSMAN
Silesian University of Technology, Department of Process Modelling and Medical Engineering,
ul. Krasińskiego 8, 40-019 Katowice, Poland

Extensive research on the mechanisms of plastic deformation undertaken recently in many R&D centers allows us to prove the existence of such methods of deformation that reduce significantly the force necessary for metal forming and increase the values of deformation limit. This paper presents the results of rolling examinations, with axial motion of working rolls and compression of cylindrical samples in conditions of oscillatory torsion. The tests were conducted on specially adapted work-stands, whose design is a unique technical solution developed at the Department of Process Modelling and Medical Engineering for testing materials. The laboratory tests made on rolling and compression have revealed some significant differences in power-energy parameters registered during the tests, in conventional conditions and conditions with forced change of deformation path. At the same time the tests on the influence of deformation conditions on the macro-, micro-, and substructure of materials are carried out.

The effects of laboratory examinations in the form of the new data describing mechanical and structural reaction of metals, in conditions of controlled change of loading pattern, are promising and encourage us in our research work.

Keywords*: deformation path, rolling, compression, oscillatory torsion*

## 1. Introduction

Research on the mechanisms of plastic deformation being carried out in many research centres allows us to find such methods of deformation that reduce significantly the value of the forces necessary for plastic forming processes and increase the values of strain that causes fracture. This research is advanced and covers both basic research and its application in laboratory and industrial conditions [1–5]. The observed effect of the reduction of forces necessary for strain continuation is due to deformation work, where a cyclic change of the vector of one of load components applied takes place. This mechanism did not find a univocal and convincing scientific explanation.

Long-term experimental examinations carried out at the Department of Process Modelling and Medical Engineering, Silesian University of Technology, reveal a high sensitivity of material to variations of external load components occurring during forming process [6, 7]. This is especially important in the case of theoretical analysis aimed at devising the method for identification of the model of plastic flow (with a change of deformation path) for its application to numerical simulations of plastic-forming processes. Devising the physical models of the material response to the change of direction and proportion of load components, against a background of plasticity

characteristics defined in conditions of proportional and monotonic strain, is being indispensable for correct designing a new technology of plastic working of metals with computer-aided simulation of processes. This is especially important in the case of metallic materials formed in plastic working processes, in cold state or at elevated temperatures. The understanding of plastic properties of metallic materials formed within a full spectrum of possible state of stress, orientation variability of main axis and values of stress components during process allows us to obtain a full plasticity characteristics of metallic materials [8, 9]. The effects obtained in basic research, in the form of new data relating to mechanical responses of metals in conditions of controlled change of loading scheme, as well as the structural effects allow us to determine technological assumptions necessary for designing the low-energy processes of plastic forming and provide a promising prognosis on possible manufacturing of high-processed products without multiple operations of interoperative heat treatment.

## 2. Test stations

The test stations are made according to the latest standards of metrology, control and registration of measurement data. They make the research procedures being based on a many-year experimental experience possible. Such stations are an integral part of research equipment for testing materials in conditions of variable deformation path [10–12]. Design of this equipment is our unique technical accomplishment.

### 2.1. Compression stand

The compression stand with oscillatory torsion is devised in order to carry out the deformation tests on metallic materials. Hence, it enables:

- conventional compression in diversified friction conditions, i.e. frictionless compression, dry friction state,
- conventional compression in closed die offering the possibility for adjustable radial flow of metal,
- compression with simultaneous oscillatory torsion in conditions of free radial flow of metal,
- compression with simultaneous oscillatory torsion in conditions of high quasi-hydrostatic pressure.

It is possible to conduct the compression tests because of additional kinematic function of equipment connected to a lower punch capable of producing oscillatory movement (Figure1). The deformation path can be controlled by changing the proportions of participation of the linear strains caused by plane motion of the punch and non-dilatational strains caused by rotating motion of punch in total strain. This equipment offers various possibilities of modelling the metal structure, of carrying out the tests of material sensitivity to the change in a deformation path, and of applying practically the operation of technological upsetting. The control system allows adjustment

of compression rate, frequency of torsion and amplitude of torsion angle. Due to its size and design the equipment is fitted for operation in the working space of testing machine. Settings of kinematic values enable us to change the torsion angle in the range from 0º to 16º. The frequency of swings of a lower punch $f_t$ is controlled by inverter within the range of 0–1.8 Hz. If necessary, the peak frequency can be increased to 2.6 Hz. Travelling speed of lower punch (related to the motion of testing machine traverse) amounts up to 0.4 m/min. Permissible compressive force is 300 kN. Compressive force $F$ [kN] and deformation path $\Delta h$ [mm] are registered by computer. The system is recording and saving the measurement data and allows also programming the course of tests (setting of specific displacement value). During the test a visual observation of force characteristics in real time is possible.

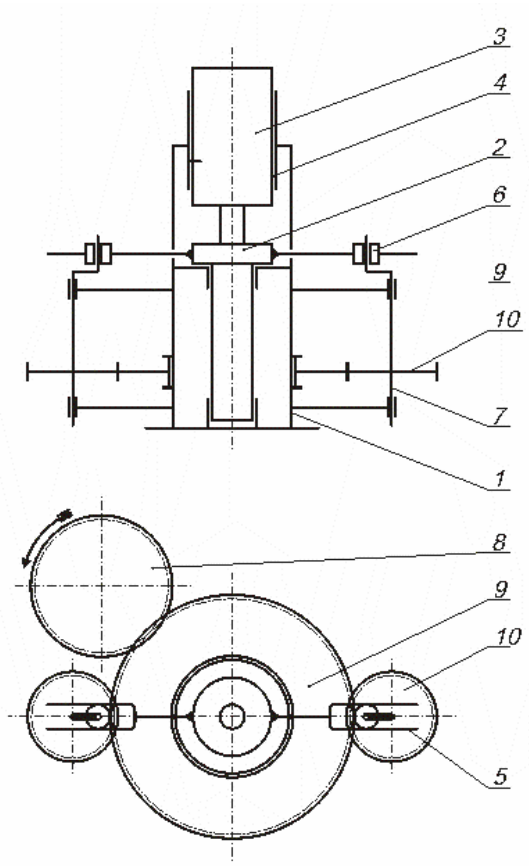


Fig. 1. Kinematic diagram of compression unit with oscillatory torsion: 1 – body, 2 – lower punch, 3 – upper punch, 4 – non-rotating slidable bearing, 5 – fork – lower punch arm, 6 – roller, 7 – crankshaft (eccentric), 8 – driving gear, 9 – toothed ring, 10 – gear

## 2.2. Rolling stand

The stand for rolling under conditions of cyclic variation of loading scheme was designed on the basis of laboratory two-high mill. Many design solutions of rolling stand were analyzed and accepted in design work and manufacture of a stand having rolls with transverse cyclic motions in the opposite directions. The kinematic diagram of the rolling stand is presented in Figure 2. Adjustment and setting of the unit allow regulation of roll deflection up to 2 mm and a frequency of transverse swings of rolls up to 3 Hz. The axial travel of rolls is possible due to eccentric lever mechanism. In a specifically established position of the eccentric-lever mechanism, the deflection is equal to zero and the unit is working as a conventional rolling stand. The mechanism of axial movement of rolls is considered to be our unique design and is protected by patent. Frequency of transverse roll swings is controlled in an infinitely variable way by means of the adjustment of rotational speed of motoreducer shaft.

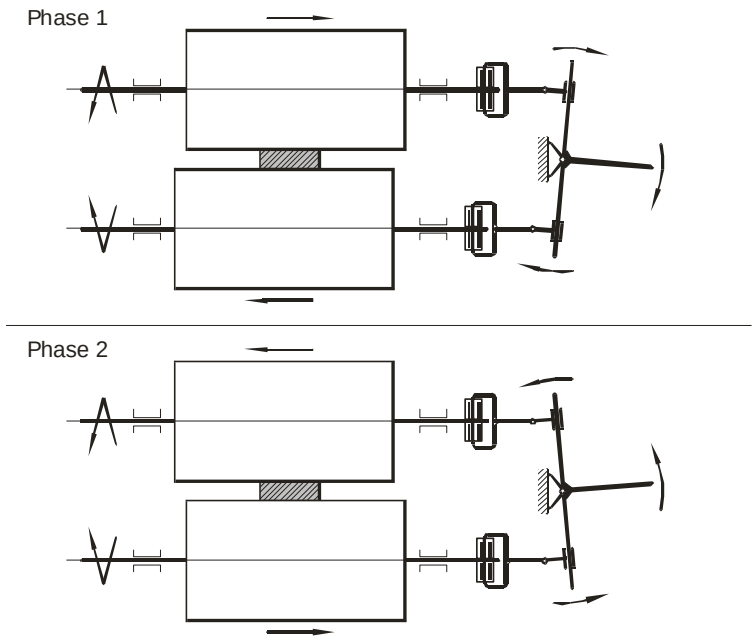


Fig. 2. Kinematic diagram of rolling stand with axial cyclic motion of working rolls

Maximum rotational speed of rolls is $n = 20$ min$^{-1}$ and can be adjusted. The stand is additionally equipped with sets of working rolls with plain faces, longitudinal passes and parallel grooves on the surface of roll face. The experimental rolling stand is fitted with the measurement system from BMCM, Germany. The measurement system, recording and processing of data, is controlled by means of NEXT VIEW 3.4 software.

## 3. Methods and results of research

### 3.1. Compression

Examinations of the behaviour of materials in the state of compression with oscillatory torsion were carried out for a group of metallic materials ($Fe_{ARMCO}$, 0H18N9, Cu, Al) in diversified initial state. Cylindrical samples with an initial size of ϕ15×22.5 mm ($h_0/d_0 = 1.5$) were taken for the test. They were compressed, and basic parameters of the process were characterized by the following variables:

- torsion angle $\alpha$ = 0º, 4º, 10º, 16º,
- swing frequency of a lower punch $f_t$ = 0.3 Hz, 1 Hz, 1.8 Hz.

The results of examination proved a high impact of the deformation path on the form of force characteristics and the stucture of materials subjected to compression with oscillatory torsion in comparison to conventional compression. In Figure 3, there are presented the characteristics of mean specific rolling pressure obtained during compression with variation of deformation path in the time of test. Oscillatory motion of a lower punch causes a definite reduction in pressure values in any phase of the compression process.

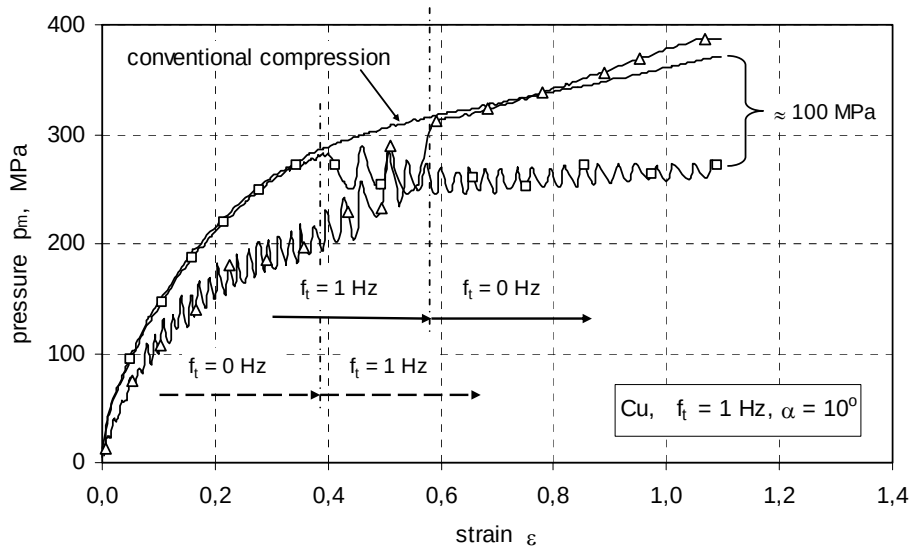


Fig. 3. Influence of the variation of deformation path on the value of mean specific rolling pressure $p_m$

The examples of characteristics of mean specific rolling pressure $p_m = f(\varepsilon)$ determined during compression with oscillatory torsion, on the background of conventional compression process, are presented in Figure 4. It can be seen in the diagrams that an increase in the frequency of reversing motion of the punch torsion $f_t$,

in the range of examined frequencies, will result in an essential drop of forces required for deformation of cylindrical samples. Such a regularity was observed for all the values of torsion angle $\alpha$ = 4º, 10º and 16º. A maximum reduction of mean specific rolling pressure, in comparison to compression without torsion, is approx. 50% (Cu – $f_t$ = 1.8 Hz; $\alpha$ = 16º, Al – $f_t$ = 1.8 Hz; $\alpha$ = 10º).

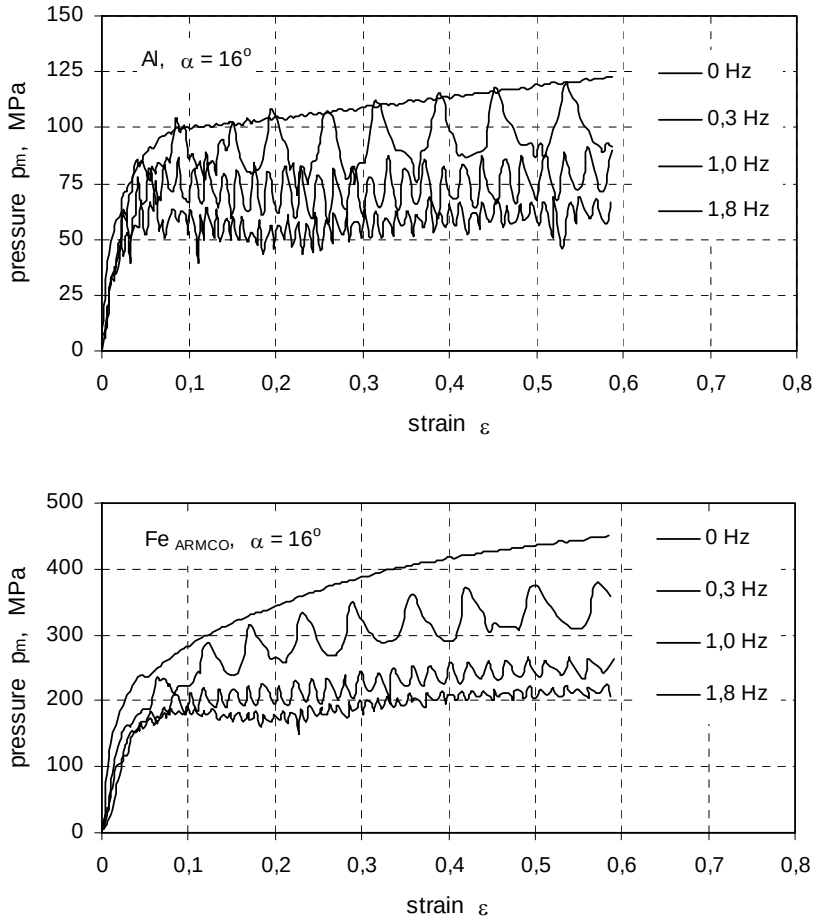


Fig. 4. Characteristics of mean specific rolling pressure defined for Al and $Fe_{ARMCO}$

A change of the torsion angle $\alpha$ at a constant frequency $f_t$ results in a decrease of the specific pressure for the torsion angles $\alpha$ = 10º and 16º and the torsion frequency $f_t$ = 1 Hz and 1.8 Hz. This regularity relates to all materials being examined. An increase of the torsion angle $\alpha$ from 10º to 16º at a constant frequency does not cause a significant drop of specific pressure values.

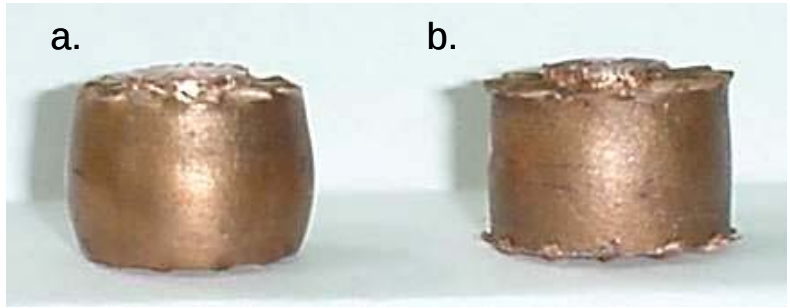


Fig. 5. View of cylindrical samples subjected to conventional compression (a) and oscillatory torsion (b)

The structural examinations carried out on the copper samples subjected to conventional compression with oscillatory torsion testified to distinct differences in the microstructure of samples. The microstructure of samples compressed under conditions of oscillatory torsion is characterized by a considerable refinement of grains, in comparison to conventionally compressed samples. A characteristic feature of the microstructure is appearence of relatively narrow dislocation bands showing considerable misorientation. Such arrangements were not observed in conventionally compressed samples. Also, the form of samples compressed with oscillatory torsion is similar to geometry of cylindrical samples compressed under frictionless conditions (lack of distinct barrel shape, Figure 5). This proves that the strain achieved in the volume of cylindrical sample is uniform.

### 3.2. Rolling

The tests of rolling were conducted on copper samples. The bands of material having initial size ($b_0 \times h_0$) of 10 × 8 mm and band length $l_0$ = 100 mm were used. The tests were carried out in the following kinematic conditions: rotational speed of rolls $n$ = 20 min$^{-1}$, amplitude of rolling deflection $\Delta p$ = 4 mm, frequency of axial rolling movement $f$ = 3 Hz. The rolls had parallel grooves on barrel surface in order to force a transverse flow of material. The copper bands were rolled in two passes with a draft, respectively, $\Delta h_1$ = 1 mm and $\Delta h_2$ = 2 mm in conditions of conventional process and with an axial, cyclic deflection of working rolls. The data relating to forces in rolling tests are presented in Figure 6. In the first pass, there was observed no essential difference in the rolling forces, independent by of the method of band deformation. The rolling force in conditions of axial, cyclic motion of rolls oscillated in the range of the rolling force obtained in conventional rolling conditions (Figure 6a). In the second pass, there was recorded a significant reduction in the value of rolling force during rolling with axial, cyclic movement of rolls (Figure 6b).

The oscillatory, regular variation of rolling force values in both passes is due to transverse movement of rolls and their response to rolled band of metal.

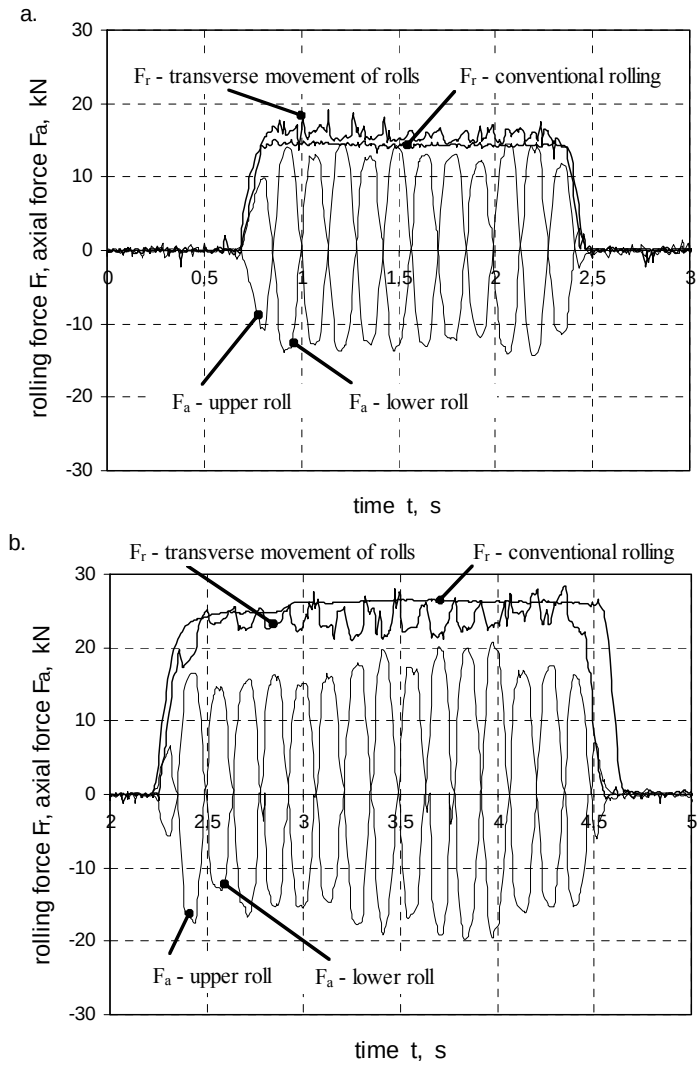


Fig. 6. Rolling force $F_r$ characteristic of conventional rolling and with transverse movement of rolls obtained in two passes: a) $\Delta h_1 = 1$ mm, b) $\Delta h_2 = 2$ mm

There was observed a strict correlation between variation of the axial force and the rolling force (Figure 7). A change of axial force produced by a lower or upper roll brings about an effect of oscillatory variation of rolling force values $F_r$. The maximum values of axial force correspond with maximum drops of rolling force. Because of this in the case of rolling process that goes on in the way described, a forced additional shear strain perpendicular to rolling direction brings an essential effect in the form of a decrease in the rolling forces.

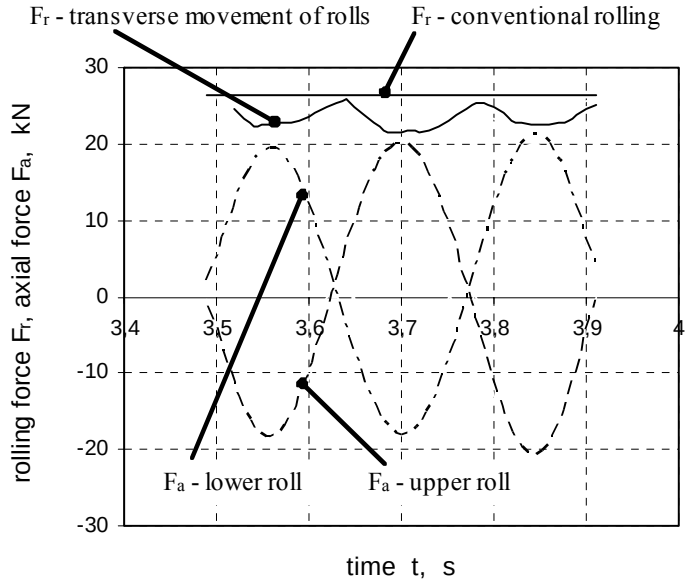


Fig. 7. Impact of rolling method on the rolling force $F_r$

A structural research allowing the observation of appropriately prepared side surface of bands (topological examinations) as well as a qualitative estimation of the evolution of the metal structure and substructure under specific conditions of loading confirms that there are essential differences in the structure of materials rolled by this method. Results of these tests are presented in report [3].

## 4. Summary

The effects observed in the form of variation of the force and structure parameters confirm the possibility of effective utilizing compression with oscillatory torsion and the rolling with transverse, cyclic movement of rolls to practical use of the conception of plastic forming with forced deformation path. The interaction effectiveness of these forming methods depends on the participation of strain components in a total strain. A univocal determination of the parameters guaranteeing maximum effectiveness of deformation in the processes analysed, expressed by reduction of the force parameters of strain, is based on finding the correlation between components of strain and structural effects, which is actually the subject of research.

The experience gathered at model stands will be used for setting the requirements for new processes of forging and rolling, which are associated with the effect of reduction of force-energy parameters, and for manufacturing the products and semi-products with special mechanical and functional properties.

## References

[1] Korbel A., Bochniak W., Kiełpiński R., Snarski P.: *Sposób wyciskania rur z metali i stopów na prasie z rewersyjnie obracaną matrycą*, Rudy i Metale Nieżelazne, 1999, R 44, nr 4, s. 153–158.
[2] Kong L.X., Lin L., Hodgson P.D.: *Material properties under drawing and extrusion with cyclic torsion*, Materials Science and Engineering, 2001, A308, pp. 209–215.
[3] Grosman F., Pawlicki J., Bochniak W.: *Walcowanie z wymuszonym odkształceniem poprzecznym*, Materiały Konferencyjne „Walcownictwo'02", Ustroń, 2002, s. 15–20.
[4] Grosman F., Pawlicki J.: *Concepts of technological applications in controlled deformation of materials*, Acta Metallurgica Slovaca, 2002, Vol. 8, No. 1, pp. 178–182.
[5] Bochniak W., Korbel A.: *KOBO Type Forming: forging of metals under complex conditions of the process*, Journal of Materials Processing Technology, 2003, Vol. 134, pp. 120–134.
[6] Pawlicki J., Grosman F.: *Wpływ zmiany orientacji osi głównych stanu naprężenia na wartość naprężenia uplastyczniające*, Rudy i Metale Nieżelazne, 1997, R 42, nr 11, s. 501–503.
[7] Pawlicki J., Grosman F.: *Wpływ przebiegu odkształcenia na wartość naprężenia uplastyczniającego materiałów polikrystalicznych*, Rudy i Metale Nieżelazne, 1999, R 44, nr 11, s. 565–568.
[8] Grosman F.: *Kryteria doboru i klasyfikacja funkcji naprężenia uplastyczniającego stosowanych w komputerowej symulacji procesów przeróbki plastycznej*, Rudy i Metale Nieżelazne, 1997, R 42, nr 11, s. 496–498.
[9] Grosman F.: *Flow-stress functions for the computer simulation of metal forming*, Journal of Materials Processing Technology, 2000,Vol. 106, pp. 45–48.
[10] Grosman F., Pawlicki J.: *Concepts of technological applications in controlled deformation of materials*, Procedings of the 7th International Conference on Technology of Plasticity, Advanced Technology of Plasticity, Yokohama, Japan, 2002, Vol. 1, pp. 1219–1224.
[11] Grosman F., Pawlicki J. et al.: Projekt badawczy PBZ/KBN 09/T08/98, *Nowe procesy kształtowania plastycznego metali i stopów oparte o kontrolowanie struktury z uwzględnieniem fizycznego i matematycznego modelowania zjawisk mikrostrukturalnych, mechanicznych i termicznych*, praca niepublikowana.
[12] Zgłoszenie do Urzędu Patentowego RP nr P-361148 wynalazku pt. *Sposób walcowania, zwłaszcza metali oraz klatka walcownicza do walcowania, zwłaszcza metali.*

## Analiza efektów siłowo-energetycznych w procesach z wymuszoną drogą odkształcenia

Badania nad mechanizmami odkształcenia plastycznego, które są bardzo intensywnie prowadzone w wielu ośrodkach badawczych, pozwoliły stwierdzić, że istnieją takie sposoby odkształcenia, które wywołują istotne obniżenie wielkości sił niezbędnych do prowadzenia procesów kształtowania plastycznego oraz zwiększenie wielkości odkształceń granicznych. Przedstawiono wyniki badań walcowania z poosiowym ruchem walców roboczych i ściskania próbek walcowych w warunkach oscylacyjnego skręcania. Próby przeprowadzono na specjalnie do tego celu zbudowanych stanowiskach, które są oryginalnym rozwiązaniem technicznym opracowanym w Katedrze Modelowania Procesów i Inżynierii Medycznej. Laboratoryjne pró-

by walcowania i ściskania wykazały istotne różnice w charakterze zmian rejestrowanych parametrów siłowo-energetycznych w warunkach konwencjonalnych oraz z wymuszoną zmianą drogi odkształcenia. Równolegle są prowadzone badania wpływu warunków odkształcania na makro-, mikro- i substrukturę materiału.

Efekty badań laboratoryjnych w postaci nowych danych na temat mechanicznej i strukturalnej reakcji metali w warunkach kontrolowanej zmiany schematu obciążenia są obiecujące i skłaniają do kontynuacji prezentowanych badań.

ARCHIVES OF CIVIL AND MECHANICAL ENGINEERING

Vol. IV 2004 No. 3

# Plasticity of Ti–48Al–2Cr–2Nb alloy

W. SZKLINIARZ, E. HADASIK, A. KOŚCIELNA
Silesian University of Technology, Krasińskiego 8, 40-019 Katowice, Poland

R. KAWALLA
Bergakademie Freiberg, Bernhard-v.-Cotta-Str. 4, 09596 Freiberg, Germany

The paper presents the results of experiments carried out in order to evaluate the plastic workability of Ti–48Al–2Cr–2Nb alloy subjected to hot compression tests. A significant influence of deformation temperature and, first of all, of the heating conditions on the results obtained has been shown. It has been found that deformation conducted under appropriate conditions and coupled with recrystallization annealing allows us to obtain a fine-grained "duplex" type microstructure. This, however, requires further research in order to define the role of the deformation parameters, initial microstructure and heating conditions in plastic forming of this group of alloys.

Keywords: *intermetallics, TiAl-based alloy, hot compression, plasticity, recrystallization*

## 1. Introduction

Owing to their low density, high specific strength as well as good oxidation and creep resistance, alloys based on ordered intermetallic phases from the Ti–Al system are an attractive, light structural material of new generation that can work at high temperatures [1–2]. They may be applied in aviation and the automotive industry as a material for combustion engine valves, turbocompressor rotors or gas turbine blades.

Alloys based on the compounds of titanium and aluminium can be divided into: ($\alpha_2$)-$Ti_3A1$-phase based alloys, ($\gamma$)-TiAl-phase based alloys, two-phase alloys and less known and more rarely used $TiAl_3$-phase based alloys [2].

The most frequently applied alloys of a two-phase microstructure ($\alpha_2 + \gamma$) contain 45–48 at.% of aluminium and three components: one from a group of elements which enhance plasticity (chromium, manganese and vanadium), the second from a group of elements which enhance high-temperature creep and oxidation resistance (niobium, tantalum, tungsten and molybdenum) and the third from a group of elements which cause grain refinement and an increase of the precipitation dispersion degree (boron, carbon and silicon). Alloys of such a chemical composition usually have a lamellar structure ($\alpha_2$ and $\gamma$ phases). Their properties depend, first of all, on the aluminium content and interlamellar spacing. A change of the aluminium content, of plastic working and of heat treatment conditions also enables obtaining a "duplex" microstructure (a structure with grains of lamellar morphology ($\gamma + \alpha_2$) and one with equiaxial grains of $\gamma$ phase). In general, the microstructure of a "duplex" type is characterized by higher plasticity, giving way, however, to the lamellar microstructure with re-

spect to crack resistance, fatigue strength and high-temperature creep resistance. The best properties are characteristic of alloys with a microstructure in which the volume fraction of the phase $\alpha_2$ ranges from 5 to 20% [3–4].

The fundamental disadvantage of those materials is their low plasticity at a room temperature and under plastic working conditions, as well as their susceptibility to brittle cracking and, finally, the difficulties which accompany the production and processing technologies. These unfavourable properties currently dramatically limit the common application of intermetallic phase-based alloys as structural materials [2–3].

There is general agreement that extended application and facilitation of processing of these alloys are conditioned by their plasticization both at a room temperature and at plastic working temperatures which can be obtained by grain refinement as well as refinement of the microstructure inside the grain. These problems constitute crucial tasks of the majority of research conducted by different research centres [4–9].

The intermetallic phase-based Ti–Al alloys belong to materials particularly difficult from the point of view of their production and processing technology. They are produced by conventional melting and casting of ingots or finished casts as well as by powder metallurgy methods.

Before plastic working, the ingots are subject to hot isostatic pressing (HIP) and homogenization, whereas alloys obtained from powders by mechanical alloying or reactive synthesis are subject to initial thickening and to HIP. After plastic working, semi-finished or finished products are subject to final heat treatment, surface treatment or possibly, to machining, as well as to quality, microstructure and property control.

Plastic working causes considerable technological problems due to low workability of those alloys, which manifests itself in low deformability and high plastic forming resistance [4, 6]. This necessitates the application of a much higher temperature of plastic working conducted with small deformations, at low strain rates, and using technologies whose state of stress is characterized by dominant compressive stresses. The high temperature of plastic working processes also requires particular surface protection by metal shields against oxidization and excessive cooling. In this connection, low-efficiency plastic working technologies are used, such as pressing and extrusion, instead of forging and rolling, the latter being commonly applied to conventional titanium alloys [6–7].

In spite of the application of two-stage plastic working as well as intermediate and final recrystallization annealing, a fine-grained and homogeneous in its cross-section microstructure of finished products is obtained only in the case of products with small cross-sections [2–3, 8].

## 2. Material and methods

The material for the investigation was a 4-component alloy, Ti–48Al–2Cr–2Nb, from the Ti–Al system with a chemical composition shown in Table 1. The alloy was

melted in an IS-III/5 Leybold–Heraeus' vacuum induction furnace, in a $SrZrO_3$-coated SiC crucible [10], and cast into graphite moulds. As charge materials for alloy melting an Al–Cr–Nb master alloy and comercially pure titanium were used. As-cast ingots were subject to 24-hour homogenization at a temperature of 1313 K, and to very slow cooling (with the furnace) after annealing.

Table 1. Chemical composition of alloy

| Chemical composition | Component | Al | Cr | Nb | O | C | Ti |
|---|---|---|---|---|---|---|---|
| Assumed | at. % | 48 | 2 | 2 | – | – | Balance |
| | wt. % | 33.35 | 2.68 | 4.79 | | | |
| Obtained | at. % | 46.88 | 2.18 | 2.69 | 0.52 | 0.17 | |
| | wt. % | 32.80 | 2.88 | 6.33 | 0.21 | 0.05 | |

Evaluation of the cast alloy's plastic workability (hot compression test) was carried out with a 320 kN servohydraulic machine. Cylindrical specimens of an initial diameter $d_0 = 5$ mm and height $h_0 = 10$ mm placed in a special vacuum Thermos were heated in an electric chamber furnace up to the temperature of 1173, 1273, 1323 and 1373 K. Immediately after the predefined temperature had been reached, the specimens were being deformed up to a half of their height, at a strain rate equal to 5 $s^{-1}$. The appearance of specimens after deformation is shown in Figure 1 and the deformation parameters as well as the specimen surface condition and maximum unit pressure are shown in Table 2. The course of the average unit pressure changes as a function of strain is presented in Figure 2.

After predefining the deformation, part of the specimens were subjected to recrystallization annealing at 1473 K for 2 hours. After annealing, the specimens were cooled with the furnace. Both in their initial state, after predefining the deformation, and after recrystallization annealing, their microstructure was examined under a Reichert light microscope. In order to illustrate better the microstructure changes caused by deformation, the investigation was carried out both in longitudinal and transverse sections. The test specimens were prepared according to a standard procedure and etched in Kroll's reagent. The results of the investigation are shown in Figures 3–5.

## 3. Results and discussion

Specimens labelled with numbers 1–3 and compressed immediately after short-term soaking at the test temperature showed defects on the lateral surface in the form of distinct scratches or cracks (Figure 1). Due to this, in the next stage of compression tests, the specimens after heating were additionally kept for 1 hour at a predefined temperature. After compression, they did not show any defects on the lateral surface (Figure 1). The application of soaking directly before the compression test did not reduce the maximum unit pressure (Table 2). The reasons for this state should not be sought in the microstructure changes because of too low a temperature and short soak-

ing time, and absence of any transformations in the alloy in this temperature range. Soaking probably increases the uniformity of heating in cross section due to low thermal conductivity of intermetallic phase-based alloys [1–2]. Thus, particular areas of a specimen are deformed uniformly, without any cracks.


Fig. 1. Specimens surface appearance after compression test

Table 2. Hot compression tests results

| Specimen number | Temperature, K /heating time | Strain rate $\dot{\varepsilon}$, $s^{-1}$ | Deformation $\varepsilon_h$, % | Maximum unit pressure $p_{śr}$, MPa | Surface state |
|---|---|---|---|---|---|
| 1 | 1173 | | | 1070 | scratches |
| 2 | 1273 | | | 930 | cracks |
| 3 | 1373 | 5 | 50 | 620 | scratches |
| 4 | 1273/1h | | | 930 | no defects |
| 5 | 1323/1h | | | 900 | no defects |

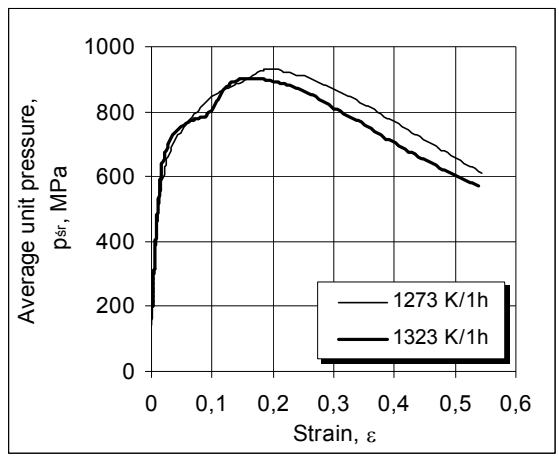


Fig. 2. Change of an average unit pressure as a function of strain

As results from the data in Table 2, the alloy investigated is characterized by high maximum unit pressure in hot compression tests. As the deformation temperature rises, the unit pressure clearly decreases from 1070 MPa at 1173 K to 630 MPa at 1373 K. At temperature of 1273 and 1323 K, the maximum unit pressure amounts about 900 MPa. A correct shape of a curve representing the dependence of the average unit pressure $p_{śr}$ on the strain $\varepsilon$ was obtained, which is shown in Figure 2. The curves

are characterized by a gently outlined maximum corresponding to 0.2 deformation and by an inconsiderable pressure fall as the deformation increases.

The microstructure of the alloy after casting and after homogenization is a typical two-phase microstructure with visible interdendritic microsegregation effects (Figure 3). It consists of regions with lamellar phases $\alpha_2$ and $\gamma$ as well as of regions of a free phase $\gamma$ located between them.

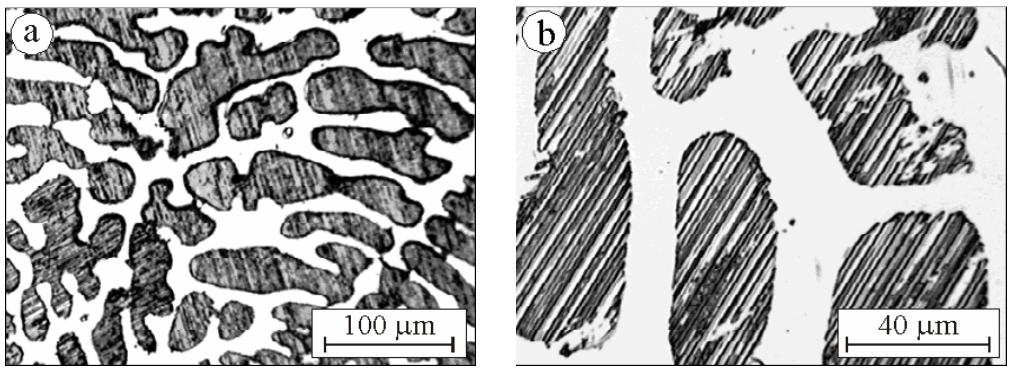


Fig. 3. Alloy microstructure in as-cast condition (a) and after homogenization (b)

As a result of the deformation in the temperature range investigated, substantial changes occur in the microstructure (Figure 4). They refer both to the changes in the lamellar regions and to the regions occupied by a free phase $\gamma$. A tendency is revealed towards the lamellar microstructure deformation and orienting it in accordance with the deformation direction, as well as towards fragmentation and spheroidization of lamellas. The same refers to the regions occupied by a free phase $\gamma$. In the microstructure of a specimen deformed at 1373 K, effects are visible which indicate the course of the recrystallization process. Thus, the microstructure of an alloy deformed at this temperature is characterized by the highest inhomogeneity.

The application of recrystallization annealing conducted in standard, for this alloy, conditions caused the occurrence of distinct recrystallization effects and grain refinement of the alloy investigated (Figure 5).

The most substantial effects of grain refinement were obtained for an alloy deformed at a temperature of 1323 K. Somewhat smaller effects were observed for an alloy deformed at 1273 K. Similar refinement effects appeared in the case of an alloy deformed at 1373 K; however, the microstructure is characterized by considerable inhomogeneity, which results from partial recrystallization occurring as early as the deformation process. Recrystallization is responsible for obtaining a duplex microstructure with grain of lamellar and equiaxial morphologies characterized by higher plasticity at a room temperature in relation to the microstructure of a lamellar morphology only.

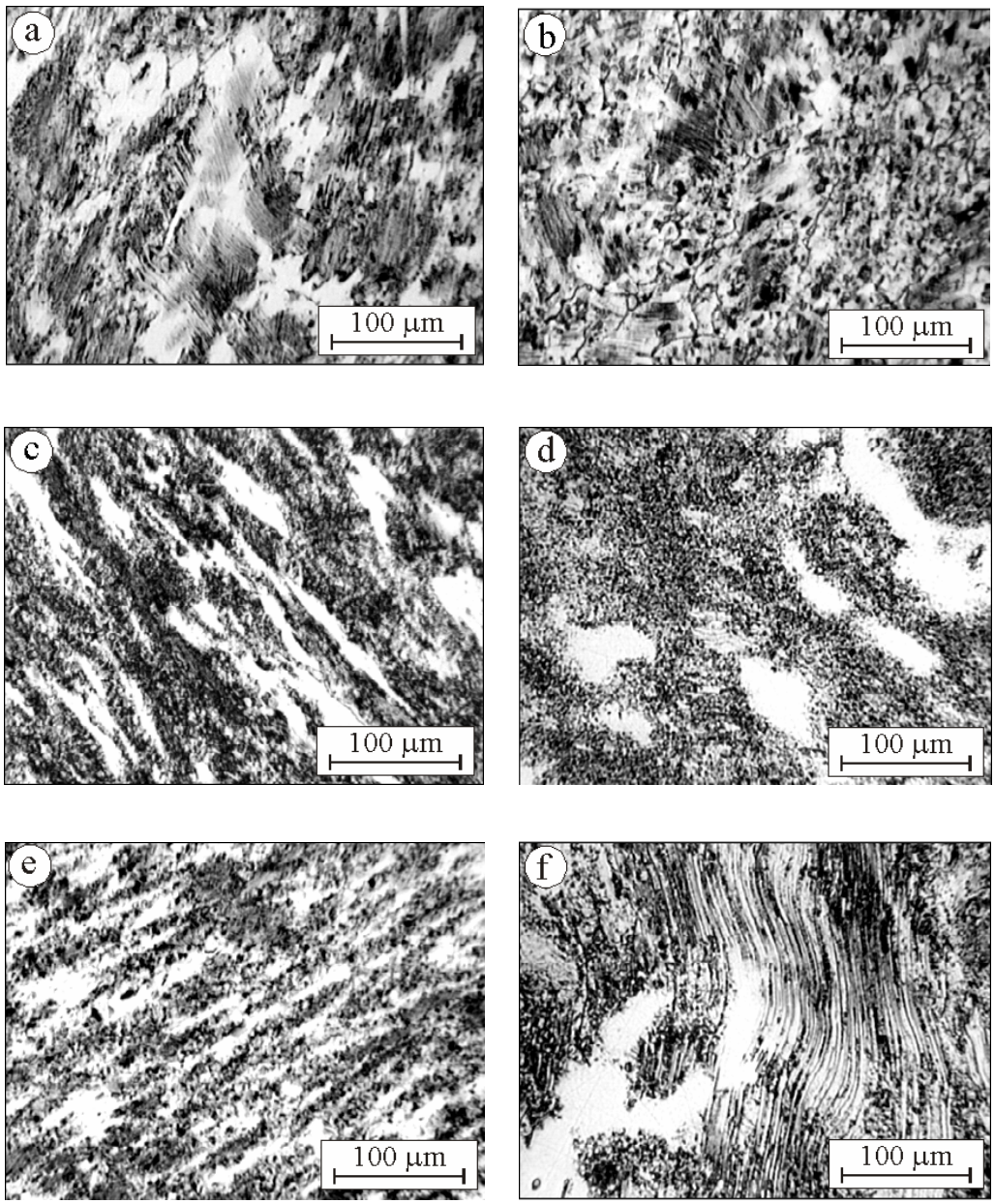


Fig. 4. Alloy microstructure after compression test: specimen 1 (a), specimen 3 (b), specimen 4 (c, d) and specimen 5 (e, f)

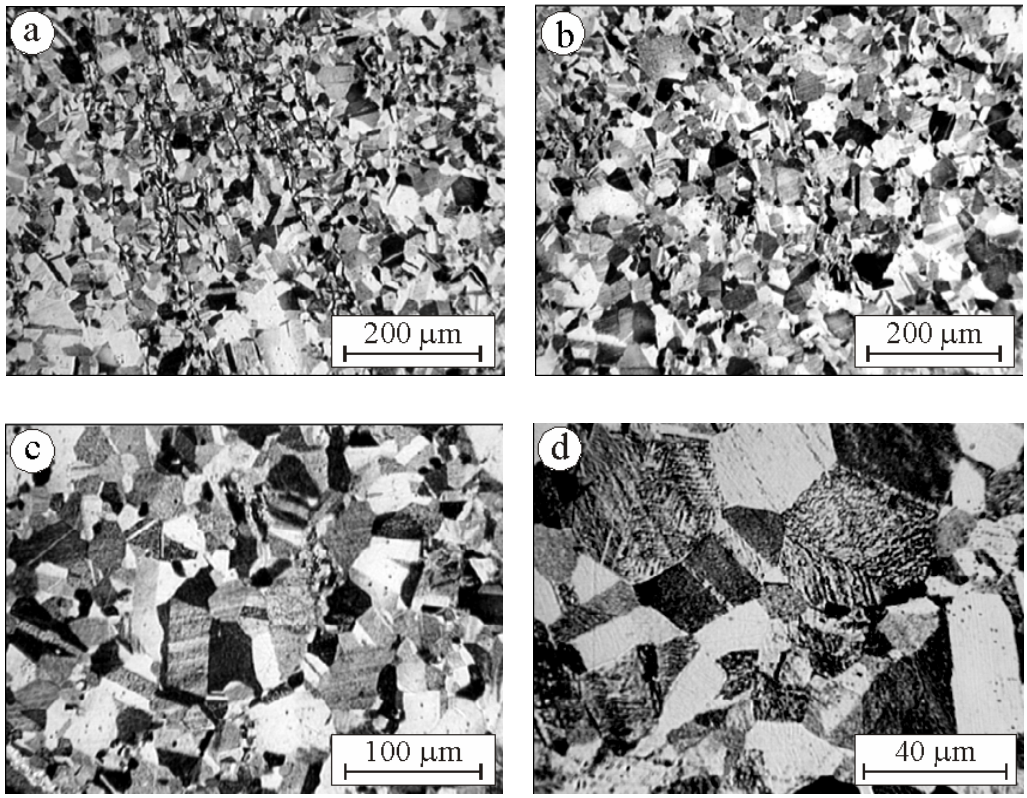


Fig. 5. Alloy microstructure after compression and recrystallization: specimen 3 (a), specimen 4 (b, c), specimen 5 (d)

## 4. Summary

The intermetallic phase-based Ti–Al alloys belong to materials particularly difficult from the point of view of their production and processing technology. Plastic working causes considerable technological problems due to low workability of those alloys, which manifests itself in low deformability and high plastic forming resistance.

An evaluation of plastic workability of the Ti−48Al−2Cr−2Nb alloy carried out based on a hot compression test has shown that the alloy is characterized by high maximum unit pressure. As the deformation temperature increases, the maximum unit pressure distinctly decreases from 1070 MPa at 1173 K to 630 MPa at 1373 K.

The curves representing the dependence of an average unit pressure on strain are characterized by a gently outlined maximum corresponding to deformation up to a strain of 0.2 and by an inconsiderable pressure fall as the deformation increases. Specimens compressed immediately after short-term soaking at the test temperature

showed defects in the form of distinct scratches or cracks on the lateral surface. The application of 1-hour soaking at the test temperature directly before the compression test, without decreasing the maximum unit pressure, resulted in elimination of those adverse effects. The reasons for this should be sought in an increase of the uniformity of the temperature distribution in cross section due to low thermal conductivity of the intermetallic phase-based alloys.

As a result of deformation in the temperature range investigated, a tendency is revealed towards the lamellar microstructure deformation and orienting it in accordance with the deformation direction, as well as towards fragmentation and spheroidization of lamellas. In the microstructure of a specimen deformed at 1373 K, effects are visible which indicate the course of the recrystallization process. The application of recrystallization annealing performed in standard, for this alloy, conditions resulted in the occurrence of distinct recrystallization effects and grain refinement of the alloy investigated. The most substantial effects of grain refinement were obtained for an alloy deformed at a temperature of 1323 K. Recrystallization is responsible for obtaining a duplex microstructure with grain of lamellar and equiaxial morphologies.

The results of the research show the possibility of deformation and recrystallization of intermetallic TiAl phase-based alloys. This, however, requires further research in order to account for the role of the parameters of the deformation process, initial microstructure and heating conditions in plastic forming of this group of alloys.

**Acknowledgements**

This work was supported by Polish Committee of Scientific Research (grant: PBZ-KBN-041/T08/2001).

**References**

[1] Yamaguchi M., Inui H., Ito K.: *High-temperature structural intermetallics*, Acta mater., 2000, Vol. 48, 307.

[2] Dimiduk D.M., Mcquay P.A., Kim Y.-W.: *Gamma Alloy Technology 1999*, Proc. of the Ninth World Conference on Titanium Titanium'99, Ed. by I.V. Gorynin, S.S. Ushkov, 1999, Vol. 1, 259.

[3] Clemens H., Kestler H.: *Processing and Applications of Intermetallic γ-TiAl-Based Alloys*, Advanced Engineering Materials, 2000, Vol. 2, No. 9, 551.

[4] Clemens H., Lorich A., Eberhardt N., Glatz W., Knabl W., Kestler H.: *Technology, Properties and Applications of Intermetallic γ-TiAl Based Alloys*, Zeitschrift für Metallkunde, 1999, Vol. 90, No. 8, 569.

[5] Hu Z.M., Dean T.A.: *Aspects of forging of titanium alloys and the production of blade forms*, Journal of Materials Processing Technology, 2000, No. 111, 10.

[6] Mitchell A.: *Melting, casting and forging problems in titanium alloys*, Materials Science and Engineering, 1998, A243, 257.

[7] Dimiduk D.M.: *System engineering of gamma titanium aluminides: impact of fundamentals on development strategy*, Intermetallics, 1998, No. 6, 613.
[8] Martin P.L.: *Effects of hot working on the microstructure of Ti-base alloys*, Materials Science and Engineering, 1998, A243, 25.
[9] Szkliniarz W.: *Strukturalne aspekty wytwarzania stopów na osnowie faz międzymetalicznych z układu Ti–Al*, Rudy i metale nieżelazne, 2002, nr 9, 434.
[10] Chrapoński J., Szkliniarz W., Mikuszewski T.: *Comparison of microstructure and phase composition of vacuum induction Ti–48Al–2Cr–2Nb alloy melted in crucibles with plasma spraying coatings*, Proceedings of the 10th World Conference on Titanium, Hamburg, 2003, Germany.

## Badania plastyczności stopu Ti−48Al−2Cr−2Nb

Stopy na osnowie faz międzymetalicznych z układu Ti–Al należą do materiałów szczególnie trudnych z punktu widzenia technologii ich wytwarzania i przetwarzania. Problemy technologiczne stwarza zwłaszcza przeróbka plastyczna tych stopów, które oznaczają się małą podatność technologiczną objawiającą się w postaci ograniczonej odkształcalności i dużych oporów kształtowania plastycznego.

Oparta na próbie ściskania na gorąco ocena podatności na kształtowanie plastyczne stopu Ti−48Al−2Cr−2Nb wykazała, że charakteryzuje się on dużym wartościami maksymalnego nacisku jednostkowego. Ze wzrostem temperatury odkształcenia wielkość ta wyraźnie maleje z 1070 MPa w temperaturze 1173 K do 630 MPa w temperaturze 1373 K.

Krzywe pokazujące zależność średniego nacisku jednostkowego od odkształcenia rzeczywistego charakteryzują się łagodnie zarysowanym maksimum odpowiadającym odkształceniu ok. 0.2 i niewielkim spadkiem nacisku w miarę zwiększenia odkształcenia.

Próbki ściskane bezpośrednio po krótkotrwałym wygrzewaniu w temperaturze próby wykazywały wady w postaci wyraźnych rys lub pęknięć na powierzchni bocznej. Jednogodzinne wygrzewanie w temperaturze próby bezpośrednio przed próbą ściskania bez zmniejszania wartości maksymalnego nacisku jednostkowego spowodowało usunięcie tych niekorzystnych efektów. Przyczyn tego stanu rzeczy należy upatrywać w zwiększeniu równomierności rozkładu temperatury na przekroju z powodu złego przewodnictwa cieplnego stopów na osnowie faz międzymetalicznych.

W wyniku odkształcenia w badanym zakresie temperatury występuje tendencja do odkształcenia płytkowej mikrostruktury i ukierunkowania jej zgodnie z kierunkiem odkształcenia oraz fragmentacji i sferoidyzacji płytek. W mikrostrukturze próbki odkształcanej w 1373 K widoczne są efekty świadczące o przebiegu procesu rekrystalizacji.

Zastosowanie wyżarzania rekrystalizującego, prowadzonego w standardowych dla tego stopu warunkach, spowodowało wystąpienie wyraźnych efektów rekrystalizacji i rozdrobnienie ziarna badanego stopu. Największe rozdrobnienie uzyskano dla stopu odkształcanego w temperaturze 1323 K. Efektem rekrystalizacji jest otrzymanie mikrostruktury typu „duplex“ z ziarnami o morfologii płytkowej i równoosiowej.

ARCHIVES OF CIVIL AND MECHANICAL ENGINEERING

Vol. IV 2004 No. 3

# Deformation geometry of copper single crystals tested in tension

M. TOKARSKI, M. S. SZCZERBA
University of Mining and Metallurgy, al. Mickiewicza 30, 30-051 Kraków

In this paper, an analysis of deformation geometry of copper single crystals tested in tension was performed. Based on a large body of experimental results it was found that the onset of deformation stage IV is connected with the change of dominant deformation system. The paper also suggests that the change of the dominant deformation system may play an important role in the onset of the deformation stage IV and its strain hardening kinetics in polycrystalline face-centered cubic materials.

Keywords: *copper single crystals, large strains, overshoot, stage IV deformation*

## 1. Introduction

To give a more precise description of the mechanisms of plastic deformation of single crystals one needs to analyze the deformation geometry of the samples, and thus, describe the evolution of active slip systems [1]. One of the main features of plastic flow of face-centered cubic (FCC) crystals, especially those of "soft" orientations, is a very strong plastic anisotropy, which is directly connected with the dominance of primary slip system, called the dominant deformation system [2]. Such a system determines the deformation path, and the rotation of crystal lattice, which is forced by the existing external constraints. In particular, the tensile axis rotates towards the operating slip direction of the dominant deformation system, and after a certain amount of plastic strain, crosses eventually over the symmetry boundary, <001>–<111>, between two stereographic triangles. This situation is widely described in the literature and known as the overshoot phenomenon. The occurrence of the tensile axis in a new basic triangle results in such a redistribution of the shear stresses operating in a crystal lattice that a new deformation system (the conjugate system) becomes the most stressed one. At the end of overshoot the stress in conjugate slip system reaches critical level and the new slip system takes over. The change of dominant slip system will obviously cause the change in deformation path. The transformation of dominant system takes place in rather abrupt manner, leading always to the localization of plastic flow. Moreover, single crystals of the initial tensile axis located far away from the symmetry line <001>–<111> need to be more strained in order to reach the end of overshoot point, and then they usually localize the tensile deformation into a heavy neck. Other crystals, which do not require such large strains to reach the end of overshoot, continue the deformation of the Lüders type in the new dominant slip system, usually at low level of hardening rate ($d\sigma/d\varepsilon$) [2]. The change of

dominant slip system can be easily detected on the work hardening curve, where each transformation generates characteristic drop and the temporary stabilization of the hardening coefficient value (Figure 1). This behaviour is characteristic of the crystals oriented near the symmetry line <001>–<111> and it is connected with strong localization of plastic flow of the Lüders type.

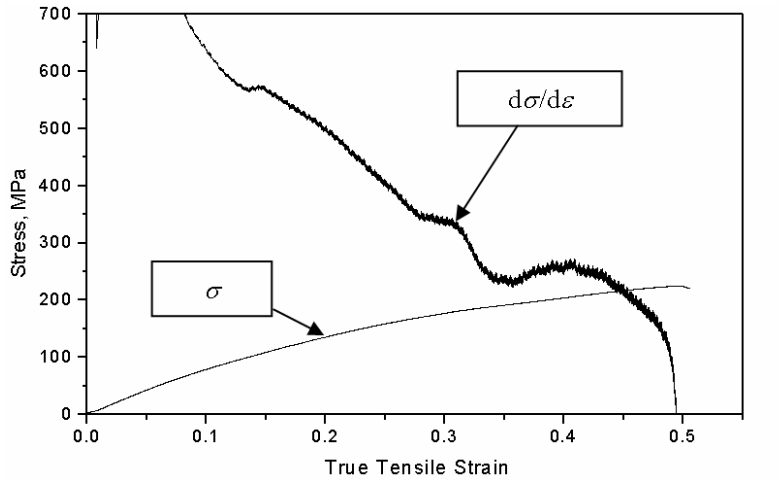


Fig. 1. The tensile stress–strain and the rate of work hardening curves of copper single crystals oriented near the <001>–<111> symmetry line

According to the present knowledge one may suggest that such a change in the work hardening rate is attributed to the onset of deformation stage IV [3]. Therefore, it is reasonable to conclude that the transformation of dominant slip system may play a deciding role in the initiation of the deformation stage IV of FCC single crystals.

In this paper, the experimental evidence of the change of dominant deformation system taking place in differently oriented tensile single crystals will be shown, and a suggestion will be made of the possibility of applying the concept of the change of dominant deformation system in the analysis of the kinetics of work hardening associated with the onset of the deformation stage IV in FCC polycrystals.

## 2. Experimental procedure

Copper single crystals of the rectangular shape ($4\times4\times70$ mm$^3$) were grown from randomly oriented seeds according to the modified Bridgman method, under the vacuum better than $10^{-5}$ hPa (Figure 2).

Based on the characteristics of the tensile tests performed on the single crystals investigated, two kinds of samples of different initial orientations of the tensile axis were selected for further investigations (orientations “2” and “5”, see Figure 2) and

strained up to a different level of work hardening. The diffractometry was performed in order to check precisely the rotation of crystal lattice and to calculate the current values of Schmid's factors. The shape changes of the cross section of the deformed samples (Figure 3) that resulted directly from the anisotropy of crystal properties were used to analyze the deformation geometry and finally a change of dominant deformation system.

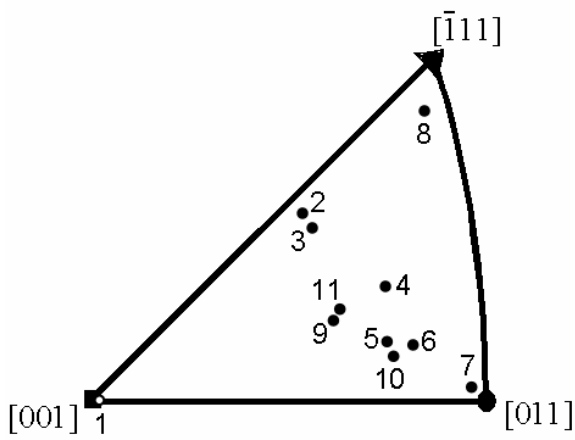


Fig. 2. The notation of the orientations of the single crystals used in the experiment

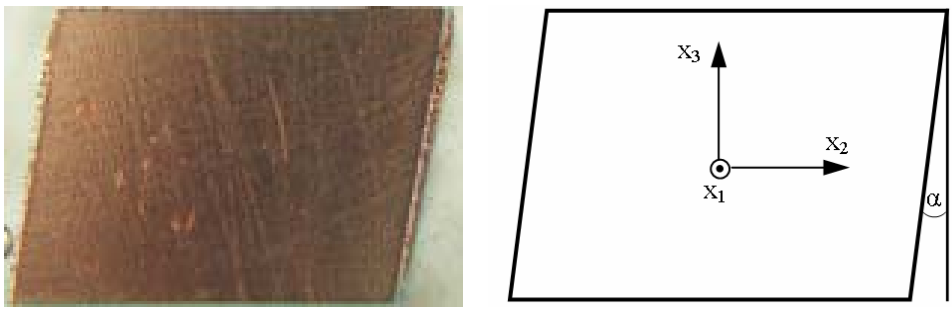


Fig. 3. Typical changes of the cross section of strained single crystals measured by means of the angle $\alpha$

The evolution of the cross section geometry was measured in the experiment by means of the angle $\alpha$ (Figure 3) and was compared with the numerical data obtained by means of a method of deformation gradient matrix [4]. This method allows us to calculate the distortion tensor for a situation, where the dominant and secondary slip systems act simultaneously, which does correspond to the assumption that the elementary shear of each operating slip system is infinitesimal, and the sum of the infinite number of the elementary shears gives a finite value. Therefore, it was possible to

determine the change of the position of any crystallographic direction or plane (for further details concerning the method of calculations see [5]).

## 3. Results and discussion

The characteristics of the tensile tests performed on eleven single crystals of different initial orientations of the tensile axis are presented in Figure 4. Clear differences that can be observed between the curves (e.g. the slope of the stress–strain characteristics and the total tensile deformation) illustrate a very individual character of the deformation behaviour of each single crystal. The different deformation paths result in different rotations of crystal lattices, so the tensile axis can cross over the symmetry line after the different amount of the tensile strain. Hence, the expected moment of the change of dominant slip system, and consequently, the onset of deformation stage IV require an individual analysis of each single crystal to be performed. To illustrate at best the quite different plastic behaviour of single crystals of different initial orientations of the tensile axis, the samples of the orientations of 2° and 20° away from the symmetry line [001]–[$\bar{1}$11] (the crystals "2" and "5", see Figure 2) were chosen for further experiment. The clearly different shapes of the tensile characteristics of the two chosen samples (Figures 5 and 6) are caused by the different deformation paths testified by the evolution of the angle $\alpha$ measured (Figures 7 and 8) and the X-ray measurements of the rotation of the tensile axis (Figures 9 and 10).

In the case of the "5" orientation of single crystal (20° from the symmetry line), the changes of the angle $\alpha$ with an increasing strain proceed in a monotonic way, there are no sudden drops on the work hardening curve, and the angle $\alpha$ increases monotonically. The tensile axis rotates towards [$\bar{1}$01] slip direction of the BIV deformation system, which is the most stressed one during almost the whole tensile deformation (Table 1).

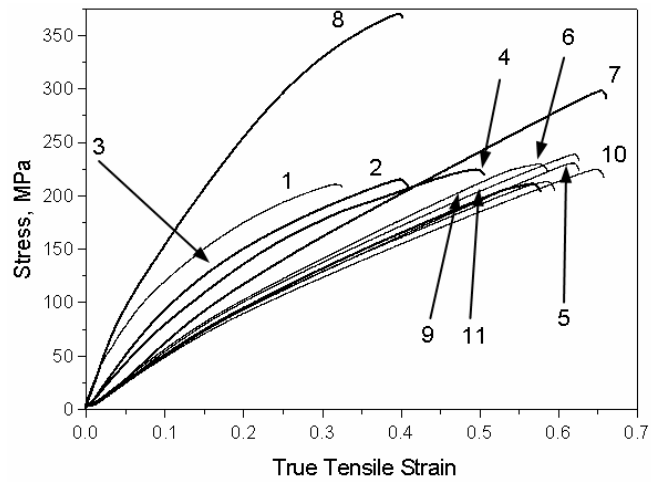


Fig. 4. The tensile stress–strain curves of the single crystals used in the experiment. The notations of the curves correspond to the numbers describing the initial orientations of the tensile axis (see Figure 2)

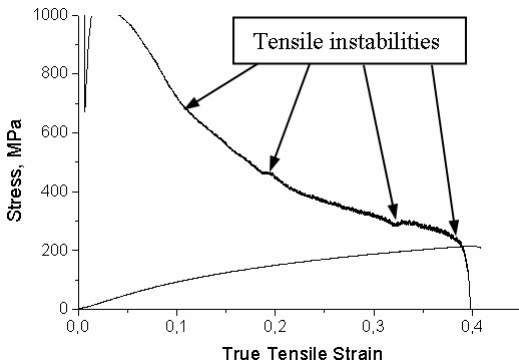


Fig. 5. The tensile stress–strain and work hardening curves of the "2" single crystal

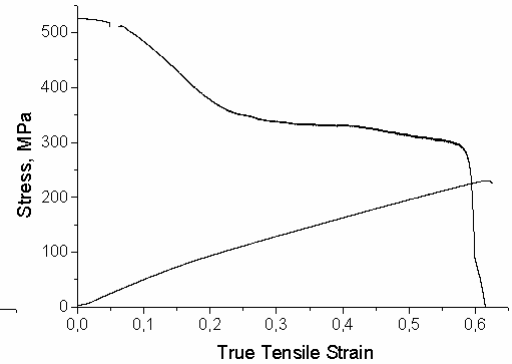


Fig. 6. The tensile stress–strain and work hardening curves of the "5" single crystal

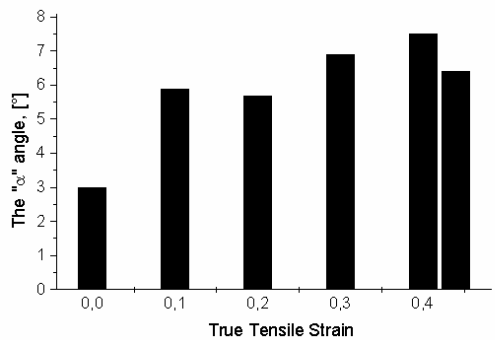


Fig. 7. The change of the angle $\alpha$ versus the true tensile strain of the "2" single crystal

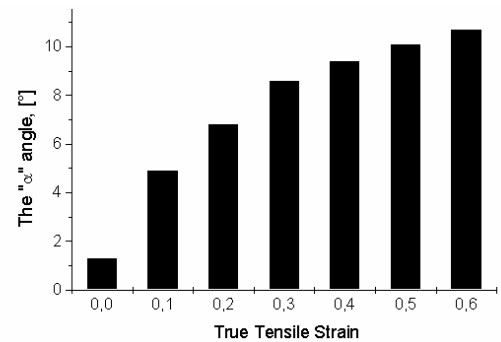


Fig. 8. The change of the angle $\alpha$ versus the true tensile strain of the "5" single crystal

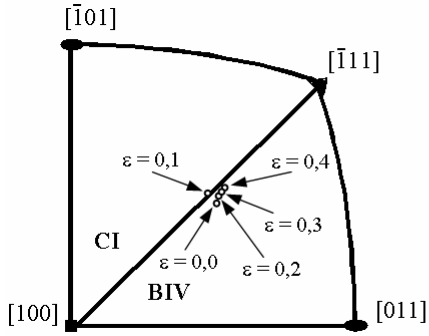


Fig. 9. The rotation of the tensile axis of the "2" single crystal

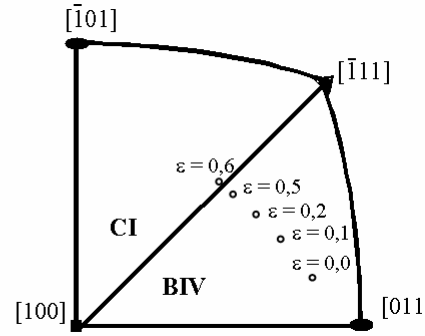


Fig. 10. The rotation of the tensile axis of the "5" single crystal

Table 1. The current values of Schmid's factors calculated for the successive strains of the "5" orientation of single crystal

| True tensile strain $\ln(l/l_o)$ | BIV Schmid's factor | CI Schmid's factor | The ratio of the Schmid's factors BIV/CI |
|---|---|---|---|
| 0 | 0.471 | 0.193 | 2.438 |
| 0.1 | 0.469 | 0.274 | 1.709 |
| 0.2 | 0.458 | 0.332 | 1.379 |
| 0.3 | 0.439 | 0.394 | 1.116 |
| 0.5 | 0.435 | 0.386 | 1.126 |
| 0.6 | 0.408 | 0.415 | 0.984 |

Table 2. The current values of Schmid's factors calculated for the successive strains of the "2" orientation of single crystal

| True tensile strain $\ln(l/l_o)$ | BIV Schmid's factor | CI Schmid's factor | The ratio of the Schmid's factors BIV/CI |
|---|---|---|---|
| 0 | 0.426 | 0.392 | 1.096 |
| 0.1 | 0.409 | 0.411 | 0.996 |
| 0.2 | 0.416 | 0.398 | 1.045 |
| 0.3 | 0.411 | 0.393 | 1.047 |
| 0.4 | 0.409 | 0.39 | 1.048 |

The transformation of the dominant slip system BIV → CI takes place at the end of the tensile test, just prior the neck, when the tensile axis takes a position of about 2°

beyond the symmetry line, and the CI slip system, which is characterized by the highest Schmid's factor, takes over.

As distinguished from the samples initially oriented far away from the symmetry line, the deformation path of the single crystals oriented closer to the symmetry line of the two basic BIV and CI triangles, (the "2" orientation of single crystal) seems more complicated. The characteristic "steps" visible in the work hardening plot (at $\varepsilon \approx 0.1$, $\varepsilon \approx 0.2$, $\varepsilon \approx 0.35$) associated with the occurrence of plastic instabilities correspond well with the non-monotonic behaviour of the $\alpha$ versus true tensile strain curve presented in Figure 7. The theoretical predictions based on the deformation gradient matrix method fully confirm the changes observed in the evolution of the angle $\alpha$ and can be explained in terms of the change of dominant slip system. The calculated distortion tensors (Equations (1) and (2)) indicate that the deformation systems BIV and CI produce just opposite off-diagonal component $\varepsilon_{23}$ (see the reference system drawn in Figure 3). This component seems to be strongly responsible for the observed current changes of the angle $\alpha$, and the tensors presented below were calculated for the "2" single crystal deformed up to 0.1 true tensile strain (the first overshoot situation).

$$e_{\mathrm{BIV}} = \begin{bmatrix} 0.408 & -0.707 & 0.289 \\ 0.236 & -0.408 & 0.167 \\ 0 & 0 & 0 \end{bmatrix}, \tag{1}$$

$$e_{\mathrm{CI}} = \begin{bmatrix} 0.408 & 0.707 & 0.289 \\ -0.236 & -0.408 & -0.167 \\ 0 & 0 & 0 \end{bmatrix}. \tag{2}$$

The X-ray studies of the rotation of the "2" single crystal lattice show undoubtedly that the tensile axis crosses over the symmetry line at least twice, at the points of about 0.1 and 0.2 of the true tensile strain. This experimental observation seems to prove that during the tensile deformation of the "2" single crystal, the redistribution of the shear strains of active slip systems does take place twice and result from the BIV-CI and the CI-BIV transformations of dominant deformation system. Moreover, taking into account the values of Schmid's factors collected in Tables 1 and 2, the analyzed overshoot phenomena seem to prove unambiguously the validation of Schmid's law for the selection of dominant slip systems in the dislocated FCC crystals. Further analysis confirms also that the mentioned instabilities of plastic flow of single crystals do belong to the end of overshoot phenomena and are directly connected with the change of dominant slip system.

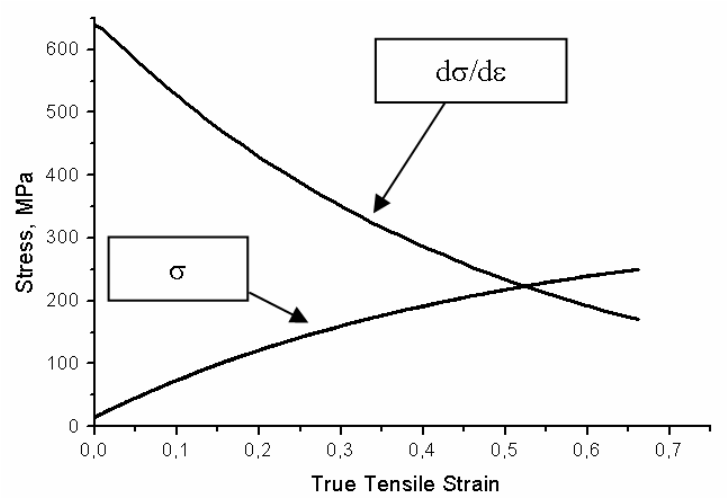


Fig. 11. The "stochastic" stress–strain and the rate of work hardening curves of eleven differently oriented copper single crystals

In the case of polycrystalline materials, which may be considered as composed of a huge number of randomly oriented single crystals, the individual features of each grain are lost, and the observed deformation behaviour is a "stochastic resultant" of the deformation paths of many separate crystals. Of course, the presence of grain boundaries should significantly enhanced the shielding effect of the individual plastic properties of each grain. It is the present authors belief that the presence of the deformation stage IV and its strain hardening kinetics of a real polycrystalline aggregate results from the change of the dominant deformation system which takes place individually in each grain. One can expect that the onset of the deformation stage IV in polycrystals will be diffused in terms of the critical strain, but the change of the strain hardening kinetics observed during the deformation stage III–IV transition will be originated by the physical process analogous to that taking place in the single crystals at the change of dominant deformation system. Let us illustrate this by considering the set of stress–strain curves for eleven differently oriented single crystal samples (Figure 4). The "stochastic" mechanical properties, which are constructed as a best statistical fit of the data points of the eleven single crystals collected in one stress–strain diagram. As one can see in Figure 11, there are no characteristic steps or drops on the stress–strain and work hardening curves.

## 4. Conclusions

Determination of the deformation geometry of single crystals is one of the useful sources of the comprehensive analysis of mechanisms of plastic flow of polycrystalline materials. The physics of the onset of the deformation stage IV in polycrystals

may be directly connected with the physics of the change of the dominant deformation system, which is easily observable during the plastic deformation of single crystals.

**Acknowledgements**

This work is supported by the State Committee for Scientific Research under grant number 4 T08A 24 and 11.11.180.255.

**References**

[1] Basiński S.J., Basiński Z.S.: *Plastic Deformation and Work Hardening*, [in:] *Dislocation in Solids*, ed. by F.R.N. Nabarro, North-Holland Publishing Company, 1979.
[2] Basiński Z.S., Szczerba M. S., Embury J.D.: Phil. Magazine A, 1997, 76, pp. 743–752.
[3] Mecking H.: *Dislocation Modelling of Physical Systems*, ed. by M.F. Ashby et al., Pergamon Press, Oxford, 1981, p. 197.
[4] Chin G.Y., Thurston R.N., Nesbitt E.A.: Transactions of the Metallurgical Society of AIME, 1966, Vol. 236, pp. 69–76
[5] Szczerba M.S., Tokarski M.: *Geometria transformacji głównego systemu poślizgu w walcowanych kryształach miedzi*, FORMING 2000, Katowice-Ustroń, 2000, p. 33.

**Geometria deformacji rozciąganych monokryształów miedzi**

Przeprowadzono analizę geometrii deformacji rozciąganych monokryształów miedzi o różnych wyjściowych orientacjach krystalograficznych. Na podstawie charakterystyk naprężenie rozciągania–odkształcenie sporządzonych dla kilkunastu różnie zorientowanych próbek zdecydowano się poddać szczegółowym badaniom sposób deformacji monokryształów, których początkowa oś rozciągania znajdowała się w odległości kątowej 2° i 20° od linii symetrii między dwoma trójkątami podstawowymi, <001>–<111>. Analiza geometryczna deformacji została określona na podstawie obserwacji zmiany kształtu przekroju poprzecznego rozciąganych kryształów. Przeprowadzone dodatkowo badania dyfraktometryczne pozwoliły określić rotację sieci krystalograficznej rozciąganych monokryształów oraz na jej podstawie obliczyć zmiany czynników Schmida–Boasa dla dominujących systemów poślizgu. Tę metodę badań uzupełniono analizą numeryczną, używając metody macierzy gradientów deformacji. Na podstawie danych zebranych eksperymentalnie oraz obliczeń wykonanych za pomocą macierzy gradientów deformacji zidentyfikowano działające systemy poślizgu. Zaproponowana metoda okazała się szczególnie przydatna do identyfikacji momentu przejścia dominującego pierwotnego systemu poślizgu w dominujący system sprzężony. Na podstawie analizy kinetyki umocnienia monokryształów dodatkowo stwierdzono, że związana z końcem *overshootu* transformacja dominującego systemu poślizgu prowadzi bezpośrednio do zapoczątkowania IV stadium deformacji.

W pracy podjęto również próbę zastosowania koncepcji dotyczącej zjawiska końca *overshootu* w monokryształach do opisu kinetyki umocnienia materiałów polikrystalicznych. Jeśli potraktuje się polikryształ jako agregat złożony z dużej liczby przypadkowo zorientowanych krystalitów, to można by się spodziewać, że sposób odkształcenia będzie wypadkową de-

formacji poszczególnych ziaren, a indywidualne cechy pojedynczego krystalitu zostaną „ekranowane" przez efekt statystycznie przypadkowego rozkładu orientacji pojedynczych krystalitów. Co więcej, „efekt ekranowania" w rzeczywistym materiale będzie spotęgowany przez istniejące granice ziaren. Na podstawie krzywych rozciągania kilkunastu różnie zorientowanych monokryształów sporządzono „statystyczną" krzywą umocnienia, która wskazuje, że już w wyniku „ekranowania statystycznego" zanikają indywidualne cechy kryształów oraz że następuje silne „rozmycie" krytycznego odkształcenia plastycznego, przy którym pojawia się początek IV stadium deformacji. Zasugerowano jednak, że fizyczne zjawisko, które powoduje zmianę kinetyki umocnienia podczas przejścia z III do IV stadium deformacji w polikryształach, powinno być analogiczne do zjawiska transformacji dominującego systemu deformacji, które odpowiada za koniec *overshootu* w monokryształach.

ARCHIVES OF CIVIL AND MECHANICAL ENGINEERING

Vol. IV 2004 No. 3

# Application of the formability limit function in prediction of the material fracture

F. GROSMAN, M. TKOCZ
Silesian University of Technology, Krasińskiego 8, 40-019 Katowice

The known criteria for predicting the ductile fracture during bulk-metal forming operations and their disadvantages are discussed. Then the authors present their own damage model that is based on the strain-path dependent ductile fracture criterion and the use of a formability limit function. The computation procedure is implemented into the Forge3 finite-element package and tested by performing the simulations of cold upsetting of austenitic-steel cylindrical billet.

Keywords: *limit deformation, state of stress, fracture criteria, upsetting test*

## 1. Introduction

Estimation of the permissible deformation range in the metal-forming processes is done based on the limit deformation value ($\varepsilon_g$) which can be defined as the equivalent strain to fracture or the equivalent strain at the moment of the stability loss.

The stability loss criterion is applied mostly in design of the sheet-metal forming processes and, in exceptional cases, in design of the upsetting and drawing operations. This criterion is determined by the geometry of a deformed element, the strain-hardening index of a material and the loading conditions. In general, it can be assumed that prediction of the stability-loss effect turns to be relatively reliable and further research on this problem is performed mostly for sheet-metal forming.

Prediction of the material fracture in the bulk-metal forming operations causes considerably more problems. Development of the numerical simulation methods which are based on the finite-element solutions has stimulated practical application of different damage models. In order to obtain a correct solution of such simulations, a mathematical model containing all important material parameters and physical phenomena involved in a specific technological process is necessary. The first attempts to apply the computer simulations in predicting the moment and location of ductile fracture were based on the models describing the fracture phenomena for structural materials. This kind of approach to solving the fracture prediction in the processes where considerable strains occur is doomed in advance. Structural phenomena that occur under conditions of great plastic strain differ significantly from the structural phenomena in the range of small elastic-plastic strain which occur during the operation of machines and devices.

## 2. Ductile fracture criteria used for prediction of the material damage

Basically, there are two kinds of models used for prediction of the ductile fracture of material. Some of them are based on the micromechanical approach, while the other are macromechanical [1, 2].

For example, the micromechanical void growth model was proposed by Oyane et al. [3]. It can be written in the form:

$$\int_0^{\varepsilon_g}\left(1+\frac{\sigma_m}{A\cdot\sigma}\right)d\varepsilon = G, \tag{1}$$

where: $\sigma$ – equivalent stress, $\sigma_m$ – mean stress, $A$, $G$ – material constant.

The other micromechanical approach was presented by Dodd [4], who assumed the occurrence of a bifurcation effect in his model:

$$\frac{1}{\sigma}\frac{d\sigma}{d\varepsilon} \le \frac{\sigma_1\left(\frac{\delta f}{\delta\sigma_1}\right)^2+\sigma_2\left(\frac{\delta f}{\delta\sigma_2}\right)^2}{\left(\sigma_1\cdot d\varepsilon_1+\sigma_2\cdot d\varepsilon_2\right)\frac{\delta f}{\delta\sigma}}, \tag{2}$$

where: $\sigma$ – uniaxial stress, $\varepsilon$ – uniaxial strain, $\varepsilon_1$, $\varepsilon_2$ – principal strain components, $\sigma_1$, $\sigma_2$ – principal stress components, $f$ – plastic yield criterion.

Many researchers used macromechanical, empirical and semi-empirical ductile fracture criteria as the basis for development of damage models. They proposed different formulae for prediction of the material fracture, for example:

- Freudenthal [5]

$$\int_0^{\varepsilon_g}\sigma d\varepsilon = C_1, \tag{3}$$

where: $\sigma$ – equivalent stress, $C_1$ – material constant;

- Cockroft and Latham [6]:

$$\int_0^{\varepsilon_g}\sigma^*\cdot d\varepsilon = C_2, \tag{4}$$

where: $\sigma^*$ – maximum principal tensile stress, $C_2$ – material constant;

- Brozzo et al. [7]:

$$\int_0^{\varepsilon_g} \frac{2\sigma^*}{3(\sigma^* - \sigma_m)} \cdot d\varepsilon = C_3, \tag{5}$$

where: $\sigma^*$ – maximum principal tensile stress, $\sigma_m$ – mean stress, $C_3$ – material constant;

- Norris et al. [8]:

$$\int_0^{\varepsilon_g} \frac{1}{(1 - c \cdot \sigma_m)} \cdot d\varepsilon = C_4, \tag{6}$$

where: $\sigma_m$ – mean stress, $c$, $C_4$ – material constants;

- Atkins [9]:

$$\int_0^{\varepsilon_g} \frac{1 + \frac{1}{2L}}{(1 - c \cdot \sigma_m)} \cdot d\varepsilon = C_5, \tag{7}$$

where: $L = d\varepsilon_1/d\varepsilon_2$ – strain ratio, $\sigma_m$ – mean stress, $c$, $C_5$ – material constants.

Most of the ductile fracture criteria are generally based on the stress and strain values integrated over the strain path. The stress and strain values must be calculated at any position in the deformed material. They can be obtained numerically from finite-element methods. Critical values for these criteria correspond to the moment and location of ductile fracture initiation.

## 3. Application of the formability limit function in the fracture prediction

The papers [1, 2, 10, 11, 12] have concluded that a universal applicability of the ductile fracture models presented is limited, since the critical values of these criteria depend on the material, the die shape and the loading conditions.

In order to eliminate the above-mentioned disadvantage, the formability limit function has been used to develop the ductile fracture criteria. The basic assumption made is that the formability of the material used is proportional to the quotient of the equivalent strain increment and the limit deformation during each phase of the deformation process.

The proposed model of the material formability utilization can be expressed in the following analytical form:

$$W_{pl} = \int_0^{\bar{\varepsilon}_g} \frac{d\varepsilon}{\varepsilon_g(k_\sigma)} \leq 1, \tag{8}$$

where: ε – equivalent strain, $\varepsilon_g(k_\sigma)$ – formability limit function.

The $W_{pl}$ indicator, which can be called the formability utilization, has an invariable critical value. According to the formula above, the ductile fracture can occur in the regions where $W_{pl}$ reaches unity.

The procedure for determination of the formability utilization assumes calculation of:

- the increment of the equivalent strain ($\Delta\varepsilon$),
- the instantaneous value of the stress triaxiality ($k_\sigma$),
- the limit deformation value that corresponds to the stress triaxiality in the given calculation step ($\varepsilon_g(k_\sigma)$),
- the $\Delta\varepsilon_{ij}/\varepsilon_g(k_{\sigma ij})_{ij}$ ratio,

at each calculation step $i$ and for each finite mesh element $j$. After each calculation step, the calculated ratios are summarized:

$$\sum_{i=1}^{n} \frac{\Delta\varepsilon_{ij}}{\varepsilon_g(k_{\sigma ij})_{ij}}. \tag{9}$$

Taking into account the fact that the formability limit function has a vertical asymptote for $k_\sigma = -0.66$ [13], the calculation procedure includes also the conditional statement with the following formula:

$$\bigvee_{k_{\sigma ij} \le -0.66} \frac{\Delta\varepsilon_{ij}}{\varepsilon_g(k_{\sigma ij})_{ij}} = 0. \tag{10}$$

The correctness of the model proposed and the operation of the code developed were tested by simulating the cold upsetting of cylinder in the Forge3 software. The procedure described above was prepared in Fortran and implemented in one of the subroutines in the cparutil_e.f file. Then, recompilation of the Forge3 elasto-viscoplastic solver was made.

In the model, the following formability limit function was used [13]:

$$\varepsilon_g = \frac{a}{(k_\sigma + 0.66)^b}, \tag{11}$$

where $a$, $b$ are material parameters determined experimentally.

Simulations were carried out on austenitic-steel billets. The shape and the form of formability limit function used in simulations are shown in Figure 1a [13]. The shape and the formula of flow stress for the steel investigated were taken from the database attached to the Forge3 software. This material characteristics is depicted in Figure 1b.

The billet was cylindrical with the aspect ratio of 2. The Tresca model with the value of 0.25 for the friction factor was used to simulate friction on the die-billet interface. Simulations were carried out until the formability utilization $W_{pl}$ reached a critical value.

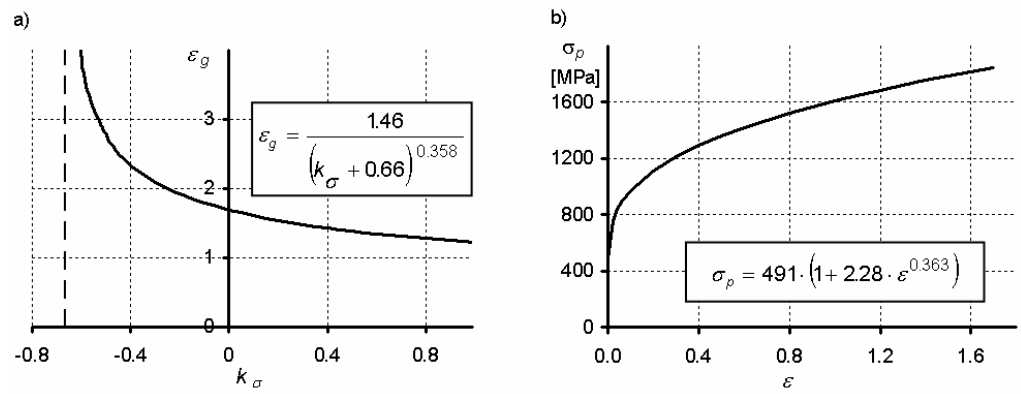


Fig. 1. The formability limit (a) and flow stress (b) functions used in simulation

The simulation results are shown in Figures 2 and 3. Figure 2 presents the top right quarter of a billet longitudinal section after 88% reduction in height. The arrow indicates the region where the formability utilization reaches unity and the ductile fracture is possible. This region is near the free surface of a billet. The local value of equivalent strain reaches 2.1 in this area. At this moment the local value of the stress triaxiality equals –0.5 there.

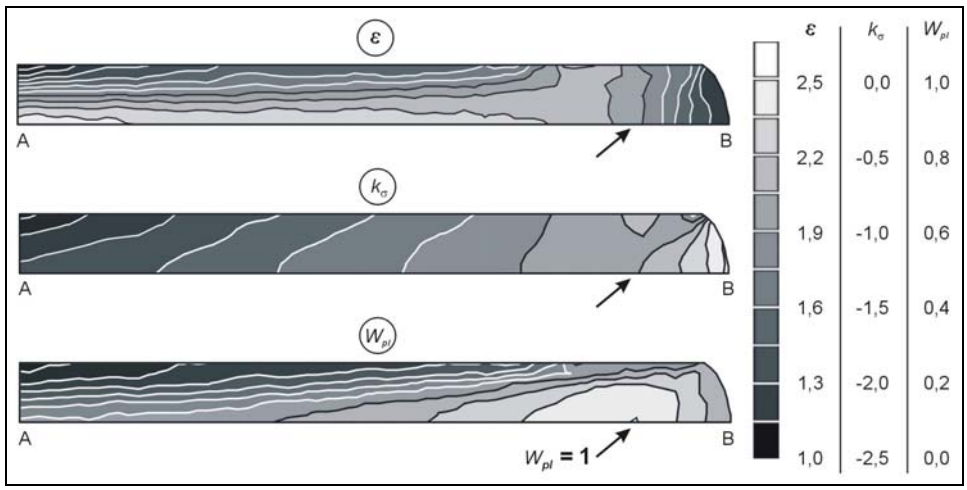


Fig. 2. Distributions of the equivalent strain $\varepsilon$, the stress triaxiality $k_\sigma$ and the formability utilization $W_{pl}$ in the right top quarter of a billet longitudinal cross-section after reduction in height $\varepsilon_h$ = 88%

The process of a material formability utilization is governed by the changes in stress state and the corresponding strain increments. The changes in the equivalent strain, the stress triaxiality and the formability utilization during upsetting in two char-

acteristic billet regions are shown in Figure 3. Point *A* represents the billet centre, and point *B* is located at the free surface on the horizontal symmetry axis. The exact position of these two points is illustrated in Figure 2.

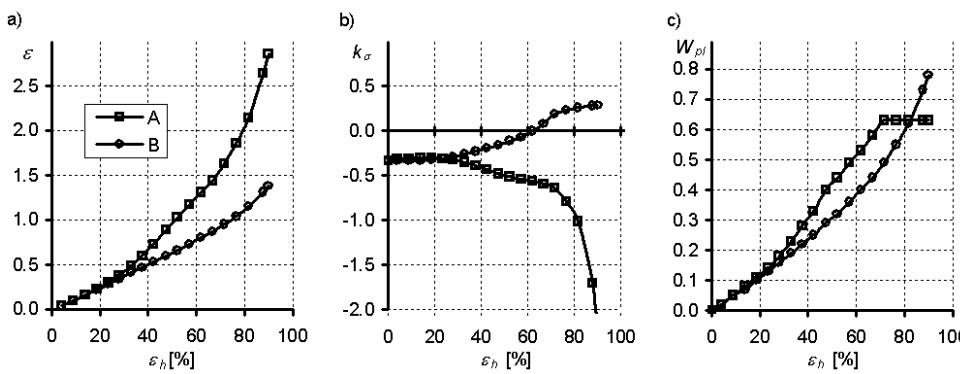


Fig. 3. Changes of the equivalent strain (a), the stress triaxiality (b) and the formability utilization (c) in point *A* located at the billet centre and point B located at the free surface on the horizontal symmetry axis (see also Figure 2)

It is clearly seen that courses of the equivalent strain $\varepsilon$ as well as the stress triaxiality $k_\sigma$ at points *A* and *B* differ significantly. When the reduction in height exceeds 30%, the stress triaxiality at the billet centre becomes considerably more favourable than the stress triaxiality at the free surface. Simultaneously, the difference between the local equivalent strain at these points becomes more and more visible. If the reduction in height is as large as 50%, the equivalent strain in point *A* is already 1.5 times larger than the equivalent strain in point *B*.

Due to such courses of the local equivalent strain and the stress triaxiality, initially the formability utilization ($W_{pl}$) is larger at the centre of a billet. When the reduction in height is large enough ($\varepsilon_h$>70%) the position of formability utilization maximum value is moved from the billet centre to the zone near the free surface. In this position, the formability utilization reaches the values close to unity.

## 4. Summary

Computer packages for numerical simulation and design of the metal-forming processes are already in common use. However, usability of such software depends heavily on the database contents. One of the most important material characteristics is the limit deformation. The possibility of predicting a material fracture in the metal-forming process is an indispensable element of the correct process design and simulation. Lack of the module for the damage prediction is a serious disadvantage of the most computer codes for metal-forming simulation. Additionally, the applicability of the damage models used is limited.

The model proposed for determination of the formability utilization is based on the strain path-dependent ductile fracture criterion. It has the following advantages over other models:

- the model is developed for the strain range and the deformation conditions that occur in the metal-forming processes,
- the model allows us to utilise the formability limit function which is already determined for many materials and a method for its determination is also widely known,
- critical value of the formability utilization depends neither on the geometry of the material deformed nor on the die shape.

The model was initially tested in the commercial Forge3 package. Based on the test results we are able to make some observations that will enable us to eliminate the model shortcomings in the future. We plan to add some new elements that make the model more useful. This especially concerns the formulae that are essential for considering the physical phenomena during deformation, i.e.:

- the phenomena of "healing" of microfractures for the stress triaxiality less than or equal to $-0.66$,
- the influence of the tensile stress components,
- the effect of the material directional properties on the limit deformation (for the anisotropic materials).

Verification of the ductile fracture model designed for the metal-forming processes performed either under warm or hot working conditions would be a crucial element in exceeding its application areas.

Full utilization of a computer software commonly used for simulation and design of the metal-forming processes is possible only when a complete technological plasticity characteristics of the material being deformed is known. In fact, only the flow stress function is necessary for a simulation. However, the possibility of predicting the moment and the position of the material fracture during a metal-forming process allows a complete and correct simulation. Only then one can be sure that the product achieved is free of defects caused by limited formability of the material.

**References**

[1] Behrens A., Just H.: *Verification of the Damage Model of Effective Stresses in Cold and Semi-Hot Forging Operations by Experimental Testing and FE Simulations*, Proc. of the 9th Conf. on Metal Forming, Birmingham, 2002, 295–301.

[2] Bramley A.N. et. al.: *The Prediction of Ductile Fracture Initiation During the Manufacture of Forged and Extruded Products*, Report FMP-13, Grant Ref GR/J61473: Development of Modelling Tools for the Forging Industry, 1995.

[3] Oyane M., Sato T., Okimoto K., Shima S.: *Criteria for Ductile Fracture and Their Applications*, J. Mech. Work. Technol., 1980, 4, 65–81.

[4] Dodd B.: *Bifurcations in Plastic Flow at Free Surfaces in Upsetting and Related Processes*, Res Mathematica, 1984, 12, 77–86.
[5] Freudenthal A.M.: *The Inelastic Behaviour of Engineering Materials and Structures*, Wiley, New York, 1950, 387–394.
[6] Cockroft M.G., Latham D.J.: *Ductility and the Workability of Metals*, J. Inst. Metals, 1968, 96, 33–39.
[7] Brozzo P., DeLuca B., Rendina R.: *A New Method for the Prediction of the Formability Limits of Plastic Sheets*, *Sheet Metal Forming and Formability*, Proc. of the 7th Biennial Conf. of the Int. Deep Drawing Research Group, 1972.
[8] Norris D.M., Reaugh J.E., Moran B., Quinones D.F.: *A Plastic-Strain, Mean-Stress Criterion for Ductile Fracture*, J. Eng. Mat. Tech., 1978, 100, 279–286.
[9] Atkins A.G.*: Possible Explanation for Unexpected Departures in Hydrostatic Tension – Fracture Strain Relations*, Met. Sci., 1981, 15, 81–83.
[10] Dung N.L., Mahrenholtz O.: *A Criterion for the Ductile Fracture in Cold Forging*, Proc. of the 2nd ICTP, Stuttgart, 1987, 1013–1020.
[11] Clift S.E., Hartley P., Sturgess C.E.N., Rowe G.W.: *Fracture Prediction in Plastic Deformation Processes*, Int. J. Mech. Sci, 1990, 32, 1–17.
[12] Landre J., Pertence A., Cetlin P.R., Rodrigues J.M.C., Martins P.A.F.: *On the Utilisation of Ductile Fracture Criteria in Cold Forging*, Finite Elements in Analysis and Design, 2003, 39, 175–186.
[13] Grosman F.: *Funkcja odkształcalności granicznej*, Obróbka Plastyczna, 1976, 15, 197–202.

**Zastosowanie funkcji odkształcalności granicznej do prognozowania utraty spójności materiału**

Opisano znane z literatury kryteria plastycznego pękania podczas operacji kształtowania objętościowego oraz ich wady. Zaprezentowano własny model zniszczenia oparty na odkształceniowym kryterium plastycznego pękania oraz wykorzystujący funkcję odkształcalności granicznej. Procedura obliczeniowa modelu została wprowadzona do kodu programu Forge3, którego podstawą jest metoda elementów skończonych, a następnie przetestowana przez przeprowadzenie symulacji numerycznych spęczania na zimno wsadu w postaci walca wykonanego ze stali austenitycznej.

ARCHIVES OF CIVIL AND MECHANICAL ENGINEERING

Vol. IV 2004 No. 3

# Structure and mechanical properties of hot deformed ferritic steel

D. KUC, G. NIEWIELSKI, E. HADASIK, K. RADWAŃSKI
Silesian University of Technology, Krasińskiego 8, 40-019 Katowice

In the paper, there are presented the results of research on the impact of parameters of hot plastic strain upon variations of mechanical properties and structure of the high-alloy ferritic steel after the process of high-temperature deformation. The tests were carried out with a torsion plastometer in the temperature range of 900–1150 °C at a strain rate of 0.04; 0.35 and 3.5 $s^{-1}$. The relations between the process parameters and the steel mechanical properties in plastometric torsion test were established. During a high-temperature deformation an intensive process of structure refinement took place.

Keywords: *ferritic steel, microstructure, deformation, recrystallization*

## 1. Introduction

The present work constitutes a part of many-year research programme developed to study the structural phenomena taking place during hot plastic strain of the high-alloy steels with diversified structure carried out at the Department of Materials Science of the Silesian University of Technology [1, 2]. The views on the recovery mechanisms of the structure of high-alloy ferritic steels with a high stacking fault energy differ widely. The majority of researchers are of an opinion that the dominating softening process of ferritic steels is a dynamic recovery [3]. It is also proved that in this group of steels at appropriate parameters of deformation process besides the recovery a dynamic recrystallization occurs as well [4].

In this paper, the influence of torsion parameters on mechanical properties and variations of the micro- and substructure of low-carbon high-chromium ferritic steel was examined.

## 2. Method of testing

A high-chromium ferritic steel was the material tested. Its comprised 0.05% of C, 25% of Cr and 0.33% of Ti. To diversify the size of initial grain, the steel samples were annealed prior to plastic strain at the temperature ranging from 1000 to 1200 °C with hold time of 60 min.

The steel samples tested were subjected to plastic strain with SETARAM torsion plastometer [5]. Torsion test was carried out at the temperature range of 900–1150 °C at the speed of 10, 100 and 1000 rpm. In order to define the impact of the process pa-

rameters upon the sample structure directly after a pre-set strain, the samples were cooled in water down to an ambient temperature.

The relation between the stress and strain $\sigma = f(\varepsilon)$ was established according to [6]. Strain conditions (temperature, speed) were set by using the Zener–Hollomon parameter (1), having previously defined the activation energy of hot plastic strain process by means of software ENERGY 3.0 [5]:

$$Z = \dot{\varepsilon} \exp\left(\frac{Q}{RT}\right), \tag{1}$$

where: $\dot{\varepsilon}$ – strain rate [$s^{-1}$], $T$ – strain temperature [°C], $Q$ – activation energy of plastic strain process [kJ/mol].

The metallographic examinations were performed with the REICHERT light microscope that magnified in the range of 100–500×, in the bright-field technique. A quantitative analysis of the structures tested was carried out by means of software "METILO v. 3.0" designed at the Department of Materials Science of Silesian University of Technology [7]. The grain size was analysed in microsections parallel and perpendicular to sample axis after the sample annealing and plastic deformation. Each time 500 grains were measured. In the structures analysed, we determined:

- average area of grain plane section $\bar{A}$ [$\mu m^2$],
- variability index of grain plane section area $v(\bar{A})$ [%];
- grain elongation index $\delta$ (Feret's index):

$$\delta = \frac{F_x}{F_y}, \tag{2}$$

where $F_{x,y}$ are Feret's diameters toward axis of the $x$- and y-coordinate system.

## 3. Test results

The results of qualitative and quantitative examinations of heterogeneity and grain size of samples after annealing of steel are shown in Figures 1–4. The steel after annealing displays a ferritic structure (Figures 1, 2). Along with the rise of an annealing temperature within the range analyzed, an average area of grain plane section enlarges in monotonic mode in the range from 1850 to 8770 $\mu m^2$ (Figure 3). Heterogeneity of grain size is changing in non-monotonic mode from 112 to 100%. The heterogeneity of the samples soaked in the temperature range of 1000–1100 °C is higher in comparison to that of the samples soaked at the temperature of 1150–1200 °C (Figure 4). In plastometric examinations, the steel samples were characterized by a low heterogeneity of grain size after annealing at the temperature of 1150 °C.

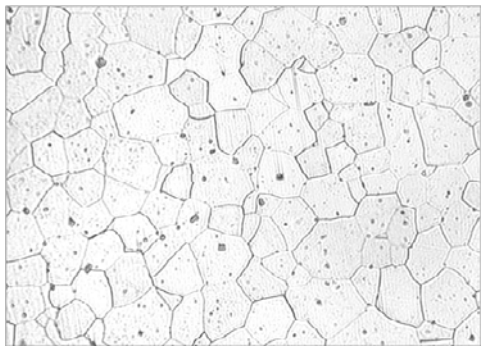

Fig. 1. Structure of ferritic steel after annealing for 60 min. at the temperature of 1050 °C. Magn. 150×

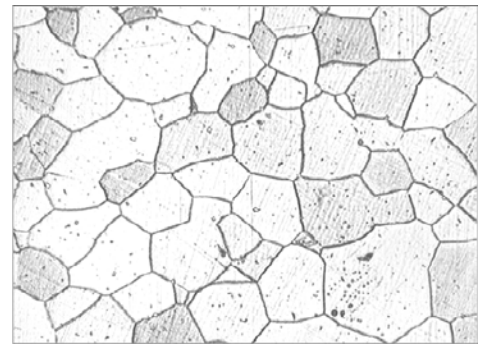

Fig. 2. Structure of ferritic steel after annealing for 60 min. at the temperature of 1150 °C. Magn. 150×

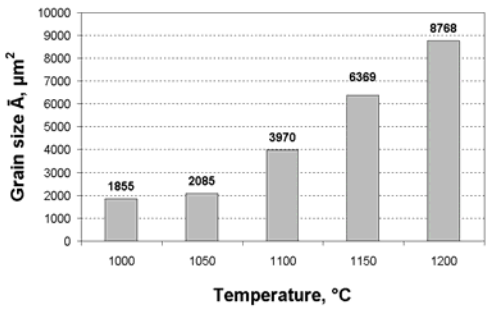


Fig. 3. Influence of annealing temperature on an average area of grain plane section $\bar{A}$

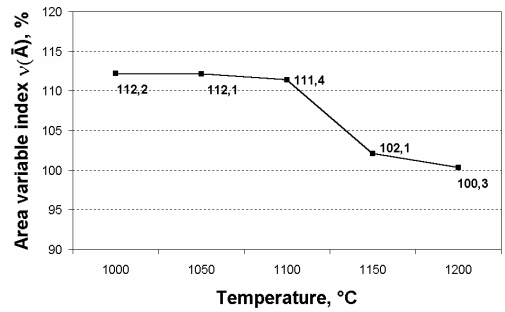


Fig. 4. Influence of annealing temperature on variability index of grain plane section $v(\bar{A})$

The examples of the stress ($\sigma$)−strain ($\varepsilon$) curves calculated on basis of the results of plastometric examinations are presented in Figures 5, 6. There is observed a reduction of plastic flow resistance together with an increase in the torsion temperature of samples in the range of 900–1150 °C (Figures 5, 6). An increase in the sample strain rate from 0.04 to 3.5 $s^{-1}$ provokes a rise of the flow stress $\sigma_p$. At each torsion temperature the flow stress after reaching its maximum is gradually dropping down until a rupture of a sample occurs. At the torsion temperature ranging from 1000 to 1150 °C, the deformability of samples is high and the strain to fracture is maintained within the range from 9 to 12.

Based on the value of the peak flow stress $\sigma_{pp}$ and the strain $\varepsilon_p$ the calculations of the activation energy for plastic strain $Q$ [kJ/mol] were made using the ENERGY 3.0 program. For high-chromium steel the activation energy amounts to 330 kJ/mol within the range of the applicable parameters of torsion process. The Zener–Hollomon parameter $Z$ [$s^{-1}$] rises substantially along with the rise of speed and a decrease in a temperature of torsion process.

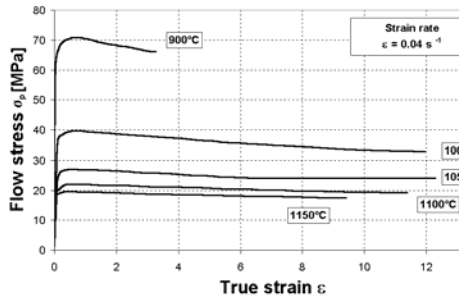


Fig. 5. Flow curves of ferritic steel after deformation at the temperature of 900–1150 °C and the rate of 0.04 $s^{-1}$

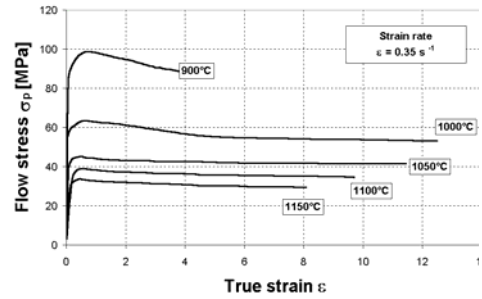


Fig. 6. Flow curves of ferritic steel after deformation at the temperature of 900–1150 °C and the rate of 0.35 $s^{-1}$

Relationships between parameters of torsion process and mechanical properties are presented in Figures 7, 8. The influence of strain conditions upon the peak flow stress $\sigma_{pp}$ and upon the strain $\varepsilon_p$ for the steel tested can be presented in the form of power functions:

$$\sigma_{pp} = 2\times10^{-7}\times Z^{5.73}, \tag{3}$$

$$\varepsilon_p = 3\times10^{-5}\times Z^{2.9}. \tag{4}$$

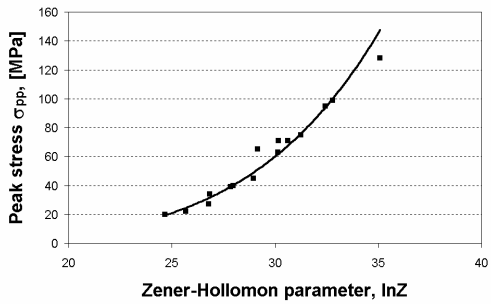


Fig. 7. Influence of strain conditions on peak flow stress $\sigma_{pp}$ of high-chromium steel

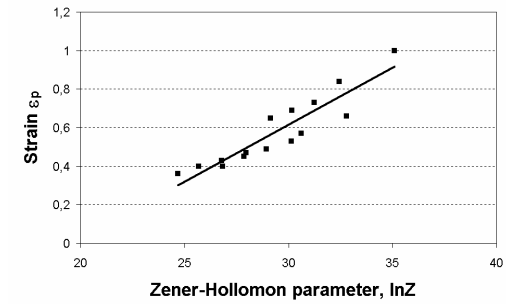


Fig. 8. Influence of strain conditions on the strain $\varepsilon_p$ corresponding to peak flow stress $\sigma_{pp}$

The impact of torsion parameters on variations of the micro- and substructure at individual stages of deformation is shown in Figure 9. During torsion at a temperature of 1100 °C there were observed processes of structure recovery in the whole range of strain rate. For a strain $\varepsilon = 1$, corresponding to peak flow stress at the flow curve, we observed fine recrystallized grains on the boundaries of elongated and corrugated initial grains (Figure 9a). Inside the grains a subgrain structure (Figure 9d) is formed. An increase in the strain to $\varepsilon = 3.2$ leads to the formation of recrystallized grains and

a gradual decay of initial grains (Figure 9b). New grains exhibit a low dislocation density with perfectly shaped boundaries of subgrains (Figure 9e), and the distribution of defects is not changed significantly (Figure 9f).

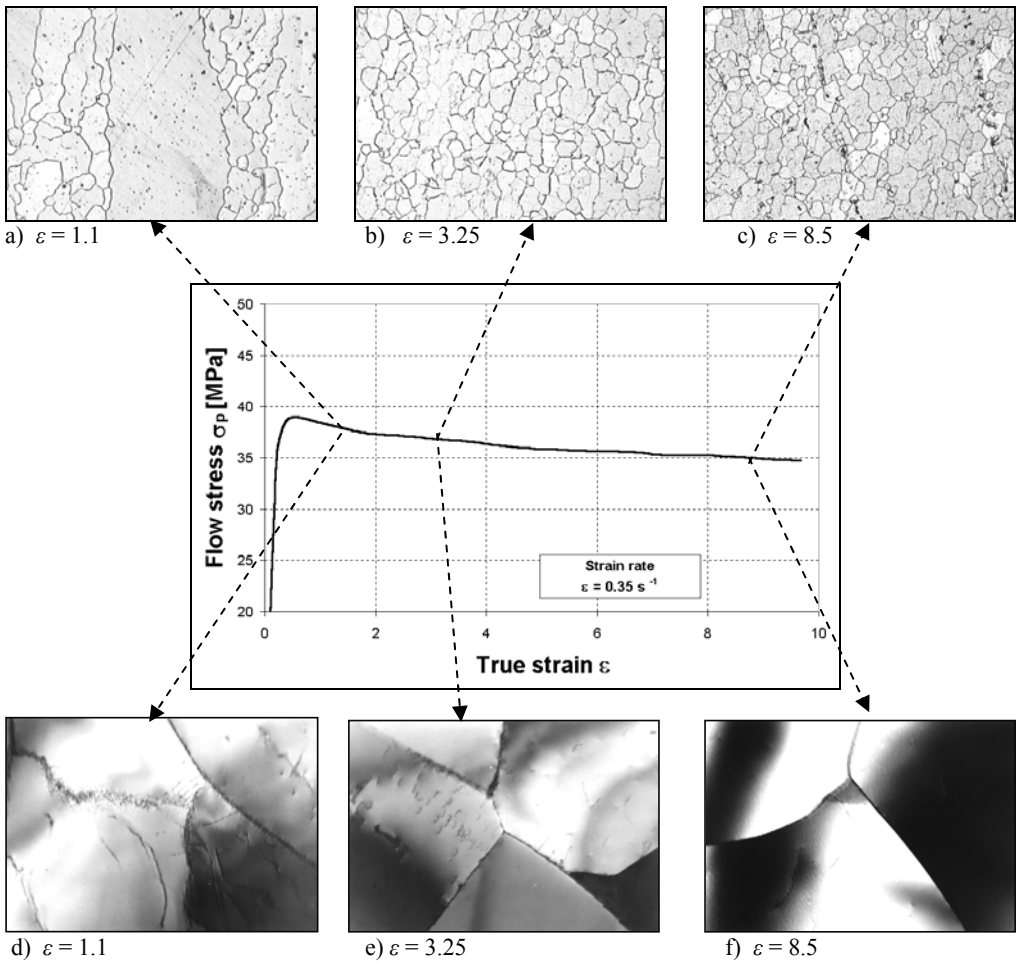


Fig. 9. Influence of deformation on variations of the micro- and substructure of the steel tested after a torsion at the temperature of 1100 °C and the rate of 0.35 $s^{-1}$; a–c – LM magn. 150×.; d–e – TEM magn. 6700×

The influence of the parameters of hot torsion upon the size, heterogeneity and shape of grains is presented in Figures 10–13. An increase in the temperature of steel deformation in the range analysed leads to an overgrowth of grain during dynamic recrystallization (Figure 10), particularly after torsion at the temperature of 1100 °C. Along with a rise of deformation temperature the heterogeneity of grain size decreases (Figure 11). An increase in the strain rate from 0.04 to 0.35 $s^{-1}$ causes an intensive,

multiple refinement of grains. An average area of grain plane section decreases from 8400 to about 1300 μm$^2$ (Figure 10). Further increase in the strain rate to 3.5 s$^{-1}$ does not longer lead to significant changes in the grain size. Instead, there is observed a reduction of grain size heterogeneity with an increase in strain rate (Figure 12).

With an increase in strain the value of Feret's index $\delta$ increases, i.e. the grain equiaxiality connected with homogeneity of structure increases (Figure 13). There was no essential effect of the strain rate and temperature on variations of the shape of recrystallized grains.

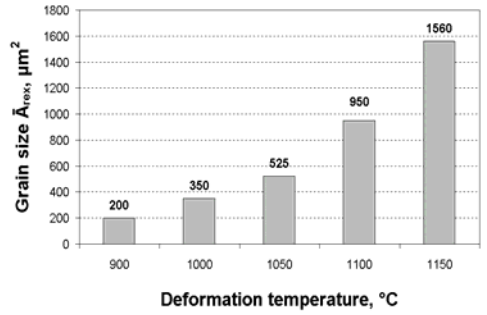


Fig. 10. Influence of deformation temperature on an average area of grain plane section $\bar{A}$. Strain rate of 0.35 s$^{-1}$

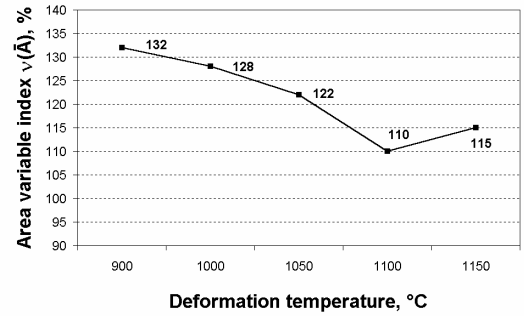


Fig. 11. Influence of deformation temperature on variability index of grain plane section $v(\bar{A})$. Strain rate of 0.35 s$^{-1}$

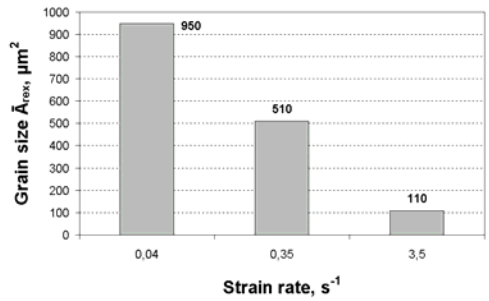


Fig. 12. Influence of strain rate on an average area of grain plane section $\bar{A}$. Deformation temperature of 1100 °C

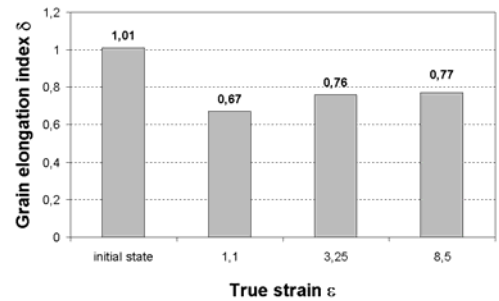


Fig. 13. Influence of strain rate on Feret's index $\delta$. Initial state – after treating solution at 1150 °C. Deformation temperature of 1100 °C, strain rate of 0.04 s$^{-1}$

## 4. Summary

The high-chromium steel after annealing within the temperature range tested has ferritic structure characterized by diversified average grain size and heterogeneity of grain size.

Ferritic steel displays high deformability, especially in the temperature ranging from 1000 to 1150 °C. In the deformation process, the value of activation energy is lower than that of austenitic steel [2] and therefore, there was observed no intensive hardening of the steel tested during deformation. The relation between parameters of deformation process and mechanical properties (the peak flow stress $\sigma_{pp}$ and strain $\varepsilon_p$) can be defined mathematically.

Within the range of variability of torsion parameters there was observed a considerable refinement of structure. In the substructure, before reaching a peak point at the flow curve, the subgrains appeared. Formation of their boundaries depends on the magnitude of strain. Refinement of structure, similar as in the case of aluminium alloys [8], can be due to the so-called geometrical dynamic recrystallization.

A rise of deformation temperature leads to an intensive grain overgrowth and reduction of grain size heterogeneity in the steel tested. An increase in the strain rate is responsible for the reduction of the grain size and its heterogeneity. An increased deformation leads to a rise of grain equiaxiality.

Our research broadens knowledge about the dynamic processes of structural variations and enables us to compare the mechanisms of structure recovery with those typical of other high-alloy hot deformed steels.

**References**

[1] Hetmańczyk M., Niewielski G., Ducki K., Lalik S.: *Structural basis of heat treatment and thermo-mechanical process of special physics-chemical properties alloys*, Inż. Mater., 1994, No. 3–4, pp. 62.

[2] Kuc D., Cwajna J. Hetmańczyk M.: *Grain size and shape of austenitic steels after hot temperature deformation*, International Conference Stereology, *Spatial Statistic and Stochastic Geometry $S^4G$*, Prague, 1999, pp. 69.

[3] Doherty R.D. et al.: *Current issue in recrystallization; a review*, Mat. Sc. and Eng., A237, 1997, pp. 219.

[4] Cizek P., Wynne B.P.: *A mechanism of ferrite softening in a duplex stainless steel deformed in hot torsion*, Mat. Sc. and Eng., A230, 1997, pp. 88.

[5] Schindler I., Bořuta J.: *Utilization Potentialities of the Torsion Plastometer*, Department of Metal Forming, Silesian Technical University, Katowice, 1998.

[6] Hadasik E.: *Procedura wyznaczania charakterystyk plastyczności w próbie skręcania*, Międzynarodowa konferencja FORMING'2002, Plastyczność Materiałów, Luhacovice 2002, pp. 103–106.

[7] Szala J.: *Computer programme for image analysis "Metilo3.0"*, Katowice, 1997.

[8] Konopleva E., Mc Queen H.: *Hot working and microstructure in 409 ferritic steel*, Mat. Sc. and Eng., A234-236, 1997, pp. 826.

This work was supported by the State Committee for Scientific Research, under grant No. 4 T08A 02922.

**Struktura i właściwości mechaniczne stali ferrytycznej odkształcanej na gorąco**

Opisano wpływ parametrów odkształcania plastycznego na gorąco na zmiany właściwości mechanicznych i struktury wysokostopowej stali ferrytycznej w procesie wysokotemperaturowego odkształcania. Badania prowadzono na plastometrze skrętnym w zakresie temperatury 900–1150 °C z prędkością odkształcania 0,04, 0,35 i 3,5 $s^{-1}$. Wyznaczono zależności między parametrami procesu a właściwościami mechanicznymi w plastometrycznej próbie skręcania. Wykazano intensywne rozdrobnienie struktury w procesie wysokotemperaturowego odkształcania.

ARCHIVES OF CIVIL AND MECHANICAL ENGINEERING

Vol. IV 2004 No. 3

# Influence of pulsatory forming on mechanical properties of stainless steel

TIBOR KVAČKAJ, LUCIA SOKOLOVÁ, MARTIN VLADO, VLADIMÍR VRCHOVINSKÝ
Technical University of Košice, Faculty of Metallurgy, Letná 9, 040 01 Košice, Slovakia.
e-mail: tibor.kvackaj@tuke.sk

ZBYŠEK NOVÝ
Comtes FHT , Plzeň, Czech Republic

Pulsatory forming of metal materials (stress cycling) is a non-conventional forging method based on the application of a variable pulsation frequency during the metal-forming process. This paper presents initial results of pulsatory forming performed with a pulsator at the Department of Metal Forming, Technical University of Košice. The basic mechanical characteristics as well as geometrical and microstructural parameters of Cr18Ni10 steel after pulsatory forming were analyzed.

Keywords: *pulsator, pulsation forming, pulsation frequency, microstructure, geometrical characteristics, mechanical properties*

## 1. Introduction

In general, the forming processes can be classified according to the energy type as follows [1]:

- processes utilizing the impact energy,
- processes utilizing the energy of pressure media,
- processes utilizing the latent energy,
- processes utilizing the energy of fields and explosions,
- processes utilizing the energy of vibration systems with a frequency effect.

Pulsatory forming, as one of non-conventional forming methods, can be classified as the category of technological processes where the energy of vibration systems with a frequency effect is utilized. The original idea to implement a volume-forming method using pulsatory forming technology arose in 1999, within the international project EUREKA E! 2336. This is a process where a tool applies a force to a formed material, while the immediate value of the force oscillates around a mean value, which can remain constant or can increase or decrease during the process. Pulses can be generated by generators based on hydraulic, electromagnetic or mechanical principles.

The idea of applying pulsatory forming resulted from looking for a new bulk forming method with the aim to increase the technological formability of material, which is in common forming processes limited by conventional conditions of technology. The pulsation frequency and amplitudes during pulsatory forming are new tech-

nological parameters and using them we can influence both important processes taking place in the formed metal (dynamic recrystallization, grain growth, transformation processes) and the contact area between the formed metal and the forming tool (the character of friction and related impacts on the deformation course and the formability). Controlling the force values during pulsatory forming (decreases and re-increases) can promote and speed up the course of dynamic recrystallization [2]. The grain size – the most important structural factor – can also be activated by pulsatory forming, resulting in finer-grained mictrostructures, while the recrystallization kinetics (its higher intensity) and the grain refinement have a positive effect on the material plasticity and formability [2, 3]. The cyclic decrease and increase of stress on the contact areas between the formed metal and the forming tool improves the conditions for elementary slips, which must take place in material flowing in the desired direction [4]. During pulsatory forming, the course of recrystallization processes is promoted, but, on the other hand, a high density of high-strength micro-areas is also promoted because of repeated "peak" stresses in the process. This has an effect on the course of transformation, for example in steel, where austenite is transformed into ferrite–carbidic microstructures. According to [5], the strengthening character of carbon steels during pulsatory forming increases the austenite stability in relation to its transformation into bainite or martensite, but, on the other hand, it speeds up the formation of pro-eutectoid ferrite. Consequently, in the resulting structure the shares of ferrite and residual austenite are promoted at the expense of the bainitic or martensitic mictrostructural shares, which is an important factor from the viewpoint of material plasticity and formability.

The paper presents initial results of research carried out with an installed pulsator, whose scheme is shown in Figure 1.

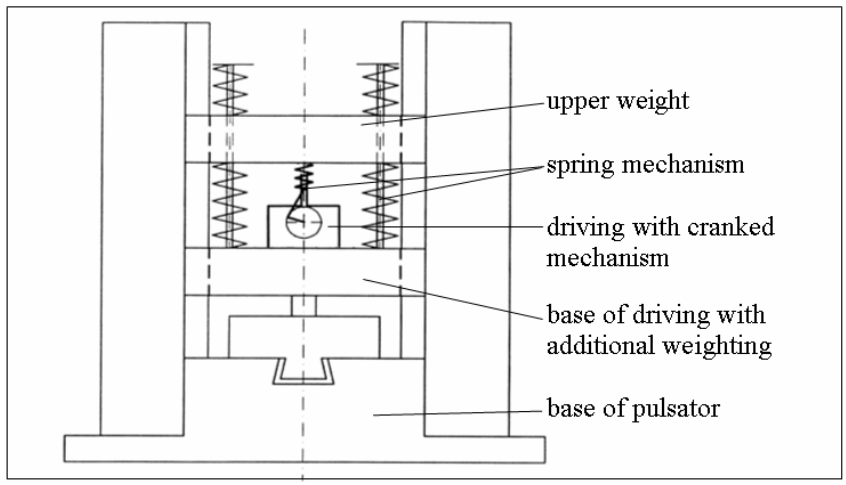


Fig. 1. Pulsator

The experimental material was exposed to pulsatory forming at a constant temperature mode (heating temperature, deformation temperature) and a variable pulsation frequency. The evaluation of the pulsatory forming results was focused on the achieved basic strength and plastic material characteristics. These characteristics are supplemented by the evaluation of the geometrical and structural parameters of the formed specimens.

## 2. Material and experimental methods

For the experiments carried out with the pulsator, cylindrical specimens with the dimensions $h_0 = 30$ mm and $d_0 = 20$ mm were used. The chemical composition of the experimental material is shown in Table 1. The experimental program, including the heating temperatures and the deformation temperatures, together with the selected pulsation frequency, is shown in Table 2. Pulsatory forming was made at deformation temperatures that represented finishing temperatures, while the as-forged structure was fixed by water quenching. After forming and quenching the specimens, the basic mechanical properties of the material (yield strength $R_{p0.2}$ and tensile strength $R_m$, plastic characteristics – elongation $A_5$ and reduction of area $Z$) were evaluated in accordance with STN 42 0321 Standard. Furthermore, the specimen geometrical characteristic $d_s/h_0$ was evaluated as a function of the forming parameters as well as the parameter $\Theta$, which was determined as the ratio $(V_{\text{barrel}} / V_0) \times 100$ [%], in order to assess the achieved barrel ratio as a function of selected pulsatory forming conditions. The results are supported by metallographic analysis using optical light microscope, where the grain size was evaluated as a function of selected pulsatory forging conditions.

Table 1. Chemical composition of steel grade 17 247 (Cr18Ni10) [weight %]

| Steel | C | Mn | Si | Cr | Ni | Ti | P | S |
|---|---|---|---|---|---|---|---|---|
| Cr18Ni10 | max. 0.08 | max. 2.0 | max. 1.0 | 18.0 | 10.0 | min. 5× %C | max. 0.045 | max. 0.030 |

Table 2. Experimental procedure

| Heating temp. [°C] | Deformation temp. [°C] | Pulsation frequency [Hz] | Note |
|---|---|---|---|
| 1100 | 850 | 10 | The specimens after pulsatory forming were quenched (water) |
| | | 20 | |
| | | 25 | |
| | | 30 | |
| | | 35 | |
| | | 40 | |

## 3. Experimental results and discussion

The deformation achieved during the pulsatory forming of cylindrical specimens made of experimental steel as a function of the pulsation frequency is shown in Figure 2.

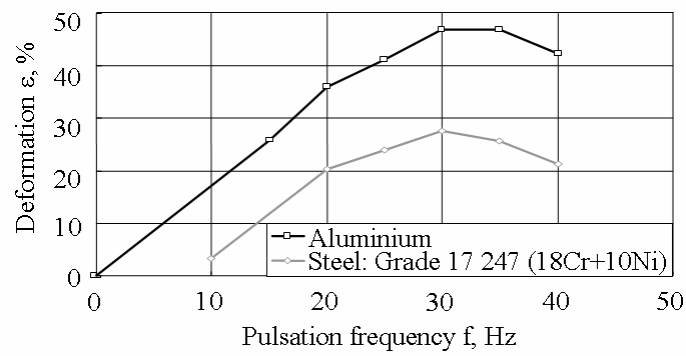


Fig. 2. Deformation as function of pulsation frequency (Al-cold forming, steel – $T_{finished}$ = 850 °C)

For comparison, the graph also shows the course for cold-deformed Al-specimens. The course of $R_{p0.2}$ and $R_m$ after deformation as a function of the pulsation frequency at a constant temperature mode is shown in Figure 3.

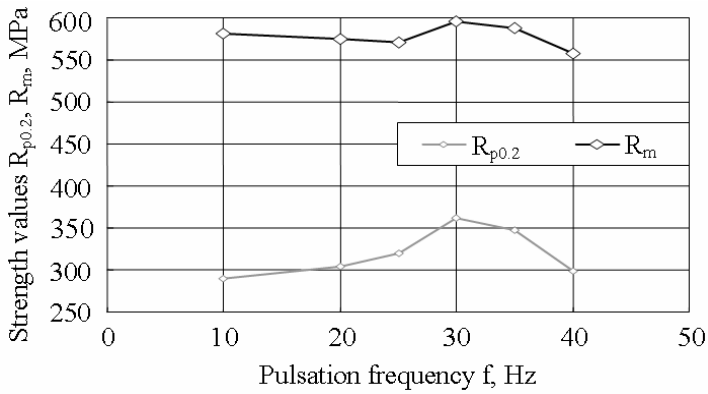


Fig. 3. Strength values as function of pulsation frequency (steel – $T_{finished}$ = 850 °C)

By increasing the pulsation frequency at the given temperature mode, maximum values of the both strength characteristics were achieved at the frequencies ranging from 25 to 35 Hz (maximum values of the both characteristics were achieved at 30 Hz). In the case of the tensile strength, the differences stemmed from varying the pulsation frequency are significantly lower than in the case of the yield strenght, while the difference between the maximum and minimum values is up to 100 MPa. The courses of elongation and reduction of area at the coincident temperature mode of heating and deformation of the experimental material as a function of the pulsation frequency are shown in Figure 4.

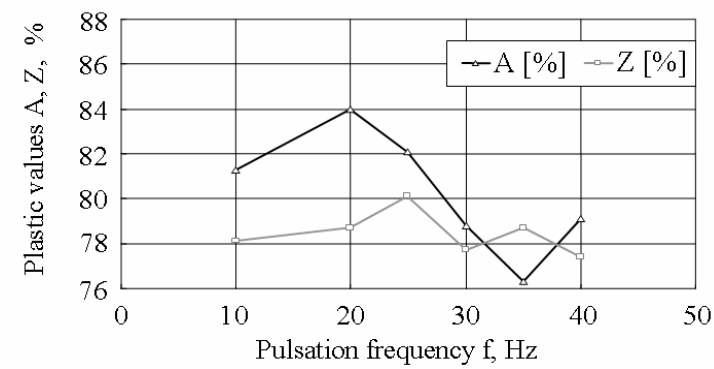


Fig. 4. Plastic values as function of pulsation frequency (steel – $T_{\text{finished}}$ = 850 °C)

The maximum value of elongation $A_5$ was reached at the pulsation frequency of 20 Hz, and a maximum value of reduction of area was achieved at the pulsation frequency of 25 Hz. At the frequencies ranging from 25 to 35 Hz, the highest strength values were obtained, the lowest elongation was achieved (at the pulsation frequency of 35 Hz) as well as one of the lowest values of reduction of area (at the pulsation frequency of 30 Hz), which corresponds to the basic course of strength – plastic characteristics of material after plastic deformation. The highest value of reduction of area (80%), which is one of the material formability indicators and which should be over 60% in forged products in order to eliminate risks during forming, was achieved at the frequency of 25 Hz, which corresponds to the tensile strength value of 570 MPa. Within the interval of the frequencies tested, the highest elongation values (over 80%) were achieved at pulsation frequencies from 10 to 25 Hz (the highest elongation was achieved at 20 Hz), while this pulsation frequency interval also corresponds to the highest achieved values of area reduction. The relationship between the final height of the specimen $h_1$ and the pulsation frequency is shown in Figure 5.

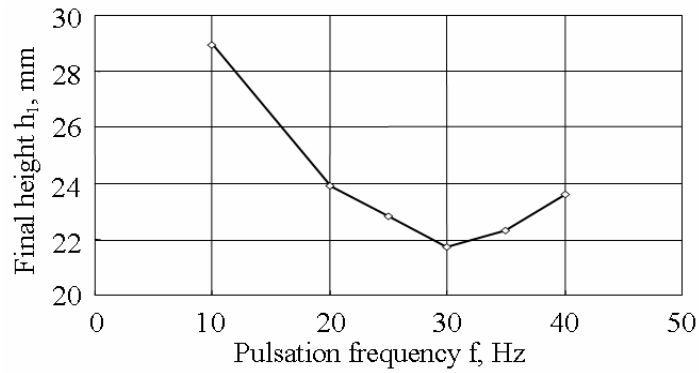


Fig. 5. Final height versus pulsation frequency (steel – $T_{\text{finished}}$ = 850 °C)

The relationship between the ratio $d_s/h_0$ and the pulsation frequency is shown in Figure 6. It results from Figure 7, where the parameter $\Theta$ calculated as a function of the pulsation frequency is shown, that the parameter $\Theta$ grows with the growing frequency in the testing interval from 10 to 40 Hz, which indicates a growth of deformation non-uniformity. This can mean a certain risk from the formability point of view. However, after exceeding the pulsation frequency of 20 Hz the growth of the barrel ratio significantly slows down.

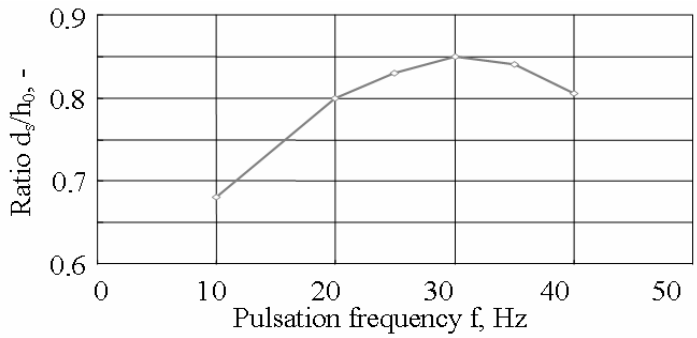


Fig. 6. Ratio ($d_s/h_0$) versus pulsation frequency (steel – $T_{finished}$ = 850 °C)

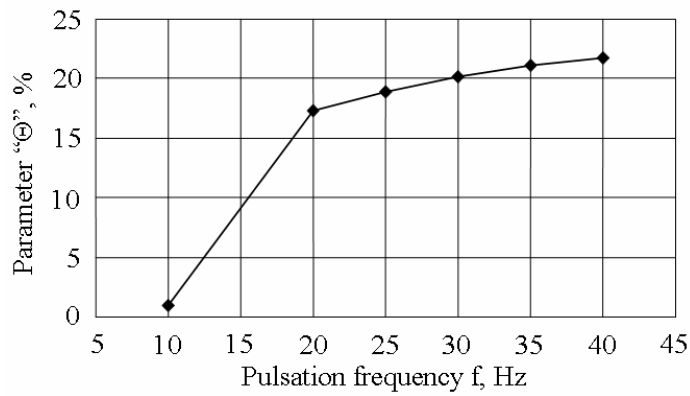


Fig. 7. Ratio of $\Theta = (V_{barrel}/V_0)\times 100$[%] versus pulsation frequency (steel – $T_{finished}$ = 850 °C)

The microstructures obtained after the pulsatory forming of the experimental material as well as in the initial state before forming are documented in Figure 8. They represent states at which the greatest grain refinement occurred. The initial grain size was 59 μm. The as-formed structure was fixed, while at the lowest pulsation frequency (10 Hz) recrystallized grains were found in the whole material volume.

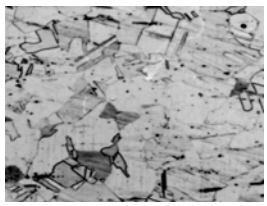

initial state
diameter of AGS: $d\gamma = 59$ μm

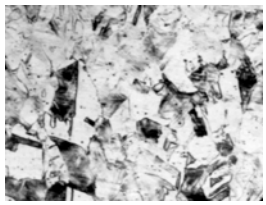

microstructure after pulsation forming
- pulsation frequency of 20 Hz; $T_{finished} = 850$ °C
diameter of AGS: $d\gamma = 59$ μm

microstructure after pulsation forming
- pulsation frequency of 25 Hz; $T_{finished} = 850$ °C
diameter of AGS: $d\gamma = 41$ μm

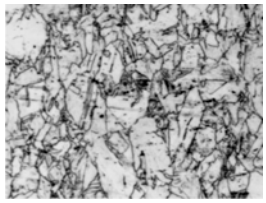

microstructure after pulsation forming
- pulsation frequency of 30 Hz; $T_{finished} = 850$ °C
diameter of AGS: $d\gamma = 40$ μm

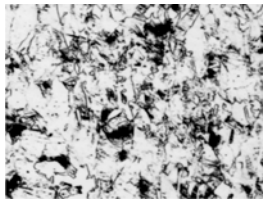

microstructure after pulsation forming
- pulsation frequency of 35 Hz; $T_{finished} = 850$ °C
diameter of AGS: $d\gamma = 39$ μm

Fig. 8. Microstructure in initial state and microstructures after pulsatory forming (magnitude 50×)

With the increase of the pulsation frequency, the size of recrystallized grain decreased and at the frequency of 25 Hz the structure mainly consisted of elongated grains. With a further increase of the pulsation frequency, the austenitic grains restored again, with a more significant heterogeneity degree. The austenitic grain size versus the pulsation frequency applied is shown in Figure 9.

The greatest grain refinement (ca 40 μm) was achieved at the frequency range from 25 to 35 Hz (relative deformation ca 25%, Figure 2), which corresponds to the fre-

quency range where a maximum contraction (80%) and elongation between 80 and 85% were achieved. In this pulsation frequency interval, we can also obtain the maximum values of strength properties, which indicates a possibility of achieving a good compromise between the strength properties and the plastic properties of the material tested.

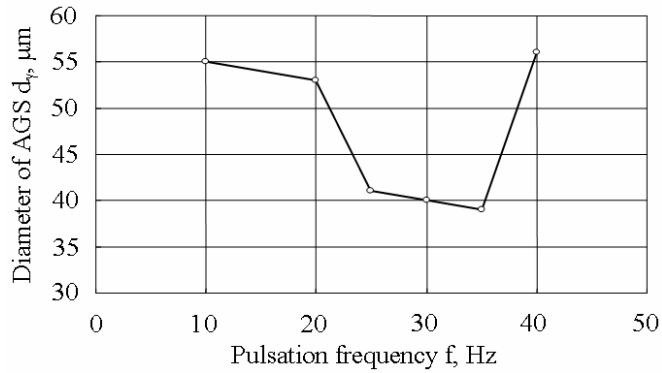


Fig. 9. Diameter of AGS versus pulsation frequency (steel – $T_{finished}$ = 850 °C)

## 4. Conclusions

Initial results of a pulsatory-forming experiment made with a pulsator installed at the Department of Metal Forming, Faculty of Metallurgy, Technical University, are presented. For the material tested, which was formed at a constant temperature mode (heating temperature: 1100 °C, deformation temperature: 850 °C), the following conclusions can be formulated:

1. The most favourable values of reduction of area, with a slight decrease of Z at the pulsation frequency of 30 Hz, were achieved within the pulsation frequency interval from 20 to 35 Hz, while this pulsation interval also corresponded to the highest achieved values of strength characteristics.

2. Within the whole frequency interval selected (from 10 to 40 Hz), the values of elongation and reduction of area are within a range ensuring reliable formability of the material tested.

3. The non-uniformity of deformation (barrel ratio of the samples) increased with an increasing pulsation frequency up to 20; above 20 Hz, further increase in the barrel ratio was less significant.

4. The grain of the material tested showed the greatest refinement (ca 40 μm) at the pulsation frequencies from 25 to 35 Hz.

**Acknowledgements**

Authors are grateful for support of experimental works by international project "Stresscycling - EUREKA E! 2336".

## References

[1] Kubíková L.: *Pulsatory forming*, PhD Thesis, KTK-HF-TU, Košice, March, 2002.
[2] Sakai T., Jonas J.J.: Acta Metallurgica et Materialia, 1984, Vol. 32, 189–209.
[3] Humphries F.J, Hatherly M.: *Recrystallization and Related Annealing Phenomena*, Pergamonn Press, 1995, 262.
[4] Polák K.: *Dynamic forming parameters*, [in:] *International Scientific Conference*, *FORMING 99*, Zlaté Hory, Czech Republic, 64–71.
[5] Cherkaoui M. et al.: Int. Journal of Plasticity, 2000, Vol. 16, 1215–1241.

## Wpływ cyklicznego kształtowania stali nierdzewnej na jej właściwości mechaniczne

Formowanie cykliczne materiałów metalicznych jest niekonwencjonalną metoda kucia opartą na zmiennej frekwencji cyklicznego obciążania w procesach kształtowania metali. Przedstawiono wstępne wyniki kształtowania cyklicznego przy użyciu pulsatora zainstalowanego na Wydziale Kształtowania Metali Politechniki w Koszycach. Przeanalizowane podstawowe właściwości mechaniczne oraz geometryczne i mechaniczne parametry stali Cr18Ni10 po kształtowaniu cyklicznym.

Kształtowanie prowadzono w stałej temperaturze 850 °C po wstępnym nagrzaniu stali do temperatury 1100 °C. Zaobserwowano także, że cykliczne odkształcanie zwiększa niejednorodność odkształceń oraz powoduje zmniejszenie rozmiarów ziaren zapewniając jednocześnie dobre właściwości plastyczne badanego materiału, konieczne do jego prawidłowego kształtowania.

ARCHIVES OF CIVIL AND MECHANICAL ENGINEERING

Vol. IV 2004 No. 3

# Modelling of casting, hot-charge rolling and cold-strip production from high-carbon steel

IVO SCHINDLER, PETR KOZELSKY, HANA KULVEITOVA, LUBOMIR CIZEK, STANISLAV RUSZ, MILOS MAREK, TOMAS KUBINA, JAROSLAV SOJKA
VSB – Technical University of Ostrava, Faculty of Metallurgy and Materials Engineering, 17. listopadu 15, 708 33 Ostrava, Czech Republic. E-mail address: ivo.schindler@vsb.cz

VLADIMIR SVINC, LIBOR CERNY
ISPAT NOVA HUT, a.s., 707 02 Ostrava – Kuncice, Czech Republic

Structure development of steel with 0.62 wt. % C during its laboratory casting, conventional as well as hot-charge rolling, cold-strip rolling and soft annealing in controlled atmosphere was studied. Effect of changes of processing parameters on final mechanical properties of a strip was determined. It was confirmed that microstructure and properties of strip produced by the effective and energy-saving hot-charge rolling could be more beneficial than after conventional rolling. Grain size seems to be more intensively effected by cooling rate and heating time of the casting than by phase transformations occurred before conventional rolling. As to final mechanical properties of thin strip from the steel applied, the ferrite fraction in the hot-rolled microstructure plays a key role. Due to higher ferrite content resulting from the finer austenite grain size, samples obtained after laboratory remelting and casting are characterized by lower yield stress and strength, together with higher ductility, which should be advantageous for subsequent processing of real strips in question.

Keywords: *high-carbon steel, casting, hot-charge rolling, cold rolling, soft annealing, microstructure, mechanical properties*

## 1. Introduction

Very effective hot-charge or even direct rolling technologies (HCR, HDR) [1, 2] integrate progressive processes of continuous near-net-shape-casting and hot forming of steels. Hot charging of slabs into the reheating furnace is of high economic interest because of the reduction of energy consumption during steel strip production in comparison with cold charging.

A laboratory complex that allows simulation of hot-charge rolling of strip from cast thin slab was developed at VSB – Technical University of Ostrava [3–5]. A steel specimen of weight up to 0.8 kg is remelted in the vacuum induction furnace and then cast in argon protective atmosphere into a simply demountable mould (Figures 1 and 2). The experimental control makes it possible to extract quickly the casting of thickness of ca 20 mm at so high temperatures that the possible phase transformation does not occur. After temperature homogenization in the electric furnace the specimen is immediately hot rolled in the computer controlled rolling mill Tandem [6] (Figure 3). In this way, hot-rolling conditions, necessary for obtaining the analogous microstruc-

ture in case of conventional and hot-charge rolling, can be evaluated.

Influence of the cast as well as hot rolled microstructure on final properties of high-carbon steel strip after its cold rolling and soft annealing was studied in laboratory conditions.

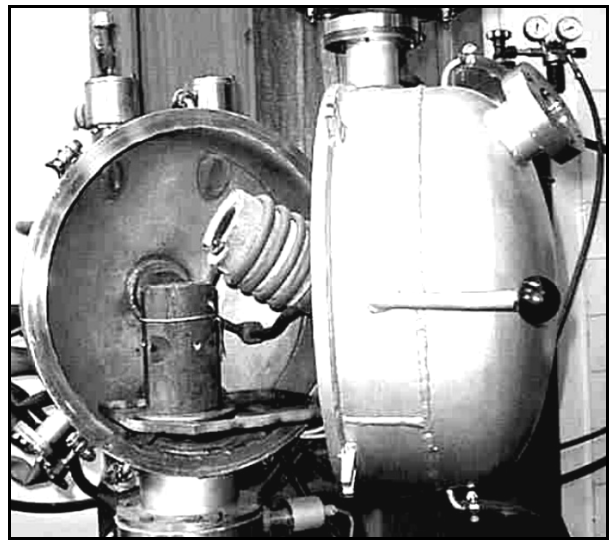

Fig. 1. Remelting vacuum furnace with mould assembly

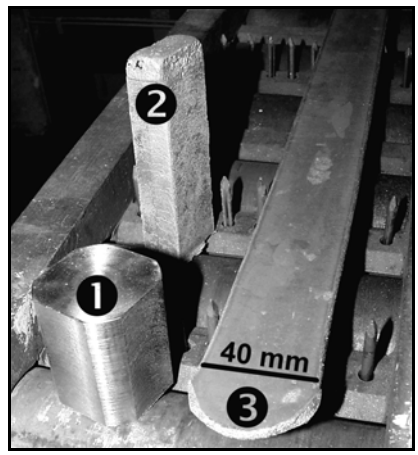


Fig. 2. Shape progress of laboratory sample:
1) machined sample before melting,
2) sample after melting and casting,
3) sample after hot rolling

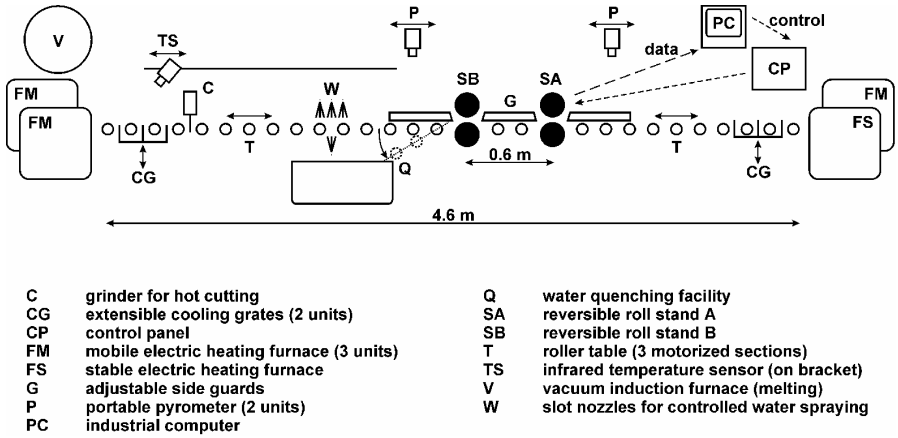


Fig. 3. Layout of the reversible laboratory rolling mill Tandem
(nominal diameter of work roll of 159 mm)

## 2. Experimental procedures

The input material was obtained in the form of a cast slab with 150 mm thickness and chemical composition as follows: 0.62 C, 0.59 Mn, 0.30 Si, 0.011 P, 0.009 S, 0.033 Al (in wt. %). The samples for subsequent hot rolling with thickness 20 mm were cut and milled from this slab or prepared by remelting and casting in the laboratory vacuum furnace, which guaranteed almost identical chemical composition. Conventional and/or hot-charge rolling was carried out in the two-stand rolling mill Tandem by 4 double-passes (individual height reductions ranging from 18 to 25%, rolling speed about 1.5 m/s) [7]. Hot-strip rolling at a reversible Steckel mill was simulated [8–10]. Three electric furnaces served for

- austenitization (equalizing temperature in the case of castings, respectively) at 1150 °C;
- simulation of a furnace coiler (see the hot strip mill P1500 in ISPAT NOVA HUT, a.s. [11, 12]) after the $6^{th}$ pass – furnace with temperature of 920 °C;
- simulation of the strip cooling in the furnace coiler with temperature slowly descending from initial temperature of 640 °C.

From the layout of the unique rolling mill P1500 (Figure 4) it may be seen that this mill is not equipped with a rougher in front of the finishing mill stand, nevertheless, it has two four-high mill stands with a vertical stand in between. Slabs soaked in the walking-beam furnace are rolled in the reverse way by five or seven double-passes. Furnace coilers are located at the entry and exit side of the mill stands and are able to maintain the rolling stock's temperature on the level up to 1050 °C. While roughing passes are performed without furnace coilers, finishing passes are carried out with furnace coilers, which makes it possible to roll even steel grades with high flow stress values.

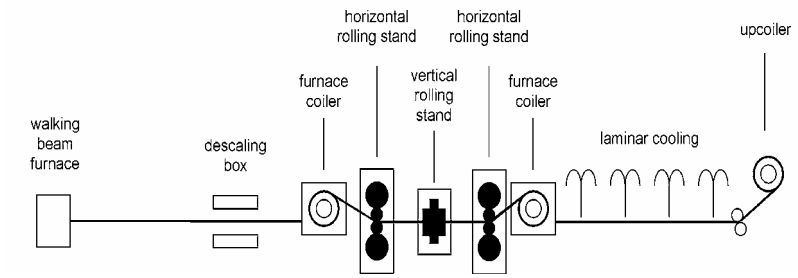


Fig. 4. Layout of the two-stand reversible Steckel hot-rolling mill in ISPAT NOVA HUT, a.s. [12]

The finishing temperature in laboratory conditions (i.e. before the 7th pass) was varied, as well as the minimum surface temperature of the cooled castings – for more detail image see Figure 5 and Table 1.

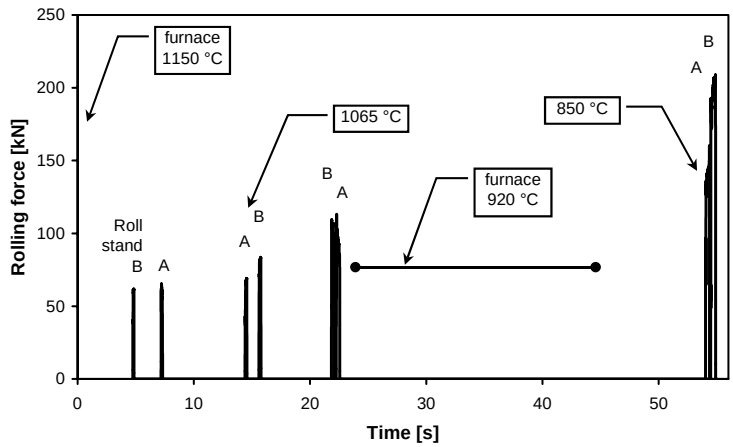


Fig. 5. Scheme of an individual hot-rolling procedure
(based on some measured variables depending on time)

Table 1. Schedule of the selected laboratory hot-rolling experiments

| samples machined from a slab |
|---|
| E – finishing 820 °C, cooling in furnace |
| F – finishing 850 °C, free-air cooling |
| G – finishing 850 °C, cooling in furnace |
| I – finishing 885 °C, cooling in furnace |
| laboratory castings (temperature: equalizing 1150 °C, finishing 850 °C) |
| K – cooling to > 1000 °C, heating, HCR |
| L – cooling to 660 °C, heating, hot rolling |
| M – cooling to 25 °C, heating, conventional hot rolling |
| N – cooling to > 1100 °C, heating, HCR |

Selected hot-rolled strips with thickness of 3.0 mm were cold rolled in the four-high mill Q110 [6] (Figure 6) as long as total height reduction of ca 53% was achived. Such thin strips with thickness of 1.4 mm were then pickled in warm hydrochloric acid and annealed in the laboratory vacuum furnace (controlled atmosphere 90% $N_2$ + 10% $H_2$) – see Figure 7. Structure and mechanical properties were studied by methods of optical metallography and standard tensile tests at ambient temperature.

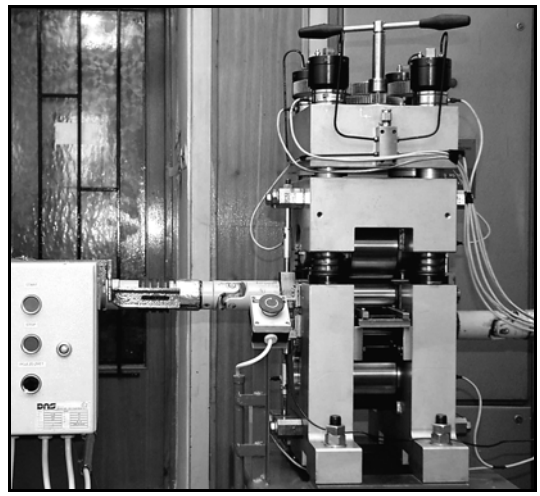

Fig. 6. Housingless laboratory mill Q110 for cold-strip rolling, prestressed by four hydraulic nuts (nominal diameter of work roll of 62 mm)

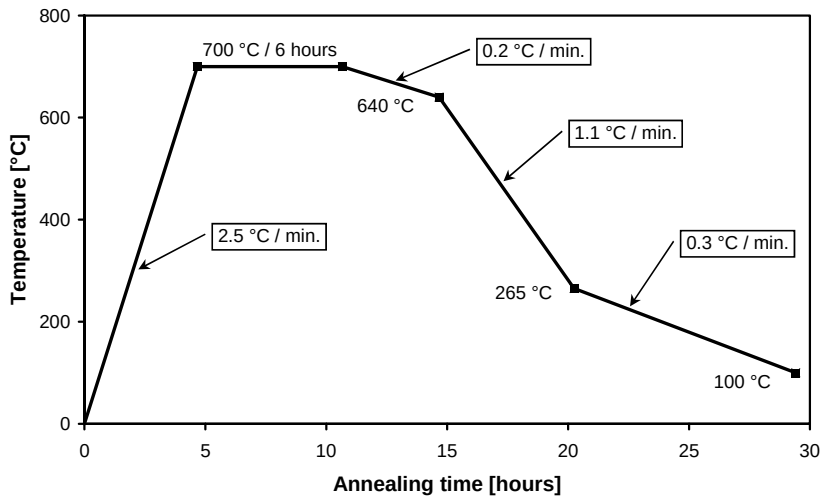


Fig. 7. Schedule of soft annealing of cold-rolled strips

## 3. Discussion of results

Microstructure of the laboratory casting and the slab are similar in as-cast state (Figure 8). Pearlite prevails and minority of ferrite (sometimes with acicular morphology) appears along the original austenite grain boundaries. Material prepared in laboratory exhibits a finer structure probably due to its faster cooling.

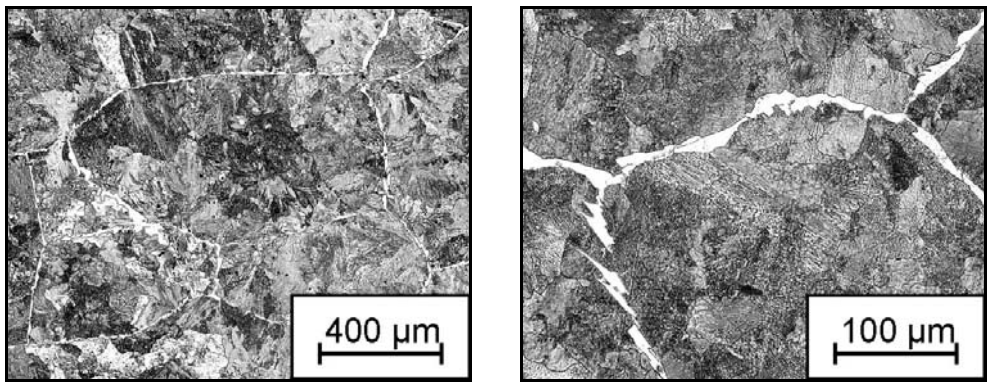


a) slab (150 mm thickness)

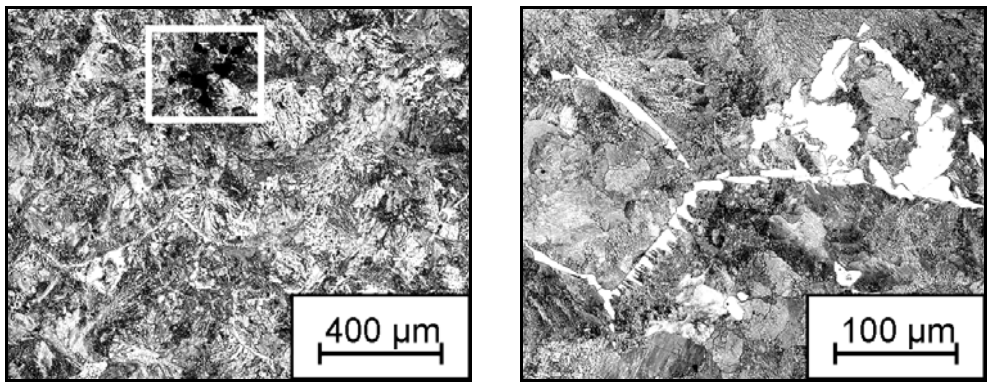


b) laboratory casting (20 mm thickness) – see central shrinkage porosity in the white rectangle

Fig. 8. Microstructure of the input material (central parts)

By comparing micrographs in Figure 9 it becomes evident that the hot-rolled samples originating from laboratory castings contain much more ferrite than those originating from a slab, which can be explained by smaller austenite grain size before the phase transformation. A greater portion of ferrite highlights banded structure. It was confirmed that laboratory cast and shortly directly heated steel (before hot-charge rolling) can exhibit a finer microstructure in comparison with that obtained by a long-term heating of cold slab before conventional rolling. Rapid cooling of hot-rolled strip prevents from originating of ferrite.

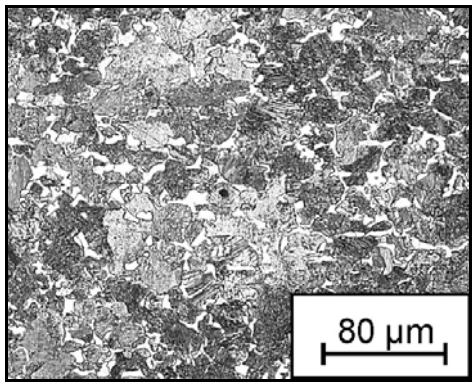


a) sample G made from a slab (slow cooling)

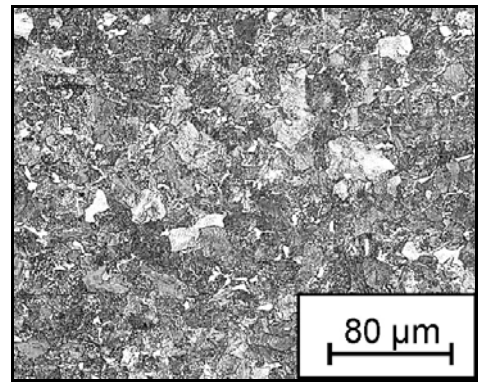


b) sample F made from a slab (free cooling)

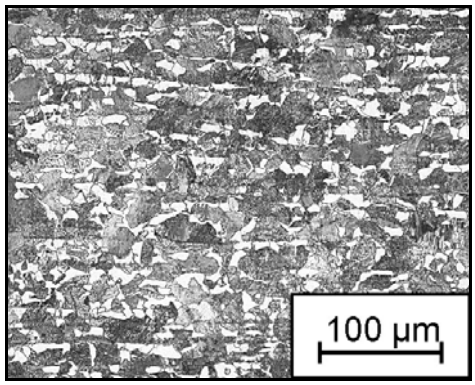


c) sample M made from a laboratory casting (conventional rolling)

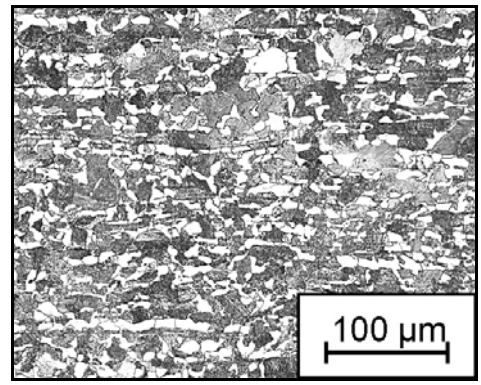


d) sample N made from a laboratory casting (hot-charge rolling)

Fig. 9. Microstructure of laboratory hot-rolled strips

Different volume fraction of ferrite markedly affects also microstructure characteristics of cold-rolled strip (Figure 10). This fact is demonstrated even by annealed structures where the perfectly spheroidized pearlite forms globules inside the recrystallized ferritic grains. These cementite globules are of much lower density in the samples rolled from laboratory castings – compare micrographs in Figures 11a, 11b and 12d.

Micrographs in Figure 12 represent a structure development during the whole experimental procedure of casting, forming and annealing with a special attention to the pearlite and ferrite morphology.

At least two tensile tests were performed for every individual laboratory strip after its annealing – for the results see Table 2. Strips made from the initial slab are characterized by larger scatter of mechanical properties. Influence of finishing temperature is negligible. Properties of the sample F (free-cooled after hot rolling) are exceptional

– this material exhibits higher strength and lower plasticity. All strips made from initial laboratory castings show higher plastic and lower strength properties. Effect of cooling conditions after casting is not evident – only strength properties of sample M (conventional hot rolling) seem to be lower and ductility of sample N (almost direct rolling) better.

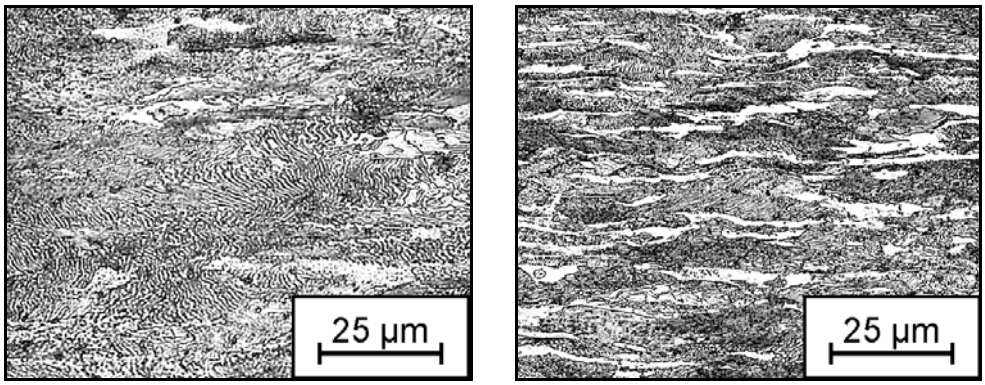


a) sample G made from a slab b) sample N made from a laboratory casting

Fig. 10. Microstructure of laboratory cold-rolled strips

Table 2. Mechanical properties of the soft-annealed strips (average values)

| Sample | $R_{p0.2}$ [MPa] | $R_m$ [MPa] | $A_{50}$ [%] | $R_{p0.2}/R_m$ |
|---|---|---|---|---|
| Samples made from slab | | | | |
| E | 402 | 540 | 25.9 | 0.74 |
| G | 402 | 538 | 25.0 | 0.75 |
| I | 406 | 547 | 25.8 | 0.74 |
| Average | 403 | 542 | 25.6 | 0.74 |
| F | 437 | 559 | 22.1 | 0.78 |
| Laboratory castings | | | | |
| M | 379 | 514 | 27.1 | 0.74 |
| L | 392 | 522 | 27.2 | 0.75 |
| K | 386 | 525 | 26.8 | 0.73 |
| N | 388 | 530 | 29.2 | 0.73 |
| Average | 386 | 523 | 27.6 | 0.74 |

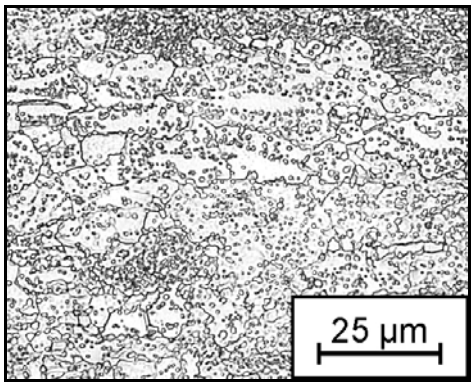


a) slow cooling after hot rolling

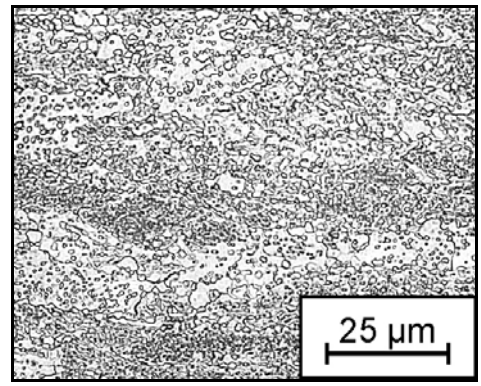


b) free cooling after hot rolling

Fig. 11. Microstructure of cold-rolled and annealed strip (samples made from a slab)

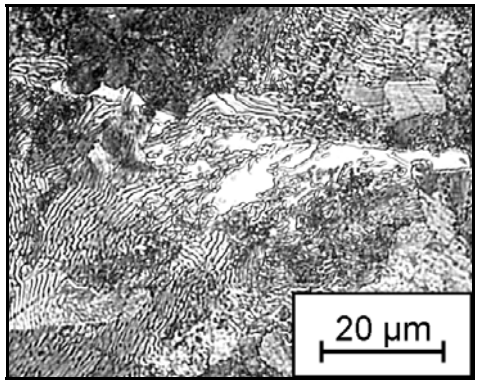


a) initial structure – pearlite + ferrite

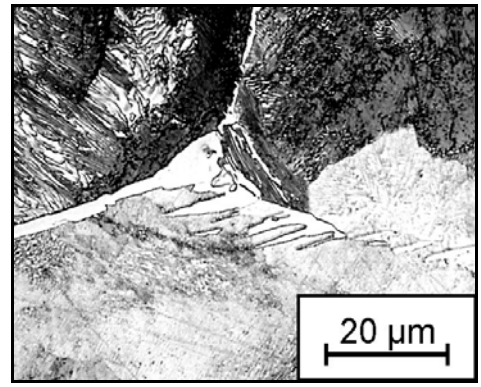


b) initial structure – acicular ferrite

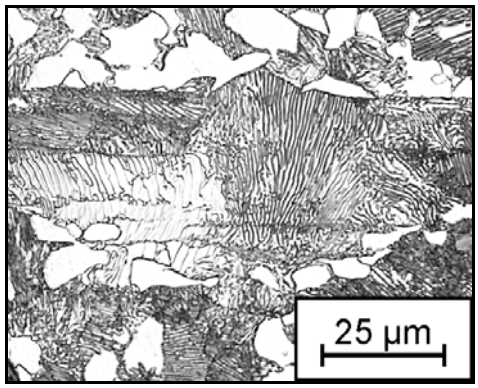


c) lamellar pearlite + ferrite after hot rolling

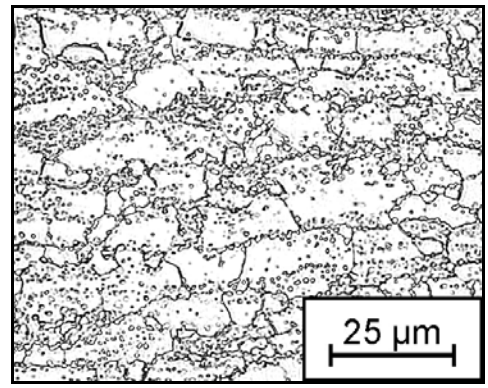


d) ferrite + globular pearlite after spheroidizing of cold-rolled strip (conventional rolling)

Fig. 12. Microstructure development of the step-by-step processed laboratory casting

## 4. Summary

• Experimental potentialities of the Institute of Modelling and Control of Forming Processes [3] cooperating with other laboratories at VSB-TUO were checked and proved at physical modelling of the complex process of high-carbon steel strip production in ISPAT NOVA HUT, a.s. – casting, conventional or hot charge rolling, controlled cooling, pickling, cold rolling and soft annealing.

• It was confirmed that structure and properties of the strip produced by the effective and energy-saving hot-charge rolling could be more beneficial than after conventional rolling [13]. Grain size seems to be more intensively affected by the cooling rate (by its dimensions) and heating time of the casting than by phase transformations occurred before conventional rolling.

• The laboratory cast flat samples with 20 mm thickness included some central shrinkage porosity. Their hot forming to the 3 mm thick strip was sufficient for entire elimination of those defects. Thus final mechanical properties of these strips had lesser scattering in comparison with samples made from an initial slab.

• Changes of the temperature parameters at hot forming disclosed that the influence of the finishing temperature on the resulting strip properties was not decisive – modification of the cooling rate was much more effective.

• As to the final mechanical properties of thin strip, the ferrite fraction in the hot-rolled microstructure plays a key role. Due to higher ferrite content resulting from a finer austenite grain size, samples obtained after laboratory remelting and casting are characterized by lower yield stress and strength combined with higher ductility, which should be advantageous for subsequent processing of real strips in question.

**Acknowledgements**

This research was supported by the Grant Agency of the Czech Republic (project 106/01/0371), Ministry of Industry and Trade of the Czech Republic (project FD-K/037), and Ministry of Education, Youth and Sports of the Czech Republic (project MSM 273600001).

**References**

[1] Bleck W.: *Metallkundliche Auswirkungen von Energiesparmassnahmen im Bereich des Warmbandwerkes auf die Eigenschaften von kaltgewaltzten Stählen*, ECSC report EUR No. 13935 DE, Brussels, 1992.
[2] Kopp R. et al.: *Casting and rolling in one heat*, Steel research, 2002, Vol. 73, No. 8, 321.
[3] http://www.fmmi.vsb.cz/model/
[4] Schindler I. et al.: *Laboratory modelling of direct rolling of steel thin slabs*, Proc. of the 5th International ESAFORM Conference on Material Forming, Akapit, Kraków, 2002, 387.

[5] Schindler I. et al.: *Dal getto alle lamine in acciaio*, Fonderia Pressofusione, 2003, Vol. 53, No. 4, 32.
[6] Schindler I., Kure F.: *Potentialities of Physical Modelling of Flat Rolling Processes at VSB – Technical University of Ostrava*, Proc. of the 6th International Conference STEEL STRIP 2001, Steel Strip Society, Ostrava, 2001, 375.
[7] Schindler I. et al.: *Laboratory casting, one-heat processing and cold strip rolling of a high-carbon steel*, Proc. of FORMING 2003, Politechnika Slaska, Katowice, 2003, 147.
[8] Groch A.G.: *TSP – The Steckel mill enters the thin slab game*, Steel Times, 1994, Vol. 222, No. 1, 28.
[9] Ramaswamy V., Benner F.G., Rosenthal D.: *Advanced hot strip Steckel mills for special steel*, Metallurgical Plant and Technology International, 1996, Vol. 19, No. 2, 70.
[10] Kramer S., Kneppe G., Rosenthal D.: *Technology and performance of modern Steckel mills*, Iron and Steel Engineer, 1997, Vol. 74, No. 7, 17.
[11] Chowaniec F. et al.: *Latest result from the production of peritectic steel grades in a medium-slab caster and a tandem Steckel mill at Nova Hut, Czech Republic*, Proc. of VAI 8th Continuous Casting Conference, Voest Alpine Linz, 2000.
[12] Cerny L., Schindler I., Boruta J.: *Research of Possibilities of Dynamic Recrystallization Initiation at Hot Rolling of Low-Carbon Steel at Two-Stand Steckel Rolling Mill*, Proc. of TECHNOLOGY 2003, SF STU Bratislava, 2003, abstract 113 + CD-ROM.
[13] Schindler I. et al.: *Structure Development at Hot Rolling of a 13Cr25 Ferritic steel*, Proc. of TECHNOLOGY 2003, SF STU Bratislava, 2003, abstract 140 + CD-ROM.

**Symulacja odlewania, walcowania z jednoczesnym nagrzewaniem oraz produkcji na zimno taśmy ze stali wysokowęglowej**

Badano rozwój struktury stali z zawartością węgla 0.62% podczas laboratoryjnego odlewania, walcowania konwencjonalnego i walcowania z jednoczesnym nagrzewaniem, walcowania taśmy na zimno oraz wyżarzania w atmosferze definiowanej. Ustalono, jak zmiany parametrów obróbki wpływają na końcowe właściwości mechaniczne. Stwierdzono, że mikrostruktura oraz właściwości taśmy produkowanej metodą efektywnego oraz energooszczędnego walcowania z jednoczesnym nagrzewaniem mogą być korzystniejsze niż po walcowaniu konwencjonalnym. Na wielkość ziarna prawdopodobnie znacznie silniej wpływa szybkość ochładzania podczas odlewania i czas nagrzewania niż transformacje fazowe poprzedzające walcowanie konwencjonalne. Zasadniczy wpływ na mechaniczne właściwości końcowe cienkiej taśmy z badanej stali ma frakcja ferrytyczna zawarta w mikrostrukturze walcowanej na gorąco. Z powodu większej zawartości ferrytu, wynikającej z drobnoziarnistej struktury austenitycznej, próbki uzyskane w trakcie laboratoryjnego przetapiania i odlewania charakteryzuje niższa granica sprężystości i wytrzymałości oraz większa sprężystość, co powinno być zaletą w obróbce wspominanych taśm.